A point-bubble model for bubble generation, transport and interaction in electrolysis

Numerical simulations of bubble flow for hydrogen production

ME55035: MSc Thesis

Nicolas David McLachlan Quiñones

TU Delft

A point-bubble model for bubble generation, transport and interaction in electrolysis

by

Nicolas David McLachlan Quiñones - 6082734

Submitted to the Process and Energy department
in partial fulfillment of the requirements for the degree of

ENERGY, FLOW AND PROCESS TECHNOLOGY - MECHANICAL ENGINEERING MASTERS DEGREE

at the

DELFT UNIVERSITY OF TECHNOLOGY

Authored by: Nicolas David McLachlan Quiñones - 6082734
Process and Energy department
November 25, 2025

Certified by: Lorenzo Botto
Complex Fluid Processing - Associate professor, Thesis Supervisor

Acknowledgments

This Masters thesis was completed as part of the graduation requirements to obtain my Mechanical Engineering Masters Degree (MSc), in the Energy, Fluids and Process Technology track. Completing it was possible thanks to the amazing people that surround me and their great support, for which I would like to thank them.

First and most importantly, my family. Despite the distance between us throughout the Masters Degree, the daily check-ups, weekly video calls and general messages of support kept me going along the way. I am beyond grateful, for both the emotional support as well as the financial support, as without any of it, I would not have been able to finish my studies. I hope the sacrifice is worthwhile and that you are proud of my work.

Secondly, my academic supervisors. From the heads of the Masters Degree track, to the professors, staff and PhD students that I have encountered during my time here, but specifically my Thesis Project Supervisor Lorenzo. Thanks to your guidance and support, I was able to clear doubts in my mind that I had regarding the thesis and direct my work where it was needed. Your knowledge on the topic is as vast as can be, and your way of dealing with students is comforting to us. I wish you all the best in your future endeavours.

Finally, to all the friends I have made along the way. Your fun and supportive attitude kept me smiling and laughing during some rough patches of the Masters. The trainings, cookouts, hangouts, random talks about subjects I hadn't even thought about, bike rides together and even events we went to, will forever be core memories linked to the good time I had in the Netherlands. I hope all of you keep being as funny, fun and amazing people as you have been to me.

Nicolas David McLachlan Quiñones,

Delft, December 2025.

THESIS COMMITTEE

Thesis Supervisor

Lorenzo Botto
Complex Fluids Processing - Associate professor
Process and Energy department - TU Delft

Thesis Defense Committee

Nicolas Valle Marchante
Energy Technology - Associate professor
Process and Energy department - TU Delft

J.W. (Willem) Haverkort
Large-Scale Energy Storage - Associate professor
Process and Energy department - TU Delft

A point-bubble model for bubble generation, transport and interaction in electrolysis

by

Nicolas David McLachlan Quiñones - 6082734

Submitted to the Process and Energy department
on November 25, 2025 in partial fulfillment of the requirements for the degree of

ENERGY, FLOW AND PROCESS TECHNOLOGY - MECHANICAL ENGINEERING MASTERS DEGREE

ABSTRACT

Green hydrogen - hydrogen produced by the electrolysis of water using renewable energy, is becoming more popular than other forms of hydrogen, due to its lower greenhouse gas emissions. Its production is forecasted to become the leading form of hydrogen generation by 2050[1] , in an attempt to limit global warming effects.

However, green hydrogen production suffers from scalability issues, as large-scale water electrolysis is limited by the efficiency of the actual electrolysis process. Such efficiency problems arise from the formation of bubbles on the electrodes, which eventually rise with the motion of the water surrounding said electrode. These bubbles in turn are capable of coalescing and producing a boundary-like layer around the electrode. This "plume" affects the efficiency of the electrolysis process.

This master thesis aims to aid in the understanding of how said bubble formation affects the efficiency of the electrolysis process, by creating point-bubble simulations to model the thought-to-be stochastic generation of bubbles on an electrode, their dynamics (growth and detachment) near the electrode, and the collision between bubbles. This will hopefully help to better understand how these bubbles evolve inside of the electrolyser.

Thesis supervisor: Lorenzo Botto
Title: Complex Fluid Processing - Associate professor

[1] As per statista: GECF. (March 14, 2024). Forecast production share of hydrogen worldwide in 2050, by technology [Graph]. In Statista. Retrieved March 19, 2025, from https://www.statista.com/statistics/1364669/forecast-global-hydrogen-production-share-by-technology:

Contents

List of Figures

Chapter 1

Introduction

1.1 Motivation

With the increase of the climate crisis and global warming effects, there is growing concern over how to reduce said effects. This has propelled the search for energy sources with a lower carbon and other green house gases footprint, than those mainly used to date. One of the most promising energy sources is green hydrogen - hydrogen produced using renewable energy sources, due to its low green house gases emissions and its high gravimetric energy density (available energy per unit mass of substance) [1]. However, a lot of research and work has yet to be done; as "green hydrogen", up until recently, accounted for a small portion of all hydrogen produced worldwide, as can be seen in Figure 1.1 (labelled "electricity"). This suggests ample room for growth and improvement of hydrogen produced by renewable energies.

One form of green hydrogen production is water electrolysis. Water electrolysis is a technique using an electric current to drive a non-spontaneous chemical reaction in which water is separated into hydrogen and oxygen molecules. The reaction that takes place in the electrode can be seen in Equation 1.1.

$$1\,H_2O + \text{Electricity} + \text{Heat} \longrightarrow H_2 + \frac{1}{2}O_2 \tag{1.1}$$

However, one of the major problems of water electrolysis processes is that their process efficiency is significantly affected by the formation and rise of hydrogen and oxygen gas bubbles on the cathode and anode, respectively; which makes the scalability of both hydrogen production methods cumbersome.

These gas bubbles are formed due to the generated dissolved gases being diffused in the supersaturated electrolyte near the electrode; nucleate in electrode areas with high supersaturation due to the increase of chemical potential of the dissolved gas molecules; and grow whilst attached to the electrode due to non-uniform concentration of said dissolved gases[3][4].

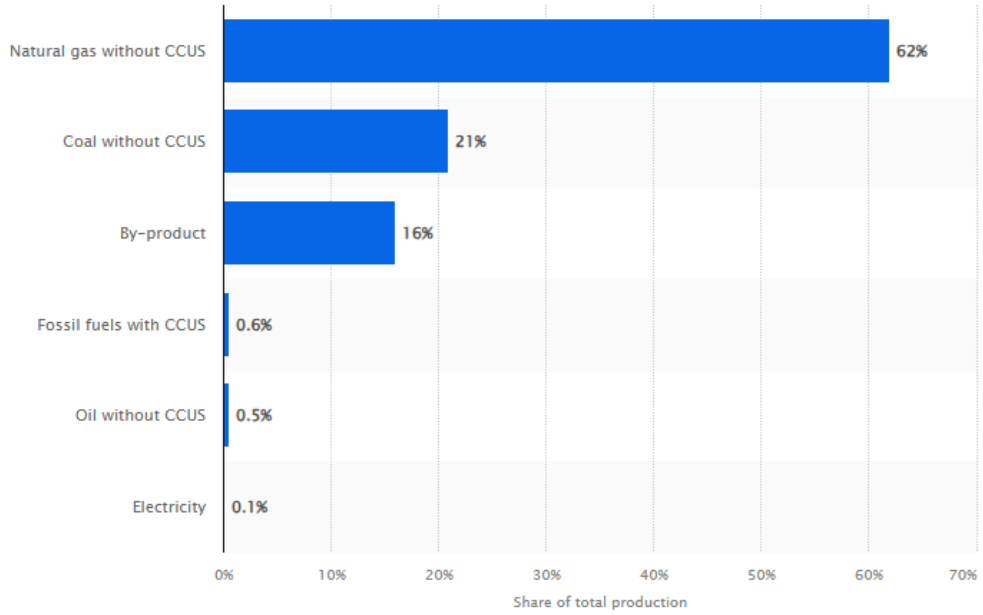

Figure 1.1: Distribution of hydrogen production worldwide in 2022, by technology. Image taken from reference [2].

These bubbles that form on the electrode are the main mode of mass transport of hydrogen and oxygen in the water electrolysis process once they detach from the electrode and are carried by the bulk flow of the electrolyte, and therefore play an important role in the performance of the electrolyser [5].

This complex and difficult to model process of bubble generation and their behaviour, have both a positive and negative impact on the electrolyser:

- As mentioned already, the major positive impact of bubbles in the electrolyser is the enhancement of mass transfer that comes along with them. Once the bubbles detach from the electrode, these enhance the mixing of the electrolyte by micro-convection near the electrode surface and macro-convection in the electrolyte bulk due to changes in the gas-liquid dispersion density and the flow of the gas-liquid dispersion parallel to the electrode. By these two modes of convection, "new" and ready-to-react electrolyte, as well as produced gases, are brought closer to the electrode, and "old" and already-reacted electrolyte is removed from the electrode's near-surrounding area [5][6].

- On the other hand, the mere existence of gas bubbles in the electrodes can lead to several problems that lead to the loss of efficiency of the electrolysis process. The root of these problems includes the blocking of electrochemically active surface of the electrode by the gas bubbles, that is, the reduction of available area for the electrochemical reactions (in this case the electrolysis of water) that take place in the electrodes, decreasing the rate of gas production; the decrease of the effective conductivity of the electrode due to the presence of bubbles - due to hydrogen gas' low electrical conductivity, the bubbles

essentially act as insulators, which in turn increases the ohmic resistance of the whole "circuit" and leads to higher energy consumption; and the increase of overpotentials, meaning more energy than expected is required to "drive" the electrochemical reactions taking place [3][7].

As bubbles, and thus multiphase flow, play such an important role in the water electrolysis process, understanding bubble growth and dynamics is key to improving and optimizing the efficiency of electrolysers.

1.2 State of the art

There are various different forms of green hydrogen production using water electrolysis such as alkaline water electrolysis (AWE), Anion exchange membrane water electrolysis (AEM), Proton exchange membrane water electrolysis (PEM) and Solid oxide water electrolysis [8]. However, amongst the aforementioned different forms of green hydrogen production, alkaline water electrolysis (AWE) and proton exchange membrane (PEM) electrolysis are considered the most promising methods for high-purity hydrogen production [3][4][9].

1.2.1 Alkaline water electrolysis (AWE)

AWE is a well-known and already settled technique that is already being used commercially in industry with capacities reaching up to megawatt scale. AWE cells use a membrane filled with an alkaline solution, in many cases 30% potassium hydroxide, to separate the electrodes. The operation of AWE cells happens at higher-than-ambient temperatures, typically ranging between 70-90 °C, and higher-than-atmospheric pressure conditions, up to around 30 bar [8][10]. The electrochemical reactions that happen in the AWE electrodes can be seen in Equation 1.2 and Equation 1.3, whilst the overall cell equation can be seen in Equation 1.4.

$$Cathode : 2\,H_2O + 2\,e^- \longrightarrow H_2 + 2\,OH^- \tag{1.2}$$

$$Anode : 2\,OH^- \longrightarrow \frac{1}{2}O_2 + 2\,e^- + H_2O \tag{1.3}$$

$$Cell : H_2O \longrightarrow H_2 + \frac{1}{2}O_2 \tag{1.4}$$

As can be seen, these reactions cause hydrogen gas to form in the cathode, and oxygen gas to form in the anode.

1.2.2 PEM water electrolysis (PEMWE)

In PEM electrolysers, water is pumped into micro-channels on the anode side's bipolar plate (electrode) where it is split into oxygen (O_2), protons (H^+) and electrons (e^-). The electrons then travel to the cathode through the external electrical circuit, which acts as the driving force of the reaction, whilst the protons traverse the proton exchange membrane that sits in between both bipolar plates (electrodes). On the cathode side of the cell, the electrons and protons recombine to form hydrogen gas (H_2). The reactions that take place in a PEM electrolyser can be seen in Equation 1.5, Equation 1.6; and the final overall cell equation can be seen in Equation 1.7.

$$Cathode : 2\,\mathrm{H^+} + 2\,\mathrm{e^-} \longrightarrow \mathrm{H_2} \tag{1.5}$$

$$Anode : \mathrm{H_2O} \longrightarrow 2\,\mathrm{H^+} + \frac{1}{2}\mathrm{O_2} + 2\,\mathrm{e^-} \tag{1.6}$$

$$Cell : \mathrm{H_2O} \longrightarrow \mathrm{H_2} + \frac{1}{2}\mathrm{O_2} \tag{1.7}$$

The operation of PEM electrolysers is done at a lower temperature range than AWE electrolysers - 20-80°C, and boasts of generally high efficiency and fast response. However, PEM electrocatalysts are mostly noble metals such as Pt/Pd which make the process costly [11].

1.3 Methodology

As for the methods to be used to complete this thesis, they are structured around the objectives and will be presented in this section :

The first methodology step is to carry out a worthy literature review, as it is needed for all three major objectives. A careful and detailed search and critical analysis of the relevant information for bubble nucleation, growth and detachment will be done. A vast range of scientific literature will be analysed, covering various different educational levels, ranging from bachelor thesis projects to conference proceedings and journal articles. Different scientific databases will be used such as Google Scholar, Science Direct , Cambridge University Press, etc.

Specifically, for the study of single bubble hydrodynamics, different correlations, algorithms and numerical methods will be evaluated, in order to pinpoint the most relevant for the case studied in this thesis. That means, correlations for the hydrodynamic forces will be tested and chosen based on the expected regime at which the fluid flow in the electrolyser operates in. As the range-of-scales is not known prior to the realization of the thesis, estimates will be used to build upon and lead to accurate solutions.

For the simulation part of the thesis, code development and optimisation is required. This includes creating codes in an interpreted language such as Python or Matlab to set the basis of the simulations. These interpreted languages are easier to write, modify and visualize in most cases, which is why the codes will be started in an interpreted language. Once these codes are known to work well and are suitable for the thesis work, they could be optimised even further and even "translated" into C++ , a compiled language. This is because compiled language is faster (takes a shorter time to run).

1.4 Challenges in modelling bubble behaviour

Modelling bubble behaviour in water electrolysers is challenging throughout the different stages of the bubble's lifespan: generation or nucleation, growth and detachment and interaction.

1.4.1 Generation or nucleation

The nucleation of bubbles is difficult to model due to its stochastic nature.

First of all, predicting where bubble nucleation[1] happens is arduous, as nucleation tends to take place in the electrode's imperfections, that in the simplest of cases and assuming the electrode is not damaged, arise from the electrode's random surface roughness. Due to the entrapment of hydrogen gas in the electrode surface's crevices, the local supersaturation of dissolved hydrogen gas in these areas becomes higher than in the areas around it, making these locations, in most cases, preferred sites for bubbles to form - known as nucleation sites. This however is not always true, as it depends on the distance between crevices in the electrode surface: when two crevices are too close to each other, as a bubble is forming in one of the crevices, dissolved hydrogen gas can be "sucked" from the nearby surface groove, leading to the depletion of dissolved hydrogen gas from this aforementioned groove. Therefore, despite the crevice, the depletion of hydrogen gas in these cases, makes the nucleation of a hydrogen bubble less likely. [12][13][14][15].

Secondly, modelling when exactly the bubbles start to nucleate is also daring. As already mentioned, bubble nucleation takes effect because of the supersaturation of dissolved gas near the electrode. The exact moment when this supersaturation level exceeds the thermodynamic barrier for bubble formation, depends on the local supersaturation gradients, surface energy and probable nucleation areas on the electrode. Proven to be challenging, some models assume instantaneous nucleation at minimal stable bubble size for simplification [10][12][16][17].

Lastly, recent study suggests that nanobubbles: much smaller bubbles than the typical bubbles that are observed to be detaching from the electrodes in water electrolysis, are also electrochemically formed on the electrodes. These nanobubbles can in turn coalesce, acting as precursors of larger bubbles. The behaviour and nucleation of these nanobubbles that are generated is not well known, therefore modelling them adds another level to the difficulty of bubble modelling in water electrolysis [16].

[1]The initial creation of a bubble from the dissolved gas near the electrode is referred to as "nucleation".

1.4.2 Detachment

Similarly, the detachment of gas bubbles from the electrodes is also complex to model.

Bubble detachment mainly occurs when the forces aiding in the removal of the bubble from the electrode, forces such as lift, buoyancy, etc; subdue those opposing the removal of the bubble, in other words, aiding the adhesion of bubbles onto the electrode: forces such as surface tension, drag, etc [2][10][5][16][17]. Accurately calculating and modelling the co-action of all of the forces acting on a bubble is strenuous, specially in the cases of the forces that are not a direct function of variables, but of the gradients of these.

Another complexity is the modelling of the bubble's contact angle on the electrode. This contact angle is dynamic and changes over time with the bubble's growth and electrolyte's flow (as it might slightly move or push a bubble over the electrode without making it detach). For the adhesion forces, such as the surface tension force, calculating and modelling said contact angle is imperative, but arduous [9].

Finally, in some cases it is possible for bubbles to detach by coalescing (merging) with bubbles in their vicinity.As bubbles coalesce, a larger and therefore more buoyant bubble is formed, leading to the increase in the bubble's detachment forces. This has proven to be computationally complex and grandiose [9][5][16][17].

1.4.3 Hydrodynamics

As mentioned already, multiphase (bubble) flow plays a great role in the operation of electrolysers. Modelling the actual multiphase flow: the hydrodynamic interactions between the bubbles and the electrolyte flow, whilst capturing the coupling of how the flow influences the behaviour of the bubbles, and vice versa, how the bubbles affect and change the behaviour of the flow; is laborious and demanding [4][10][5][12][17].

At the same time, bubbles do not have a rigid, undeformable shape. Bubble geometry and shape depends on the hydrodynamic forces that act on the bubble due to its interaction with its surroundings - electrolyte flow, other bubbles, the electrode, etc. The change of shape of a bubble requires intricate numerical techniques capable of tracking the gas-liquid interface. As a simplification, throughout this masters thesis, the shape of a bubble is considered to be perfectly spherical and non-deformable [10][16].

The influence of factors such as the bubble size, velocity of the electrolyte flow and shear rate of the flow can drastically change the bubble dynamics. Therefore, accurately selecting the values for said variables is of great importance during the simulations and can be complicated without previous experience or knowledge [3][9].

[2]All of these forces will be explained in more detail later on in the document, in the bubble dynamics section of the literature review chapter (section 2.2).

Finally, as both the relevant length and time scales of the bubbly-multiphase problem in water electrolysis are small, numerically resolving these small scales accurately, tends to be computationally very demanding, specially for the cases in which a large number of bubbles is simulated. Having said so, simulations are often limited to small-scale operation (small-scale electrolysers and small number of simulated bubbles) as well as short periods of simulation time. Simplifications and assumptions are needed in order to lighten the computational burden, although if chosen badly, the accuracy of the results could plummet.

Despite all of these challenges and complexities, accurate and physically-real models can be created to model bubble behaviour and influence in water electrolysers. This study aims to help provide exactly that.

1.5 Thesis research goal

The overarching research goal of this thesis is to better understand how the bubbles are produced near the electrode and how they evolve in the electrolyser, in order to better understand how these affect the electrolysis process.

More specifically, the research goal of this thesis is to be able to simulate and model bubble growth, detachment and flow near the electrode, and the collisions between bubbles:

- To be able to generate realistic bubble distributions on the electrode by coming up with an algorithm to do so. This includes both the location of the bubble on the electrode as well as the initial bubble size with which it nucleates. To do so, a systematic review of methods to generate statistical distributions of bubbles on a wall that are realistic for water electrolysers must be done. A thorough and extensive survey of existing literature on both experimental studies and numerical models of bubble nucleation is needed: statistical information on bubble size and location distribution will be taken from experimental studies, and compared to the results obtained from different nucleation theories based on and used in boiling and phase change phenomena modelling.
- To do an assessment of the hydrodynamics that influence bubble behaviour in water electrolysis. This means evaluating the importance of each of the hydrodynamic forces that might affect bubbles that are just nucleated, in the regime of Reynolds number (Re), shear rates, and volume fractions that are relevant to electrolysis. This means evaluating the hydrodynamic forces that act on bubbles, once the regime of operation has been established, during bubble growth (once a bubble has nucleated) and detachment from the electrode. Special interest will be given to the lift and drag forces, as well as the buoyancy and weight forces.

  All of this will include: estimating the range of Reynolds number valid for the simulations based on typical bubble sizes and velocities in water electrolyte flow conditions; obtaining a valid shear-rate range, both close to the wall and in the bulk flow, based on

already existing knowledge of electrolyte flow between vertical electrodes; and studying bubble volume fractions typical in water electrolysis, that essentially means understanding the scale of "how many" bubbles are created during the process.

Finally, if possible, to study the bubble-bubble interaction happening near the electrode that account for hydrodynamic interactions, detachment and even collisions between different bubbles. This requires reviewing existing models for bubble collision and interaction.

- To build a code capable of modelling the collision between bubbles. This will enable the study of bubble-bubble interactions happening near the electrode that account for hydrodynamic interactions, detachment and even collisions between different bubbles. The code will also be able to give an insight as to how multiple-bubble interactions happen near an electrode surface, making it possible to then try modelling the collision force on a bubble numerically. The numerical model of the collision force on a bubble could simplify the calculation of collisions and interactions between bubbles, thus potentially helping decrease the computational demand of collision simulations.

  The will include determining the relevant forces acting on bubbles during collisions, defining said forces and implementing them numerically. Apart from that, a statistical study of the results obtained from the collision simulations will be done in order to see whether a specific model suits the collision force best.

  Different methods such as periodic boundary conditions, cut-off distances and force smoothing; present in other fields of study such as Molecular Dynamics (MD), will be used in order to make the collision simulations code more efficient and rid off numerical artifacts.

By simulating and coming up with models of said processes, research questions such as the following will be answered:

- "Is the generation or formation of bubbles on the electrode a fully stochastic process?"
- "Can the formation of bubbles on the electrode be modelled for a planar vertical electrode?"
- "Is the lift force acting upon a bubble significant during the detachment of the bubble from the electrode?"
- "Is the collision between rising bubbles and bubbles attached to electrode significant enough to promote the detachment of said attached bubbles from the electrode?"
- "Can the collision force between bubbles be modelled? What forces does it depend on?"

The answers to the proposed research questions will help in the understanding and achievement of the overarching project goal described above and will hopefully aid in the understanding of the drop of electrolysis efficiency and scalability problem.

Chapter 2

Literature Review

In this chapter, a more in depth view of bubble formation, growth detachment and collisions is given using established literature for this field of study.

2.1 Bubble formation and growth

This section is divided into two subsections, one for bubble nucleation, and the other subsection for bubble growth.

2.1.1 Bubble nucleation

As already mentioned in the introduction, the first step in the life cycle of a bubble is the formation, also known as nucleation.

Following the electrochemical reaction in which water is transformed into hydrogen gas (as explained in section 1.1), this hydrogen gas is dissolved in the electrolyte. Once enough hydrogen gas is dissolved in the electrolyte, the latter becomes supersaturated. When the supersaturation limit exceeds the thermodynamic barrier for bubble formation, nucleation begins [4][18].

Nucleation can happen via two different methods: homogeneous or heterogeneous nucleation [19].

Homogeneous nucleation is the spontaneous genesis of gas nuclei within the electrolyte, that is, the bulk liquid, without necessarily being on the electrode. This generally requires a high degree of supersaturation to overcome a hefty energy barrier.

Heterogeneous nucleation on the other hand comprises the creation of bubbles at specific sites on the electrode: mostly surface imperfections such as cracks, cavities on the surface, micro-concave areas due to the surface's roughness, or intentionally engineered sites; and are known as "nucleation sites" [16] [20]. In practical electrolysis systems, heterogeneous nucleation at the electrode surface or existing defects, is more favourable as it requires

overcoming a lower energy barrier than homogeneous nucleation [19][21].

As for the rate and location of bubble nucleation, the actual electrode surface and its properties are of crucial importance. Properties such as the surface wettability[1] and presence of hydrophobic regions help assign nucleation sites. On the other hand, parameters such as the flow rate of the electrolyte, solvent concentration and cavity distance; determine the growth rate, number density of microbubbles and nucleation location of these [20].

Although stochastic in nature due to the influence of random-like parameters such as the surface's roughness, studies have explored the possibility of controlling bubble nucleation. By actively modifying or pre-designing the surface of the electrode, a certain degree of control can be obtained. For example, in previous studies, micromachined pillars and superhydrophobic cavities have been fabricated and used as preferential nucleation sites. These help with controlling the location of nucleation by tailoring the energy landscape of the surface and in the case of superhydrophobic cavities, these enable to control the supersaturation distribution along the electrode: in these superhydrophobic cavities, the electrolyte is "repelled" as it contains water molecules, leaving the space for the dissolved gases to accumulate, leading to a higher concentration gradient and therefore supersaturation at that location. These control methods have been tested for different conditions, including pressure pulse propagation, ultrasound exposure, turbulent boiling, and liquid flow conditions [12].

Finally, recent studies have focused on the formation of nanobubbles: gaseous domains on immersed substrates in the nanoscale. This has provided insight on the critical nuclei size and formation rates of bubbles [4][20][21].

However, for this project, nanobubbles will not be dealt with. Attention will be given to microbubbles, that is bubbles with sizes within the micrometers; and larger. This is because in industrial scale electrolysers, bubbles will range in sizes mentioned already, between the micro and milli-meter scale.

2.1.2 Bubble growth

Once a bubble nucleates (is formed), the next step it follows in its life cycle is to grow, resembling that of living creatures.

Bubble growth happens primarily due to the diffusion of surrounding dissolved gases (in supersaturated regions of the electrolyte) towards the gas-liquid interface, that is, the bubble interface [10][5][18]. Typically, the initial growth rate of bubbles is rapid, but with time slows down due to the concentration of dissolved gas in the electrolyte diminishing, i.e the liquid becomes depleted of dissolved gas. This decrease in the dissolved gas concentration in the immediate surrounding area to the bubble's surface, creates a dissolved gas concentration gradient between said area and the bulk flow area. The region where this concentration gradient is substantial is known as the bubble diffusion layer. The bubble diffusion layer's

[1] Surface wettability: degree of hydrophilicity (water-loving) or hydrophobicity (water-fearing) of a surface.

thickness however is not constant - it changes in time. With time, as the concentration of available dissolved gas in the area closest to the bubble interface becomes less and less, the region of lower concentration expands. The evolution of this gas diffusion layer can be approximately modelled by Equation 2.1, where δ_b is the gas depletion in the radial direction, D is the diffusion coefficient of the dissolved gas, and t is time [12].

$$\delta_b \sim \sqrt{\mathrm{Dt}} \tag{2.1}$$

Electrolytic bubble growth can be described by a power law relationship between the bubble's radius (R) and time (t) as can be seen in Equation 2.2:

$$\mathrm{R} \propto \mathrm{t}^{\beta} \rightarrow \mathrm{R} = \mathrm{bt}^{\beta} \tag{2.2}$$

where β is a time exponent constant that depends on the dominant bubble growth mechanism and is empirical, and b is a dimensional growth coefficient that depends on the electrode [16].

Three main growth mechanisms have been observed:

- Inertia controlled growth is the first stage of bubble growth after nucleation. This stage is fast as it typically only lasts in the range of decimals of a second, and is controlled by the inertia of the liquid surrounding the bubble. In this stage, the time exponent can be considered the unit value: $\beta \approx 1$, meaning the bubble's radius grows linearly in time; and therefore the power law describing this stage can be written as Equation 2.3 [10][16].

$$\mathrm{R} \propto \mathrm{t} \tag{2.3}$$

- Diffusion-limited growth: this stage is often observed after the inertia controlled growth stage, and is regulated by the diffusive transport of dissolved gas to the bubble. The time exponent of this growth stage can be approximated to $\beta \approx \frac{1}{2}$ [10]. This stage mostly happens in water electrolysis when the characteristic time of diffusive transport to the bubble ($t_{db} \approx R_e^2/D$) is smaller than that of the diffusive gas transport to the electrode ($t_{de} \approx R^2/D$); i.e the dissolved gases produced at the surface of the electrode are more prone to diffuse into an already existing bubble adhered onto the electrode than across the electrode, as it takes less time for them to do so [12]. The ratio between both mentioned characteristic times is known as the Damköhler number: $Da = \frac{t_{de}}{t_{db}}$, therefore diffusion-limited growth is suggested to happen when $Da >> 1$. The power law describing this stage can be written as Equation 2.4 [16][10]:

$$\mathrm{R} \propto \sqrt{\mathrm{t}} \tag{2.4}$$

- Reaction-limited growth: This stage happens when the rate of the electrochemical reaction that produces the dissolved gas limits the growth of the bubble. This regime is more common for relatively small active electrode surfaces, that is, for small active

electrode surfaces when compared to the size of the bubble attached to the electrode. An example of this is micro-electrodes. The time exponent of this stage can be approximated as $\beta \approx \frac{1}{3}$, and therefore the power law describing this growth stage is as seen in Equation 2.5 [12][10].

$$\mathrm{R} \propto \mathrm{t}^{\frac{1}{3}} \tag{2.5}$$

Worth mentioning is that a small Damköhler number value (Da) suggests reaction-limited growth, whilst a large Damköhler number value (Da) suggests diffusion-limited growth.

However, the aforementioned power laws to describe bubble growth are the result of experimental data fitting. The rate of bubble growth in electrolysis can be described in a more fundamental way by relating it to the mass transfer of the dissolved gas through the gas-liquid interface, using Fick's Law [5]. Fick's Law relates the diffusive flux to the gradient of concentration as:

$$\mathrm{J}=-\mathrm{D}\nabla\varphi \tag{2.6}$$

where J is the diffusive flux and $\nabla\varphi$ is the gradient of the concentration φ.

Then, by equating the rate of change of the mass within the bubble to the diffusive flux of hydrogen dissolved gas through the bubble interface, Equation 2.7 can be obtained [5]:

$$\dot{N}_b = \frac{P_0}{RT_0} 4\pi R_b^2 \frac{dR_b}{dt} = \int_{\partial V} D_{H_2} \nabla C_{H_2} \cdot \hat{\boldsymbol{n}}_{\boldsymbol{b}} dA \tag{2.7}$$

where $\dot{N}_b$ is the rate of change of moles within the bubble, P_0, T_0 and R are the ambient pressure, ambient temperature and universal gas constant, respectively; and R_b is the bubble's radius at the specific time instant. On the right hand side of the equation is an integral over the bubble surface boundary ∂V, in which D_{H_2} is the diffusivity coefficient of dissolved hydrogen gas across the bubble's interface, ∇C_{H_2} is the concentration gradient of dissolved hydrogen gas (acting as $\nabla\varphi$ in Equation 2.6) and $\hat{\boldsymbol{n}}_{\boldsymbol{b}}$ is the bubble's interface unit outward pointing normal vector.

From Equation 2.7, the bubble growth rate, ie. the rate of change in time of the bubble's radius ($\frac{dR_b}{dt}$) can be obtained as Equation 2.8 suggests:

$$\frac{dR_b}{dt} = \frac{RT_0}{P_0} \frac{1}{4\pi R_b^2} \int_{\partial V} D_{H_2} \nabla C_{H_2} \cdot \hat{\boldsymbol{n}}_{\boldsymbol{b}} dA \tag{2.8}$$

Note, this equation works for assumed constant pressure inside of the bubbles, throughout the whole bubble growth (this assumption is valid for bubbles whose radius is larger than $50\mu m$).

Finally, the non-dimensional bubble Sherwood number, formally defined as the ratio of the total mass transfer rate (convection + diffusion) to the rate of diffusive mass transport, can

be used to characterize the mass transfer of dissolved gas into the bubble and the efficiency of the mass transfer process, and can be calculated as:

$$\mathrm{Sh}_b = \frac{2\,\dot{R}_b \mathrm{R}_b\,\mathrm{RT}_0}{\mathrm{P}_0\,\mathrm{D}_{\mathrm{H}_2}(\mathrm{C}_{\mathrm{H}_2,\mathrm{e}} - \mathrm{C}_{\mathrm{H}_2,\mathrm{sat}})} \tag{2.9}$$

where $\dot{R}$ is the bubble radius rate of change in time, $C_{H_2,e}$ is the concentration of dissolved hydrogen gas at the electrode and $C_{H_2,sat}$ is the saturation concentration of said dissolved gas at the bubble interface.

Bubble growth is affected by various factors, ranging from the degree of supersaturation of the dissolved gas in the electrolyte, to the hydrodynamic conditions of the bulk flow in the vicinity of a bubble [10] [5]:

- The current density in the electrolyser can influence the bubble size distribution on the electrode. Higher current densities generally lead to larger bubbles, whilst lower current densities in the range of $0.15\check{}0.35\frac{A}{cm^2}$ are shown to produce a higher number of smaller bubbles [9].

- The concentration of the electrolyte as well as the electrolyte pH, can also play a role in bubble residence time (time that a bubble stays detached to the electrode) and detachment size. For example, increasing sodium sulfate concentration in an electrolyte made up of water and the aforementioned neutral salt, decrease bubble residence time and detachment size. Experimental results suggest strong alkalinity may facilitate quicker detachment of the bubbles from the electrode.[7].

- The surface tension of the electrolyte also influences the bubble growth. Lowering said surface tension by adding surfactants suggests the formation of smaller bubble clusters [7]. Apart from modifying the surface tension and enhancing mass transfer, the addition of surfactants can also affect the inertial separation of bubbles [16][18].

- Flow conditions can also affect bubble growth. As will be explained in more detail in section 2.2, increasing flow velocity or linear share-rate can cause the lift force acting on a bubble to increase and therefore bring forward the bubble detachment onset [22].

- The operational pressure of the electrolyser can also modify the bubble growth: increasing the operational pressure slows down the growth process as it causes higher hydrogen density [10].

- The presence of external fields, such as magnetic fields, also affects bubble evolution [4][5][16].

- Gravity can also affect bubble growth. As some of the hydrodynamics forces that act on a bubble are a function of gravity, the value of gravitational acceleration may also affect bubble residence time and therefore bubble detachment size [23].

2.2 Single bubble dynamics near vertical planar electrodes

A single bubble growing on a vertical planar electrode will be subjected to different forces acting upon it. Both the direction of these vectorial forces, as well as their absolute value depend on the bubble's shape, size, proximity to the electrode and even the electrolyte flow. The interplay of mentioned forces will determine the bubble's behaviour and will ultimately dictate whether the bubble stays attached to the electrode where it is growing, or if it will detach.

Before going straight into the different hydrodynamic forces that act on a bubble during water electrolysis, four dimensionless numbers need to be mentioned, as some of these hydrodynamic forces depend on the hydrodynamic regime which the bubble is in, which is given by these dimensionless numbers.

The first dimensionless number worth mentioning is the Reynolds number (Re), which is the ratio of inertial forces to viscous forces. This non-dimensional number can help predict the fluid flow patterns, as depending on its value, the scale of either inertial or viscous forces will be much larger than the other, and therefore the aforementioned forces will dominate. The bubble Reynolds number can be calculated as seen in Equation 2.10. For the case of microbubbles in water electrolysis, the range of expected values for the Reynolds number is $Re \approx [0 - 10]$.

$$Re_b = \frac{2U_{rel}R}{\mu} \tag{2.10}$$

where U_{rel} is the relative velocity of the bubble with respect to the fluid flow, R is the bubble's radius (characteristic length of the bubble) and μ is the dynamic viscosity of the fluid in which the bubble is immersed, in this case the electrolyte.

The second dimensionless number to be mentioned is the non-dimensional shear number (Sr), which indicates the relative intensity of the shear field in the fluid, that the bubble experiences, in relation to the motion of the bubble. Therefore, a high Sr value means that the shear forces that the bubble is experiencing are significant compared to other forces. Sr can be calculated as:

$$Sr_b = \frac{2R\alpha}{U_{rel}} \tag{2.11}$$

where α is the shear-rate of the fluid flow.

As for the expected range of Sr values for microbubbles, the expected Sr values are given using experimental wall shear-stress values in the range of $[0.01 - 1]\frac{1}{s}$, as presented by N. Valle and J. W. Haverkort [24], and knowing that Sr is inversely proportional to the diameter of a bubble.

The third relevant non-dimensional number is the Eötvös number (Eo), which is the ratio of gravitational forces to capillary forces. This number is commonly used to characterize the

shape of drops or bubbles moving in a fluid. The Eötvös number can be calculated as:

$$Eo_b = \frac{(\rho_l - \rho_b)\, g\, (2R)^2}{\sigma} \tag{2.12}$$

where ρ_l is the density of the electrolyte, ρ_b is the density of the bubble (gas inside of the bubble), g is the gravitational acceleration value, R is the bubble's radius and σ is the surface tension value.

The fourth relevant dimensionless number is the capillary number (Ca). This number is the ratio between viscous forces and surface tension forces acting on a fluid flow. This number is mainly used alongside the Eötvös number to characterise the flow in porous media or multiphase flows. The Capillary number (Ca) can be calculated as:

$$Ca_b = \frac{\mu V}{\sigma} \tag{2.13}$$

where μ is the dynamic viscosity of the fluid, V is the characteristic velocity and σ is the surface tension between bulk fluid (electrolyte) and bubble.

Once the relevant non-dimensional numbers have been defined, the hydrodynamic forces acting on a bubble can be presented:

The Buoyancy force (F_B) arises due to the difference in densities between the bubble, ie. the hydrogen gas that makes up the bubble (ρ_b), and the electrolyte in which the bubble is immersed in (ρ_l). By Archimedes' principle, the fully immersed bubble in the fluid, is "pushed" up by a force equal to the weight of the fluid displaced by the bubble. The direction of this force is upward, opposing gravity, due to the nature of this force given by Archimedes' principle, and due to the gas being lighter than the electrolyte it is immersed in. The buoyancy force therefore can be calculated as can be seen in Equation 2.14

$$F_B = \frac{4}{3}\pi \rho_l g R^3 \tag{2.14}$$

where g is the value of the acceleration due to gravity, ρ_l is the electrolyte's density and R is the bubble' radius.

The weight force (F_W) is the gravitational force acting on the bubble due the bubble having mass. It follows the same direction as gravity and can be calculated using the bubble's density (ρ_b) and volume. The weight force for hydrogen gas bubbles in electrolysers is generally much smaller than the buoyancy force and therefore in most cases can be considered negligible. However, it can be calculated using Equation 2.15:

$$F_W = \frac{4}{3}\pi \rho_b g R^3 \tag{2.15}$$

The drag force (F_D) is a viscous force that opposes the relative motion of the bubble in the electrolyte. Both its magnitude and direction depend on the magnitude and direction

of the bubble's relative velocity vector with respect to the electrolyte flow; as well as the bubble's shape and size and the viscosity of the fluid the bubble is immersed in. The generally accepted way of calculating the steady drag force is [25]:

$$F_D = C_D \rho_f \pi \frac{(2R)^2}{8} |\boldsymbol{U} - \boldsymbol{V}|(\boldsymbol{U} - \boldsymbol{V}) \tag{2.16}$$

where C_D is the drag coefficient, ρ_f is the carrying fluid density, $\boldsymbol{U}$ is the velocity vector of the electrolyte in the absence of the bubble and $\boldsymbol{V}$ is the velocity vector of the bubble. Note: in Equation 2.16, the difference between absolute bubble velocity ($\boldsymbol{V}$) and flow velocity ($\boldsymbol{U}$) is the relative velocity of the bubble, as defined in [26]. However, in this thesis, the relative velocity of the bubble with respect to the fluid velocity will be called U_{rel} like in Equation 2.10.

However, there is not a universally accepted way of calculating the drag coefficient, as it is a function of the Reynolds number (Re), and therefore has been investigated for some time: $C_d = f(Re)$.

There are many different studies that suggest different ways of computing the drag coefficient for a rising bubble in shear flow, depending on the bubble Reynolds number and the bubble's shape and deformations:

- For Low Reynolds ($Re < 1$), the drag coefficient for a rigid sphere in a uniform flow with no-slip boundary conditions and in the creeping flow (Stokes flow) limit, is given by Stokes [27] as:

$$C_{D,Stokes} = \frac{24}{Re} \tag{2.17}$$

  Meanwhile, Hadamard and Rybczynski (1911) stated that for a clean bubble (mobile, stress-free interface) in stokes flow with slip-free boundary conditions, the drag is two thirds that of a rigid sphere [25], leading to

$$C_{D,H\&R} = \frac{16}{Re} \tag{2.18}$$

  From Oseen's expression for flows at low Re, which corrects Stoke's correlation by including a correction term for the convection momentum [28][29]; Taylor and Acrivos (1964) presented a correlation for small amounts of deformation at low Re [30]:

$$C_{D,T\&A} = \frac{16}{Re}\left[1 + \frac{Re}{8} + \frac{8}{15}(\chi - 1)\right] \tag{2.19}$$

  where χ is the aspect ratio. For a nearly spherical bubble ($\chi \approx 1$), this approaches Oseen's expression.

- For intermediate Reynolds Number ($1 \lesssim Re \lesssim 1000$), many empirical correlations have been established such as the extensions of Stoke's drag correlation as seen in Equation 2.17. An example is an expression for full slip conditions which holds for

higher Reynolds numbers, given by [31], in which it is stated that the second part of the correlation becomes relevant at $Re \approx 43$ and higher.:

$$C_{D,T} = \min\left[\frac{16}{Re}\left(1 + 0.15Re^{0.687}\right), \frac{48}{Re}\right] \tag{2.20}$$

On the other hand, Ishii and Zuber (1979) presented a viscous drag correlation [32]:

$$C_{D,Visc} = \frac{24}{Re}(1 + 0.1Re^{0.75}) \tag{2.21}$$

Mei et al. also presented a commonly used correlation that aims to cover a wider range of Re for bubbles. This correlation transitions between Hadamard-Rybczynski at low Re and asymptotic behaviour at large Re [25]:

$$C_{D,Mei}(Re) = \frac{16}{Re}\left[1 + \left(\frac{8}{Re} + \frac{1}{2}\left(1 + \frac{3.315}{\sqrt{Re}}\right)\right)^{-1}\right] \tag{2.22}$$

As stated in [25], this correlation agrees well with the results obtained from DNS simulations [2].

- At high Reynolds Number ($Re \gtrsim 1000$), bubbles may suffer deformations, as the flow becomes less "regular" and more turbulent. Therefore, many drag coefficient correlations for this regime consider said deformation of the bubbles. For example, Moore's correction to Levich's well-known high Reynolds number correlation [33], considers how the transport of vorticity in the wake produced at the bubble surface lowers the drag experienced by the bubble [34]:

$$C_{D,Moore} = \frac{48}{Re}\left(1 - 2.21\sqrt{Re}\right) \tag{2.23}$$

However, this correlation can yield non-physical negative values at low Re values. Figure 2.1 is a representation of said error in Moore's correction.

As already mentioned, bubbles may deform at high Re values, making the drag coefficient dependent on the bubble's deformation. As a result, the drag coefficient becomes a function of the Eötvös number. Tomiyama et al. [31] presented a correlation for for the drag coefficient as a function of Eo that can be seen in Equation 2.24:

$$C_{D,Tom}(Eo) = \max\left[\min\frac{16}{Re}\left(1 + 0.15Re^{0.687}\right), \frac{48}{Re}, \frac{8}{3}\frac{Eo}{Eo + 4}\right] \tag{2.24}$$

Legendre and Magnaudet (1998) [26] suggest that in viscous linear shear flows, a bubble's drag coefficient may be affected by the non-dimensional shear rate (Sr). Equation 2.25 is an empirical correlation to account for the aforementioned Sr dependence:

$$C_D(Re, Sr) \approx C_{DU}(Re)[1 + 0.55Sr^2] \tag{2.25}$$

where $C_{DU}(Re)$ is the value of the drag coefficient at uniform flow at the same Re values.

[2] DNS simulations will be explained more in depth in subsection 2.4.2

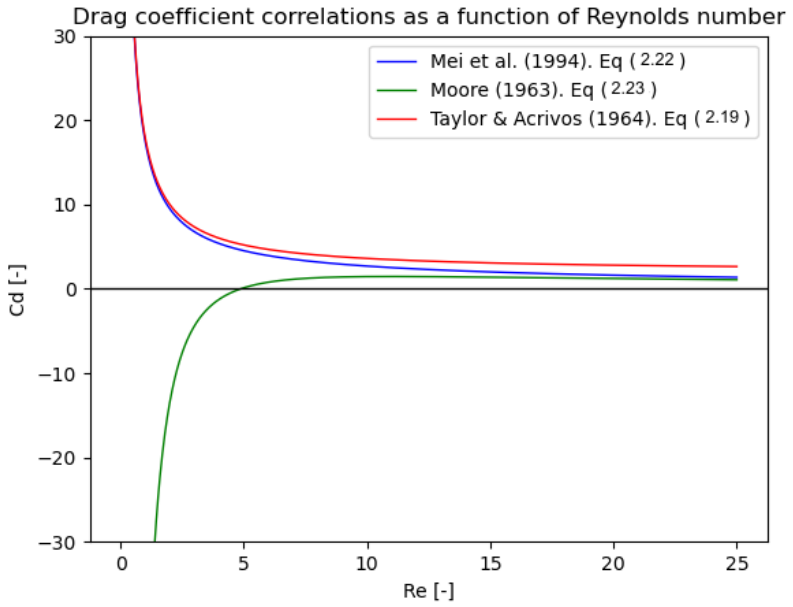

Figure 2.1: Visualization of non-physical Cd values given by Moore's correction for low Re values. Comparison between Low - Intermediate - High Re correlations. Plot inspiration taken from reference [35].

- Finally, for bubbles in the electrode's immediate proximity, Takemura et al. (2002) [36] suggest that the drag coefficient also depends on how close the rising bubble is to the wall (electrode). This empirical study mentions that different correlations are needed for different L^* cases, where L^* is the dimensionless separation defined as the ratio between the distance from the bubble centre to the wall and the viscous length scale ν/U (ν being the dynamic viscosity and U being the velocity of the fluid). However, this study does not explicitly provide correlations, but instead mentions that said correlations are adaptations of Oseen's approximations and Magnaudet, Takagi & Legendre's (2002) theoretical predictions.

Having mentioned all of these drag coefficient correlations, as mentioned previously, the expected values of the Reynolds number for this thesis project are expected to lie in the "Low Reynolds number" range, and therefore only the correlations mentioned in the "Low Reynolds number" section are expected to be used. Additionally, no deformations in the bubble's interface or shape are expected at said low Reynolds number values, and therefore will be neglected for this project.

The lift force (F_L), is a force that arises due to shear (velocity gradients) in the flow surrounding the bubble or due to the bubble rotation. This force acts perpendicular to the relative velocity of the bubble. Thus, for a bubble attached to the electrode or in the electrode's vicinity, the lift force will aid in detaching the bubble from the electrode, or will add to the bubble's movement perpendicular to the electrode; as long as the bubble's relative velocity vector mainly points in the direction parallel to the electrode. As for the lift

force's magnitude and direction, these depend on several factors such as the bubble Reynolds number, the shear rate, and the bubble's shape and deformability; similarly to the drag force; and consequently there are many ways of calculating the lift force. Additionally, methods to compute the lift force in three dimensions have been studied for years: its definition is arduous and complex as it involves vorticity and non-axisymmetric flows. As there are a vast number of methods/correlations used in literature to calculate the lift force and the lift coefficient, too many to state in this work, only a few relevant correlations are presented:

- McLaughlin (1991)[37] extended Saffman's technique (1965) to obtain an expression for the lift force and lift coefficient for Reynolds number values much smaller than unity ($Re \ll 1$) and shear parameter ($A_w = \frac{d|\nabla U|}{U_{rel}}$) values much smaller than unity ($A_w \ll 1$) as well [25]:

$$C_L = \frac{27}{2\pi^2\sqrt{ReA_w}} J(\epsilon) \tag{2.26}$$

$$F_L = C_L m_f \left(\boldsymbol{U_{rel}} \cdot \boldsymbol{\nabla U}\right) \tag{2.27}$$

  where C_L is the lift coefficient which depends on Re, A_w and $J(\epsilon)$. $J(\epsilon)$ is a monotone function of the dimensionless variable epsilon, which depends on the Reynolds and non-dimensional shear numbers:$\epsilon = \sqrt{\frac{Sr}{Re}}$. Also, m_f is the displaced fluid's volume, $\boldsymbol{U_{rel}}$ is the bubble's relative velocity vector, and $\boldsymbol{\nabla U}$ is the gradient of the flow velocity.

- The lift force in inviscid shear flows, which involves evaluating the velocity perturbation by solving the Helmholtz equation and the pressure at the surface of the bubble (sphere), was calculated by Auton (1983) for regimes in which the shear parameter is much smaller than unity ($A_w \ll 1$) [38] [25]:

$$F_L = C_L m_f \left[\boldsymbol{U_{rel}} \times (\boldsymbol{\nabla} \times \boldsymbol{U})\right] \tag{2.28}$$

  where the only difference with Equation 2.27 is that instead of the dot product of the relative velocity of the bubble with the gradient of the flow's velocity being used, the cross product of the bubble's relative velocity with the curl of the fluid flow velocity is used in Equation 2.28. Note that the lift coefficient in this case is assumed to be constant: $C_L = \frac{1}{2}$.

- Finally, Legendre and Magnaudet (1998) [26] proposed a way of calculating the lift force as a function of the monotone function $J(\epsilon)$ and the magnitude of the drag force on the bubble in creeping motion (F^0):

$$F^0 = 4\pi\rho_l \nu R|U_{rel}| \tag{2.29}$$

$$F_L = \frac{J(\epsilon)}{\pi^2} R\sqrt{\frac{\alpha}{\nu}} F^0 = \frac{4}{\pi}\rho_l\sqrt{\nu}R^2|U_{rel}|\sqrt{\alpha}J(\epsilon) \tag{2.30}$$

where $J(\epsilon)$ is once again the monotone function, R is the bubble's radius, α is the shear rate and ν is the kinematic viscosity of the bulk fluid (electrolyte), ρ_l is the density of the fluid, and $|U_0|$ is the absolute value of the undisturbed flow velocity at the bubble's location. As for the monotone function, the definitions given by McLaughlin (1990) [37] for the lift force on a small sphere in an unbounded fluid, are suitable and yield coherent results when paired with Equation 3.5.

The surface tension force (F_σ) acts at the gas-liquid interface, tending to minimize the surface area. This force is most relevant when the bubble is attached to the electrode, as at the contact point between the electrode and the bubble interface (gas-liquid interface), known as the three-phase contact line, the surface tension force aids in keeping the bubble attached to the electrode. The magnitude and direction of this force depend on the contact angle between the bubble and electrode, and of the geometry of the electrode-bubble contact line. Said contact angle however changes with the bubble's growth or with slight movement whilst still attached to the electrode or as the bubble deforms [4]; and therefore has to be considered a "dynamic" contact angle (θ_d). The dynamic contact angle θ_d is a function of the theoretical contact angle (θ_0) that can be calculated using various different methods/correlations. Equation 2.31 is a way of calculating the dynamic contact angle proposed by Klausner et al. [39], as a cubic function of the polar angle (ψ), relating it to the advancing (α) and receding (β) contact angles. A simpler and commonly used way of calculating the dynamic contact angle can be used instead, known as the Hoffman-Voinov-Tanner Law. A modified version of this law can be seen in Equation 2.32 which depends on the non-dimensional capillary number (Ca) [40]. This equation is simpler to use, which is why it is commonly used in multiphase flow simulations and CFD studies.

Once the dynamic contact angle is computed, then the surface tension force (F_σ) can be calculated as shown in Equation 2.35:

$$\theta_d(\psi) = \beta + (\alpha - \beta)\left(3\frac{\psi}{\pi} - 2\left(\frac{\psi}{\pi}\right)^3\right); 0 \leq \psi \leq \pi \tag{2.31}$$

$$\theta_d = \theta_0 + kCa^n \tag{2.32}$$

$$F_\sigma = \sigma L_c \sin(\theta_d) \tag{2.33}$$

Equation 2.31 ensures that the derivatives of the function at the front ($\psi = 0$) and rear ($\psi = \pi$) ends are both 0, i.e. a continuous function.

In Equation 2.32, k and n are empirical constants that depend on the system, and Ca is the non-dimensional Capillary number.

In Equation 2.35, σ is the surface tension once again, L_c is the contact line length between the bubble bubble and the electrode, and θ_d is the dynamic contact angle.

For a bubble with a circular contact area of radius r_c, the contact line length can be calculated as the perimeter of the circular contact area: $L_c = 2\pi r_c$, so the surface tension force can be calculated as [7]:

$$F_\sigma = 2\sigma\pi r_c \sin(\theta_d) \tag{2.34}$$

However, as modelling the dynamic contact angle of a bubble on an electrode can be cumbersome, in practice and although less accurate, the surface tension force F_σ can be calculated as the product of the surface tension σ and the radius of the bubble R:

$$F_\sigma = \sigma R \tag{2.35}$$

This form of calculating the surface tension force helps both reduce the complexity of the numerical model as well as the computational demand of the numerical methods used during the calculation, as no dynamic contact angles have to be calculated, and therefore no implicit iterative methods have to be used for said calculation.

The added mass force (F_M) accounts for the changes imposed on the fluid as the bubble accelerates. Any body of mass moving through a fluid at non-constant velocity, i.e. accelerating, will displace the fluid in its surroundings as it moves, changing the flow field. This is known as the "added mass" or "virtual mass" effect. From [25], the added mass force can be calculated as is seen in Equation 2.36, where m_f is the volume of the displaced fluid, which can be calculated as the density of the fluid (electrolyte) times the volume of the bubble that displaces the fluid: $m_f = \frac{4}{3}\pi R^3 \rho_f$; $\frac{\partial U}{\partial t}$ is the change of the fluid velocity in time (rate of change of the fluid's velocity), i.e the fluid's acceleration; $\frac{dV}{dt}$ is the change of the bubble's absolute velocity over time (rate of change of bubble's absolute velocity), i.e the bubble's acceleration; and C_m is the added mass coefficient. From [17] and [25], $C_m = 0.5$ for spherical bodies independent of their nature.

$$F_M = C_m m_f \left(\frac{\partial U}{\partial t} - \frac{dV}{dt} \right) \tag{2.36}$$

Assuming an electrolyte quasi-steady flow, the partial derivative of the flow's velocity can be considered zero, therefore Equation 2.36 is simplified as:

$$F_M = -C_m m_f \left(\frac{dV}{dt} \right) \tag{2.37}$$

for which an iterative or integral numerical method is needed to calculate the derivative of the bubble's absolute velocity with respect to time.

The Marangoni force (F_{MA}) arises from gradients in surface tension along the bubble interface ($\nabla_s \sigma$). Said Marangoni force acts tangential to the bubble interface and can be calculated as the integral over the bubble's surface area :

$$\mathbf{F}_{MA} = \int_A (\nabla_s \sigma) dA \tag{2.38}$$

In alkaline water electrolysis, solutal marangoni forces due to gradients of the electrolyte's concentration exist and aid in the bubble's detachment, as this solutal marangoni force is often directed away from the electrode [10][5][7].

The history force (F_H) accounts for the non-stationary effects of the viscous boundary layer that develops around the bubble when its velocity changes over time. As the name suggests, it depends on the history of the bubble's relative motion with respect to the bulk flow (electrolyte flow), given that the possible generated vorticity due to the bubble requires a finite time to diffuse over a distance and therefore the surrounding flow needs time to readapt to the new conditions imposed on it. This force can be important in flows with significant accelerations. The general correlation to calculate the history force in a uniform flow is [25]:

$$\mathbf{F}_H(t) = \mu d \int_0^t K(t-\tau)\left(\frac{\partial U}{\partial \tau} - \frac{\partial V}{\partial \tau}\right) d\tau \tag{2.39}$$

where μ is the dynamic viscosity of the bulk fluid, $K(t-\tau)$ is the kernel, that depends on the diffusion of the vorticity; U is the bulk flow's velocity, V is the bubble's absolute velocity, and τ is a time variable.

For a clean bubble (no surfactants inside of it), the history force is negligible in most cases and therefore can be considered zero: $F_H = 0$ [25].

The differential pressure force (F_P) can also affect a rising bubble's dynamics. This force comes about due to a difference in pressures between the top and bottom of the bubble. This difference in pressure can originate from the fluid (electrolyte) flow or from the bubble's curvature, in which case the difference in pressures in known as "Laplacian pressure".

Finally, in cases where surfactants are present in the electrolyte, the electrostatic repulsion force (F_E) between the charged electrode and the similarly charged bubble interface, may affect the dynamics of the bubble. This is possibly due to surfactants increasing the electrical conductivity of the electrolyte, making the bubble's interface more electrically charged [7].

The most significant forces acting on a singular spherical rising bubble produced during water electrolysis can be seen in Figure 2.2.

Bubble detachment occurs when the sum of the forces aiding in bubble detachment exceed the forces wanting to keep the bubble attached. This applies to both relevant axis in the three dimensional problem, the axis parallel to the electrode and the flow direction, in the case of Figure 2.2 the z axis; and the axis perpendicular to the electrode, the y axis in Figure 2.2 [4][5][7]. Whilst this is applicable to the detachment of single bubbles, for a multitude of bubbles in one same electrode, detachment may be promoted by other mechanisms such as bubble collision or coalescence [18]. Also, for both single bubbles and groups of bubbles on the electrode, the detachment size and detachment time are a function of the hydrodynamic forces, which in turn are a function of the size and shape of a bubble. Therefore, generally, larger bubbles tend to detach earlier than smaller bubbles, as their buoyancy force, which changes with the cube of the bubble radius, acts as the main promoter of said detachment.

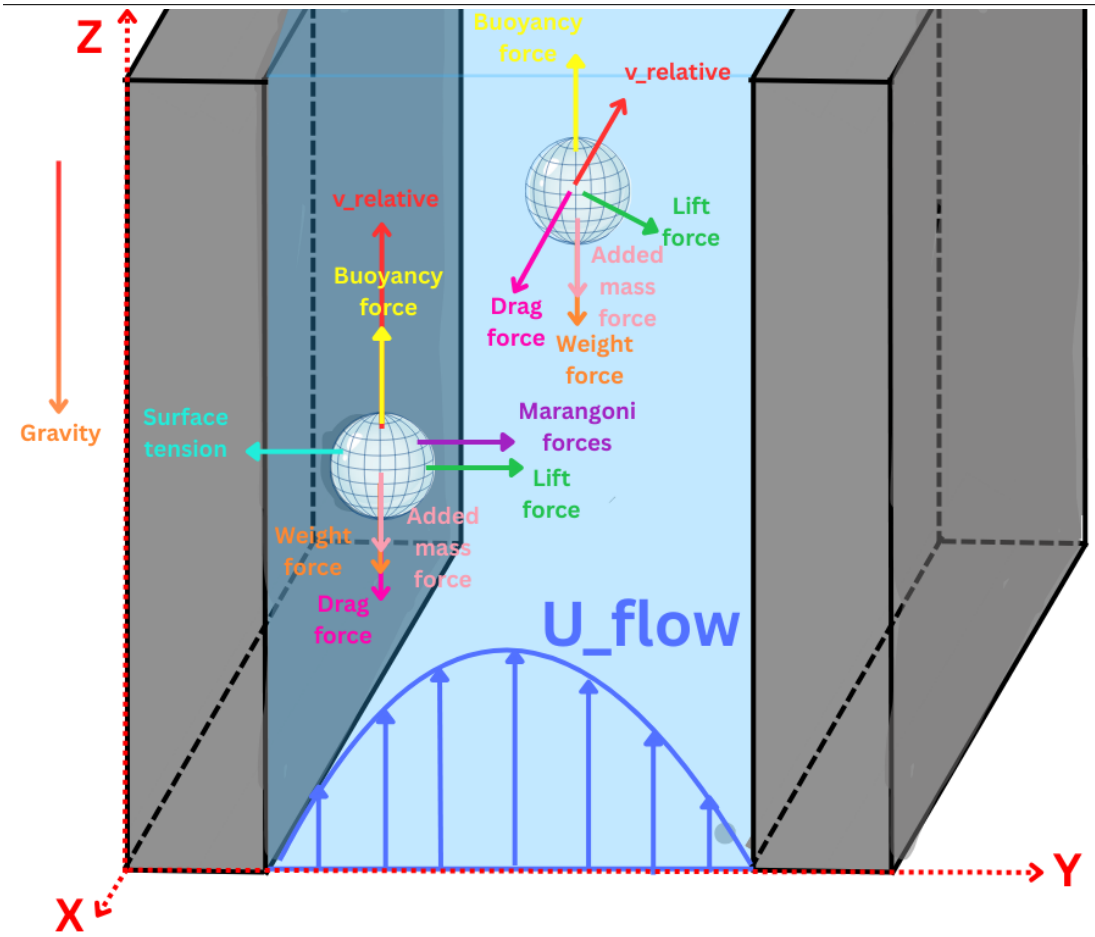

Figure 2.2: Visualization of the main hydrodynamic forces acting on a bubble attached to the electrode and a bubble already detached. Image was created assuming the bubbles to be perfectly spherical throughout the simulation .

This is why in microgravity, bubbles tend to grow to larger sizes and remain attached to the electrode for longer times: an absence of significant buoyancy force is suffered in said microgravity circumstances, making the Lift and Marangoni forces more relevant to bubble detachment [20][23]. Finally, and despite having mentioned the importance of buoyancy in bubble detachment, the importance of Lift force in relation to the bubble's detachment motion perpendicular to the electrode is still somewhat unknown, but may be of great importance.

2.3 Bubble-bubble and multiple bubble collisions

Bubble collisions in electrolysers come hand-in-hand with bubble coalescence.

Bubble collision and coalescence are important to the performance of electrolysers, as both phenomenon have been proven to alter the size and shape distribution of bubbles, altering therefore the physics of bubble detachment from the electrode and dynamics, changing the size and shape of the swarm of bubbles or bubble layer that is produced near the electrode, and therefore modifying the efficiency of the overall electrolysis process.

Two bubbles may collide: bouncing against each other, and end up separating; or their shape and size will be modified due to the collision, until a point is reached when they no longer are capable of continuing independently. In this later case, they end up merging or coalescing into one bigger bubble. This competition between the process of bubbles merging together and bubbles just bouncing off of each other depends on the circumstances of the collision: the velocity with which the bubbles are approaching each other, the type of fluid the bubbles are in, etc.

The coalescence process of gas bubbles in liquids is said to follow three steps [41].

The first step of the process can be described as the approach and film formation: two gas bubbles in a liquid approach each other, squeezing out the liquid in between them. This squeezing produces a thin film in between both bubbles that is typically around 1 to 10 μm. This first stage is governed by the hydrodynamics of the bulk liquid and by the way the bubbles are formed. The second step, is the film thinning step: after the already mentioned thin film is formed between the gas bubbles, this thin film starts to become even thinner as the bubbles are pushed closer together and the liquid in the film drains. This stage is governed by the interplay between the collision forces acting upon the gas bubbles (the forces pushing them closer to each other) and the capillary or surface tension force (trying to keep the gas entrapped in the bubble). The last step, is the film rupture and merging step: once a critical size or thickness of the film is reached, i.e the bubbles are pushed too close to each other, a spontaneous rupture/ break of the thin film of liquid between the gas bubbles occurs. Once this happens, the short range van der Waals pressures become dominant, which lead to the rapid formation of a hole (area where there is no liquid or gas present). Surface tension then expands this hole, resulting in the formation of a bubble as a single entity and combination of both previous colliding bubbles [42].

All three different steps of the coalescence process of gas bubbles in liquid can be seen in figure Figure 2.3. The leftmost rectangle represents the approach and film formation stage, the second rectangle represents the film thinning phase, in which the red cloud in the image represents the liquid film between both bubbles and the red arrows represent the direction of motion of that thin film being squeezed, and the last rectangle represents the merging of both bubbles to form one single entity.

The aforementioned coalescence process is the ideal low Reynolds number case, in which the liquid is pure. However, for gas bubbles in low viscosity liquids, high Reynolds number fluids or non-pure liquids; the competition between the process of coalescence and the bouncing of bubbles before rupture of the thin film is less one-sided, meaning bubbles can collide and bounce against each other without merging together [42].

For gas bubbles in pure liquids for cases with low Weber number ($We = \frac{\rho U_\infty^2 R_b}{\gamma}$), meaning the surface tension force of the bubbles dominate over the inertial forces acting upon the bubble, the inertial forces in the gap between both bubbles are not strong enough to halt the motion of the bubbles before the film rupture, leading to coalescence of bubbles.

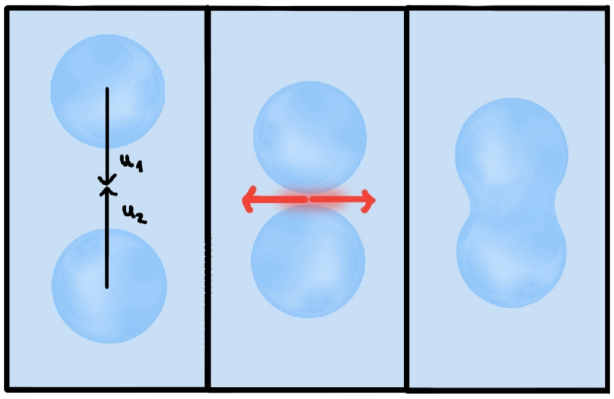

Figure 2.3: Visualization of the three different steps of gas bubble coalescence in liquids.

In the case of low viscosity liquids, the deformation of the bubble interface increases their surface area, leading to an increase in the free energy of the system at the cost of a decrease in the kinetic energy of the bubbles related to their relative motion. As this kinetic energy decreases, the bubbles slow down or decelerate. If they slow down enough and the thin film in between the bubbles has not yet ruptured, then the bubbles will bounce against each other and head in opposite directions.

In the case of non-pure liquids, i.e liquids with electrolytes and surfactants as is the case of the fluid used in electrolysers, the coalescence of bubbles is delayed and/or inhibited [42] [41]. This is believed to be due to several different phenomena such as double layer electrostatic repulsion, Gibbs-Marangoni effect, changes of liquid viscosity, decrease of gas solubility and other surface effects such as a change of the bubble interface surface area.

Pure collision between bubbles is dominated by both hydrodynamic (inertial) forces and nonhydrodynamic short range forces present in non-pure liquids.

For perfectly spherical and non-deformable bubbles, apart from the forces driving the motion of the bubbles such as the buoyancy force, the lubrication force is of utmost importance. This force arises when the separation or gap between bubble surfaces separated by a fluid becomes small relative to the actual size of the bubbles. Once this happens, the fluid separating the bubbles and that lies in between them, is "pushed" by the motion of said bubbles, as already mentioned.

Lubrication can be divided into two different scenarios: scenario a) in which two bubbles have a relative translation along their line of centres (both bubbles move straight towards each other), known as the "squeeze flow problem" ; and scenario b) in which the bubbles move in the plane perpendicular to the motion plane of scenario a), i.e, they flow in a parallel direction to each other; known as the "shear flow problem". Both scenarios share the the fact that the separation between both bubbles $h_0 = \kappa R$ is very small, making the gap distance (h_0) a ratio of the bubbles' radius (R), where the size of this ratio is given by κ; therefore, $\kappa << 1$. For both cases, as $\kappa \to 0$ the force necessary to bring both bubbles to rest diverges. However, the form of divergence for both cases differs: for the shear flow problem, the force

diverges as can be seen in Equation 2.40 , while for the "squeeze flow problem", the force diverges as in Equation 2.41 [43].

$$\mathbf{F}_{sh} \sim \mu R U_{rel} \log \kappa \tag{2.40}$$

$$\mathbf{F}_{sq} \sim \mu R U_{rel} \kappa^{-1} \tag{2.41}$$

where μ is the dynamic viscosity of the fluid the bubbles are surrounded in, R is the radius of the bubble and U_{rel} is the relative velocity of the bubble with respect to the fluid flow, and κ represents the gap in between both bubble's surfaces.

Having said this, the order of magnitude of the squeeze flow problem force is much larger than that of the shear flow problem: assuming one bubble is at rest and the other is in motion and both have the same radius, for a separation of 1% of the radius, i.e $h_0 = 0.01R$, the ratio between squeeze flow force and shear flow force is $F_{sq}/F_{sh} \approx 50$. Thus, in some cases, the force attributed to the shear flow problem, F_{sh}, is neglected when calculating the collision force between bubbles.

For the squeeze flow problem, the physical principle behind it is that pressure in the gap becomes very large in a small area closest to each of the bubbles; and although this area is very small, it is not small enough for the forces acting upon the bubbles to not diverge. This force, known as the lubrication force, can be calculated using three basic arguments.

Firstly, assuming the spheres to be perfectly round and the flow to be axisymmetric, given that the bubbles are moving straight towards each other with their centres of mass in one same line, thus using cylindrical coordinates, the bubbles' surfaces can then be approximated by paraboloids (for small distances from the axis of symmetry, i.e the axis where both centres of mass lie):

$$h(r) \approx h_0 + \frac{r^2}{2}\left(\frac{1}{R_1} + \frac{1}{R_2}\right) = h_0\left(1 + \frac{r^2}{2R_{red}h_0}\right) \tag{2.42}$$

where h_0 is the minimum distance between bubble interfaces, r is the distance from the axis of symmetry, and $R_{red} = R_1R_2/(R_1 + R_2)$ is the reduced radius.

Secondly, the velocity profile of the fluid in between both bubbles (given by u and w in their respective axis) can be calculated by considering the lubrication theory. Lubrication theory states that when the gap between bubbles is very small ($\kappa << 1$ as stated previously), the axial z-velocity scale is much smaller than the radial r-velocity scale, as defined in figure 4.7 of "A physical introduction to suspension dynamics" [43]. This can be proved from the continuity equation:

$$\frac{1}{r}\frac{\partial(ru)}{\partial r} + \frac{\partial w}{\partial z} = 0 \tag{2.43}$$

where u is the velocity in the r-axis and w the velocity in the z-axis.

As the scale of the velocity in the z-axis is W, then for the continuity equation to be obeyed, the scale of the velocity in the r-axis must be of the same order of magnitude and therefore: $U >> W$. This means that the fluid flow can be considered unidirectional, confirming that the fluid is pushed out of the gap between the bubbles in the radial direction.

Using the same difference in scales between both r and z directions, the Laplacian of the flow velocity ($\nabla^2\mathbf{u}$) in the r-component of the Navier Stokes Momentum Equation (NS) can be reduced to $\mu\frac{\partial^2 u}{\partial z^2}$ (as $\frac{\partial^2 \mathbf{u}}{\partial z^2} >> \frac{\partial^2 \mathbf{u}}{\partial r^2}$). Thus, the r-component of the NS equation can be defined as:

$$-\frac{\partial p}{\partial r} + \mu\frac{\partial^2 u}{\partial z^2} = 0 \tag{2.44}$$

And assuming that the order of magnitude is smaller than the order of magnitude W, Equation 2.44 reduces even further to:

$$\mu\frac{\partial^2 u}{\partial z^2} = 0 \tag{2.45}$$

from which the no-slip boundary condition at the bubble interfaces can be taken: $u = 0$.

Using the same pressure order of magnitude rule in the z-component of the NS Momentum equation, it can be seen that $\frac{\partial p}{\partial z} \gg U$. Therefore, $\frac{\partial p}{\partial z} = 0$, meaning that the pressure is constant across the gap and is a function of the radial position $p = p(r)$.

With all of this knowledge, including the no-slip BC, solving Equation 2.44, yields the velocity profile of the unidirectional fluid flow in the gap between the bubbles, as a parabolic profile:

$$\mathbf{u}(r, z) = \frac{1}{2\mu}\frac{dp}{dr}\left[z - z_1(r)\right]\left[z - z_2(r)\right] \tag{2.46}$$

Third, as the fluid being squeezed out of the gap has to obey the conservation of mass, meaning that the flux of fluid being squeezed out of the gap over any radius must be equal to the volume of fluid displaced by the bubbles, the pressure gradient is obtained. Integrating this pressure gradient with respect to r and applying the zero-pressure BC at infinity, yields the pressure field:

$$\mathbf{p}(r) = \frac{3\mu W/R}{\kappa^2 \left(1 + \frac{r^2}{2R^2\kappa}\right)^2} \tag{2.47}$$

Finally, the lubrication force can then be obtained by integrating the pressure field (shown in Equation 2.47) over the surface of either bubble:

$$F_l = \int_{r=0}^{r\to\inf} p(r) 2\pi r dr = 6\pi R^2 W/h_0 = 6\pi R W/\kappa \tag{2.48}$$

From which it can be seen that the lubrication force is inversely proportional to the size of the gap between both bubbles, and therefore diverges as the bubbles get closer to each other at a fixed relative velocity.

In the case of non-pure liquids, as already mentioned, electrostatic - nonhydrodynamic repulsive forces aid with bubble bouncing and delay or inhibit the coalescence process.

As already mentioned, these forces arise from the microscopic nature of the liquid and the possible charged particles in it. Due to the presence of ionic salts or surfactants in the liquid, the bubble interface, i.e the bubble's external surface, can "stack up" on electrically charged particles thus leading to nonhydrodynamic repulsive forces in the form of electrostatic repulsion between bubble interfaces. The exact reason for this electrostatic repulsion is not well known, however it is believed to be due to the creation of a hydration layer on the bubble interface [3], modification of the Debye screening length in the diffuse double layer near the interface, the steric interaction between surfactants on bubble interfaces or the polarization of the bubble's interface by surfactants [44].

In order to prevent coalescence by stopping the bubbles' motion before coming into close contact with one another, it is believed that the repulsive pressures acting upon the bubble interface, i.e the repulsive force per unit area of bubble interface, must be larger than $2\gamma/a$, where γ is the surface tension of the bubble interface and a is the bubble's radius [44]. This minimum pressure accounts for the change in curvature of the bubble surface in the case that the bubble surface is modified due to the collision.

In some papers, this nonhydrodynamic short range repulsive force is obtained by combining a series of equations for the fluid flow near the bubbles, the boundary conditions at the different parts of the bubble interface (such as the inner and outer region)[4] and a form on Newton's second law. By doing so, one can obtain the following equation:

$$-g_1(0)\rho\frac{4\pi a^3}{3}\frac{dU}{dt} = -A(t)\frac{2\gamma}{a} \tag{2.49}$$

[3] a hydration layer is a layer of water molecules strongly associated or related with large cations that is stuck to or adsorbed to something, in this case the bubble interface

[4] to see the definition of the inner and outer region of the bubble interface, as well as the equations for the fluid flow and the boundary conditions, please refer to reference [44]

Where ρ is the density of the surrounding fluid, a is the radius of the bubble, $\frac{dU}{dt}$ is the rate of change of the bubble's velocity in time, that is, the bubble's acceleration; γ is the surface tension of the bubble interface; and $A(t) = \pi(a\alpha)^2$ is the area of the inner region of the bubble, which is a function of its radius and the radial extent[5] α.

This equation, Equation 2.49, states that although the bubbles' mass inside of it is negligible, the bubbles act as if they do in fact possess an added mass of coefficient $g_1(0)$ and volume $\frac{4\pi a^3}{3}$; and that these bubbles decelerate due to a short range nonhydrodynamic force that equals the area of the inner region of a bubble (region of the bubble interface affected by the collision) times the surface tension of said interface. This means that as the bubbles come closer to each other, the area of the inner region of the bubble becomes larger and therefore the force becomes larger. In other words, the nonhydrodynamic repulsive force is inversely proportional to the distance between bubbles, as is the case of other forces seen in nature such as the lubrication force, electrostatic forces, Van der Waals forces, Lennard-Jones potential force, etc

2.4 Numerical methods and simulations

This section will delve into the numerical methods and simulation techniques relevant to the study of the flow of bubbles in water electrolysis. Special focus will be placed on the generation of realistic statistical distributions of bubbles on a wall, the assessment of hydrodynamic forces on said bubbles, and collisions between perfectly spherical and non-deformable bubbles; which align with the main objectives of the thesis. As mentioned in chapter 1, numerical methods already exist, however they present various flaws and challenges. In this chapter, relevant numerical methods and simulation approaches are stated.

2.4.1 Methods for Generating Statistical Distributions of Bubbles on a Wall

Generating a realistic statistical distribution of bubbles on an electrode surface requires knowledge of already existing and used numerical modelling approaches , and the validation of said approaches by means of comparison with experimental observations.

Experimental Observations of Bubble Nucleation and Distributions

Experimental studies provide relevant information into what really happens during nucleation, growth and detachment of bubbles during electrolysis. Most of these studies use real-time visualization techniques, such as high-speed photography; or parameter control methods, such as micro-engineering the electrodes to be studied [4][10][18].

[5] the radial extent α is the angle between the centre of symmetry of the bubble interface and the outermost point of contact between both colliding bubbles. For further understanding, please refer to FIG 4. of [44]

High-speed photography allows for the observation of the bubble's evolution whilst attached to the electrode, contributing information to the nucleation site density and bubble detachment size and time [9][18]. Studies using this, or similar experimental techniques, have found that the size distribution of detached bubbles is influenced by current density across the electrolyser, electrolyte concentration and electrode material [9]. Some studies even suggest that the bubble size distribution near the electrode surface is bimodal initially, and then evolves into a log-normal distribution at higher current densities [18].

Micro-engineering the electrode surface enables studies to control the nucleation and growth sites of bubbles. By doing so, conclusions on bubble nucleation and growth and their dependency on surface topology can be drawn: superhydrophobic locations and micromachined pillars have a higher probability of becoming a nucleation site [12].

The aforementioned experimental findings are crucial to be able to validate numerical models whose aim it is to re-create a realistic generation of bubble distributions.

Numerical Approaches to Model Bubble Nucleation

As for the numerical methods to re-create the already mentioned experimental findings, most of them focus on heterogeneous nucleation from pre-existing nucleation sites, as it is a more practical approach than homogeneous nucleation modelling for macroscopic bubbly flow simulations [19]. This is because homogeneous nucleation is an often stochastic process in nature that is relevant at the nanoscopic scale, making the direct simulation of said bubble generation from a supersaturated solution a complex task [16][20][21].

To model the presence of stochastic variations that determine preferential nucleation sites, such as the existence of surface defects, cavities, or variations in wettability , numerical models simply define specific locations on the electrode surface where bubbles are "allowed" to nucleate [20].

Diffuse interface models set a basis to study the thermodynamics of phase change (such as heterogeneous nucleation at solid surfaces) by considering the free energy of the solid-fluid interaction and its influence on wetting properties. Although computationally demanding, diffuse interface models contribute extensive insight into bubble nucleation.

Generating Statistical Distributions of Bubbles

To generate realistic statistical distributions of bubbles on a vertical wall for a large number of bubbles, different methods can be used:

- Empirical, experimental-data based models are one way of creating realistic statistical bubble distributions. Both the nucleation site distribution and initial bubble size distributions can be obtained from observing and studying experimental data under relevant experimental conditions [9][18]. These distributions can then be used to stochastically generate bubbles on a flat surface, to then use in numerical simulations. One of the main advantages of this method is that it allows for tighter control of

parameters that influence the nucleation rate and other characteristics of the generated bubbles; as well as already including the validation of the method in its nature, as it is built from experimental data. The main drawback however is that the replication of the experimental data needs to very accurate, as it allows small margins of error, outside of which the methods would be termed "unrealistic".

- Probabilistic models, such as Poisson processes, are another method that can be employed to simulate the random activation of nucleation sites over time and space, as this process is also random in nature as mentioned previously. Additionally, the rate at which bubbles nucleate on the surface can be a function of local conditions at the electrode surface, such as supersaturation concentration [16]. A combination with empirical experimental-data based models can be done to predict initial bubble size distributions.

- Agent-Based Modelling, uses the concept of treating each nucleation site as an "agent" with specific bubble activation and generation rules that incorporate the randomness and dependency on local environmental factors that influence bubble nucleation. This method however seems more computationally demanding, as a set of rules for each nucleation site is needed, which in the case of simulations for high number density of bubbles can be extreme.

Applying said methods, a minimal code to statistically generate a realistic distribution of bubbles on a surface can be done following the steps below:

1. Define the geometry of the surface where the bubbles are going to be generated, which in the case of water electrolysis would be on an electrode.

2. Use either one of the methods previously described or experimental data to establish the number density of nucleation sites on the defined geometry.

3. Stochastically distribute the nucleation sites determined in the previous step.

4. Assign an activation time and initial bubble size to each of the distributed nucleation sites based on an empirical distribution or a simplified model.

Worth mentioning, is that in order to continuously generate nucleation sites and bubbles, after say an already grown bubble has detached, a simple way of doing so would to repeat the aforementioned process, starting from the second step, but for a singular nucleation site instead of a distribution. This process would have to be iterated as bubbles detach from the electrode. Nonetheless, this method would not consider how nucleation site distribution is based on variables such as the existence of hydrophobic sites and energy landscapes. So, once the nucleation sites are initially distributed, it means that the probability of a bubble nucleating in those distributed nucleation sites is higher than for other random locations on the surface. This fact would be violated by just continuously assigning random nucleation sites.

2.4.2 Numerical modelling of bubble hydrodynamics

Accurately resolving the hydrodynamic forces of bubbles at a microscopic length scale can be done using several different methods, each of them having their advantages and disadvantages.

Direct Numerical Simulation (DNS) aims to accurately resolve all relevant scales of the hydrodynamic and concentration boundary layers around growing and detached bubbles [10]. This method can capture the detailed flow field around the bubble and accurately model the interfacial forces by resolving/calculating the governing equations: Navier-Stokes equations, species transport equations and potential equation; for each bubble. DNS is a deterministic method, since it is able to predict the evolution of a bubble based on physical laws given initial conditions. However, DNS is extremely computationally demanding for high volume fraction of bubbles, since it requires the physical equations that govern a bubble's evolution to be resolved for each bubble iteratively at each time step as well as for the flow around the bubbles, considering the previous time steps for the calculations [22]. Having said this, DNS has proven to be useful to obtain accurate results in simulations. Examples of this are simulations such as that of a singular hydrogen bubble attached to a vertical cathode, using an immersed boundary method within a DNS framework, to study the effects of flow rate, pressure and velocity boundary conditions [10]; and the simulation of bubble formation and detachment from a horizontal electrode in which the bubble's size and trajectory were tracked throughout the simulation [5].

Interface-Resolved Simulations, which are related to DNS, focus on accurately capturing the gas-liquid interface of the bubble and its evolution over time [5] apart from resolving over the whole domain (including the electrolyte flow). Techniques like the immersed boundary method or body-fitted grids are used to track the bubble shape and movement in response to the hydrodynamic forces acting upon it [10]. These simulations can model the growth due to diffusion of dissolved gas and the detachment of bubbles [5]. As mentioned, Interface-Resolved simulation is very similar to DNS. In fact, DNS is a type of highly resolved (high resolution) interface-resolved simulation.

Point-particle methods are more suitable for simulating larger systems with many bubbles. This method simplifies bubbles to be points in the domain and models the hydrodynamic forces acting upon the bubbles (or points) using closure laws, i.e. simplified extra equations such as boundary conditions, or models, needed to be able to solve the system of equations that makes up the problem. Simplified, less accurate models are needed initially as a first approximation, to then as the simulation progresses, be able to make the problem more complex [17]. For example, simple expressions for buoyancy and surface tension forces are initially used, but as the bubbles grow and the flow field develops, more complex drag and lift force models are incorporated.

Deterministic models based on predefined nucleation sites incorporate the already mentioned concept of specific nucleation sites on the electrode surface. Bubble generation and evolution using these models can be deterministic, despite the randomness or statistical determination of the initial location sites. The simplified model described in [17] explores a

more controlled environment, rather than a statistical one, in which bubbles are generated at random points on the electrode, whilst also having a predefined grid of nucleation points on said electrode. This makes the model somewhat resemble nature, as the bubble nucleation process is stochastic, while having locations on the electrode where it is more likely for bubbles to nucleate. Meanwhile, [12] studies the evolution of a single bubble on a predefined, micro-engineered electrode, hinting at the possibility of using numerical methods to simulate bubble behaviour from said chosen nucleation site.

In early studies, such as Dukovic and Tobias' (1987) study on the influence of attached bubbles on the potential drop and current distribution at gas-evolving electrodes [45], an axisymmetric model was used to simplify the simulation of the growth of a bubble attached to an electrode in a stationary flow. Despite being limited by the axisymmetric assumption, these models are capable of providing a deterministic way to study the influence of a single bubble on its surrounding environment.

Molecular Dynamics (MD) Simulations can be used in the case of micro or nanobubbles simulations. This simulation method, as the name suggests, is normally used in molecule simulations as it is capable of delivering deterministic results based on intermolecular forces and the state/circumstances of the environment. Therefore, MD can be used to simulate the initial stages of bubble formation, as at this stage the problem consists of very small length and time scales.

Fast Interface Particle Interaction (FIPI) is a numerical method used to describe and simulate problems involving suspended particles in binary fluids (gas-liquid for example) and interacting liquid interfaces of complex morphology. One of the main objectives of FIPI is to be able to simulate systems with large number of particles interacting with fluid interfaces, without the need of state-of-the-art computer hardware such as supercomputers. It is intended for investigating phenomena like particle adsorption/desorption and particle-induced surface tension modification in multiphase systems such as froth flotation and drop/foam stabilisation [46]. FIPI resolves interfacial structures and hydrodynamics on length scales much larger than the particle size and solves particle-level physics using empirical or semi-analytical expressions, which help ease the computational load. As for the fluid-particle coupling, it uses a Euler-Lagrangian method: the fluid in question is treated on a grid (Eulerian) and individual particles are tracked (Lagrangian). Also, FIPI uses a diffuse-interface method, meaning the interface (layer between fluids) has a non-zero thickness and therefore is "diffused". This allows for easier resolve of interface breakup and coalescence. The phase field variable[6] in this method provides information about the local distance of a particle to the fluid interface,

[6]Phase field variable references the partial differential equation that describes the interface and can take values between two distinct integer values (for example 0 and 1). In the case of 0 and 1 values, a 0 value is set to one of the phases (A), and 1 is set to the other phase (B). For the interface, a value between 0 and 1 will be given depending on a specific pre-set definition of the phase-field variable, such as the volume fraction of one of the phases, the distance to one of the phases, etc. Therefore, in the example using 0 and 1, if the phase variable were to be defined as the volume fraction of phase (A), a value of 0.5 on a location of the interface would mean that at that location the volume fraction of the interface is half of phase (A) and half of the other phase (B). A value of 0.7 would mean there is more of the phase(B) than of the phase (A).

which can be used to calculate capillary forces. The way FIPI applies said methods, is by being divided into three different modules: an interface module that provides the location of the interface; a tracking module that tracks the particles and provides a force term to the fluid module; and a fluid module that solves the momentum equation on the fluid domain and provides the fluid velocity field to the other two modules. FIPI shares one common limitation with point-particle methods: using the drag force definition given in the FIPI code, prescribing the unperturbed fluid velocity at the particle position when calculating the drag force is challenging. Having said all of this, FIPI presents major potential for gas bubble simulations in water electrolysis, as said bubbles can be treated as the "particles" interacting with the interface mentioned in [46].

It is worth mentioning that the mentioned numerical methods and simulation methods aim to be deterministic despite including stochastic elements such as the location and timing of bubble nucleation on the electrode. Whilst having stochastic elements, these methods are based on actual physical laws and defined conditions, and therefore can provide a deterministic way of simulating bubble evolution in water electrolysis.

Chapter 3

Results and discussion

This section will be divided into three different subsections, each one presenting and discussing the main results obtained during the completion of this project.

3.1 An algorithm for bubble generation

To model the formation of a bubble on the electrode, an algorithm was created to generate the distribution of bubbles on a flat electrode that can recreate that of real life.

First of all, as already mentioned in the literature review, there are two types of bubble formation or nucleation, however, in this project only heterogeneous nucleation, i.e when bubbles form on the electrode, was modelled.

The main objective of this algorithm was to be able to generate a realistic distribution of large number of bubbles on an electrode, to then be used in further Point Particle simulations, for the reasons already mentioned.

The algorithm can be explained using a flowchart (Figure 3.8) where red rectangles are the starting point and ending point of the algorithm, blue rhomboids represent input and output, amber squares are processes and green diamonds are bifurcations or conditions, where the algorithm can go either one way or another.

To start the algorithm, a number of dimensions (either 2D or 3D) must be specified, as well as the number of bubbles to be generated. The dimensions refer to the coordinates of each bubble, therefore by making it 3D, each bubble will have x , y and z coordinates, whilst a 2D case will only have two of those, representing for example the coordinates of a bubble on a specific plane. The number of bubbles to be generated can be either explicitly or implicitly determined: the code can be modified to generate the exact of bubbles wanted, or it can be modified so that a number or volume fraction within the simulation domain (2D and 3D cases, respectively) is achieved.

At the same time, the user must also input the maximum number of attempts desired.

The maximum number of attempts refers to the number of times the algorithm/computer is allowed to try to generate the random coordinates of the bubbles. As it is possible that whilst generating random coordinates for different bubbles, these are the same; once this happens, the algorithm detects it and generates random coordinates again whilst using up an additional attempt. This maximum number of attempts will therefore determine the accuracy of the algorithm.

The algorithm can be modified to change the minimum distance the bubbles should have between them whilst being generated. The user is capable of making said distance larger or smaller, to their own convenience. Having said this, for a limited domain size and specified number of bubbles to be generated, having a higher minimum distance between bubbles will render a higher chance of overlap between them and therefore less accuracy of the algorithm and a higher computational demand and run time.

Similarly, the size of the bubbles to be generated has to be specified before the algorithm can continue, as well as the domain size (which refers to the size of the electrode in the case that bubbles are to be generated on an electrode), and the type of bubble distribution wanted, which can be either monodisperse (meaning all generated bubbles have the same size) or polydisperse (the size of the generated bubbles is varied). In the monodisperse case, as the size of all of the bubbles is the same, the inputted size is a singular variable. However, in the polydisperse case, a range of sizes must be inputted instead. This range of sizes follows a log-normal distribution, which follows and adheres to results taken from experimental studies of the size of bubbles forming on electrodes during water electrolysis.

Sequentially, once all of the aforementioned data is inputted into the algorithm, the algorithm creates the necessary data structures to continue. The most important one is the array of dimensions and number of bubbles, which is the final output of the algorithm. Initialised as an array of zeros with the shape $[m \times n]$ where m is the number of dimensions and n is the number of bubbles to be generated, this array stores the coordinates of each and everyone of the generated bubbles.

Once the array of coordinates is initialised, the algorithm enters an iterative loop that runs as many times as there are bubbles to be generated, and each iteration accounts for one of the generated bubbles. That means that if there are , for example, 5 bubbles to be generated, the iterative loop will have 5 iterations, each iteration corresponding to one of the bubbles. This iterative loop makes sure that all bubbles are assigned coordinates, as the loop does not pass from one iteration to the next unless the current iteration bubble's coordinates are valid.

Valid coordinates are those that make the current iteration's generated bubble not overlap with any previously generated bubbles.

For each iteration, the first thing to be done is to assign the bubble its fixed coordinate, in the case that the bubbles are to be generated on the electrode. In this project, the fixed coordinate is y, as by doing so, the bubble will be generated on the electrode (as can be seen in Figure 2.2. For the case where bubbles are to be randomly generated in a domain where

they are not bound to anything, then this step can be skipped.

Subsequently, the non-fixed coordinates are randomly generated. Because this project was undertaken using MATLAB and python, as these include random number generation algorithms already in them, a random number generator algorithm was not additionally created. In the case that this algorithm is used in a software that does not include random number generators in them, or any third parties that can be included, then creating a random number generator is of course needed for the completion of the bubble generation algorithm.

Once the coordinates for all dimensions have been assigned to the bubble, before making them final, the algorithm proceeds to check for overlaps. What this means, is that the algorithm will compare the coordinates of the bubble that is currently trying to be generated with all other already generated bubbles. For the algorithm to consider a bubble overlap, all coordinates must coincide: in the case of 2D, both dimensions' coordinates must coincide; whilst in 3D all three dimensions' coordinates must coincide.

Worth mentioning is the fact that because this algorithm was created for its intended use in a Point Particle simulation, as each bubble is considered a point in space, the overlap between bubbles is defined as coordinates being the same. In the case that this algorithm is wished to be used in a different type of simulation where bubbles are not considered points in space, but rather entities that take more than one point in space, then the overlap between bubbles can be configured to be triggered if parts of the bubble interface are in overlap. That means that for example, the overlap can be if coordinates fall in a range centred around the coordinate of the bubble's centre of mass, and limited by a distance equal to the bubble's radius.

The check for overlaps is the first instance where the algorithm can take either one route or another. If there is no overlap, the algorithm will confirm the bubbles coordinates and said coordinates will not be changed anymore. However, if there is overlap, then the algorithm proceeds to check if the maximum number of attempts to place the bubble, i.e to generate the bubble's coordinates, has been reached.

When checking the maximum number of attempts, the algorithm encounters the second instance in which it can continue through different paths. If the maximum number of attempts to place the bubble has not been reached, then the algorithm goes back to the stage in which the non-fixed coordinates of the bubbles are generated, to try once more. Because the algorithm has already "used up" one attempt to place the bubble, but has failed, the number of attempts left is reduced by one and thus the number of attempts gets closer to that maximum number of attempts limit.

On the other hand, if when the algorithm reaches this second instance where it can take different routes, and the maximum number of attempts has been reached, it will proceed to generate a fallback position.

The fallback position is the last resort at placing a bubble. This method of placing a bubble steps away from the randomness to ensure that the bubble will be generated without

overlap. Given that at this point, the algorithm has failed to place the bubble randomly, a "fallback" position is created and assigned to the bubble in this loop iteration, that does not necessarily comply with other placement rules set beforehand (such as minimum distance between bubbles if previously stated). The basic concept of this fallback position is that it is the optimal position/space based on the other bubbles already placed. The way the algorithm finds this optimal position is by doing an " overlap avoidance search", meaning that the algorithm checks all spaces in the domain and decides the best spot to place the bubble based on where there is more "breathing room", i.e where there is more free space available. To compute this, the algorithm compares the minimum distance between all bubbles, and where this minimum distance is largest, is where there is most space available. This is implemented to ensure placement without overlap.

This check for minimum distance can be done in different ways. For this project, the way this was achieved was by dividing the simulation domain into a grid/mesh-like pattern and for each subdivision of the mesh/grid, checking for the distance between bubbles and those subdivisions.

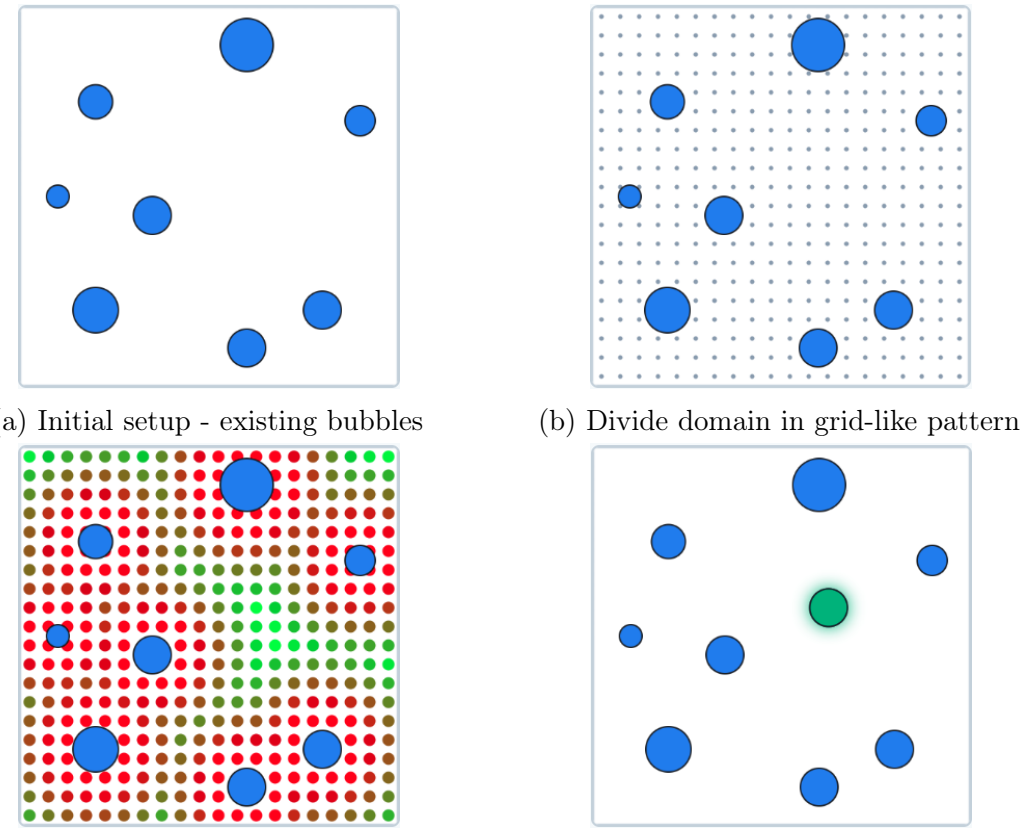

(a) Initial setup - existing bubbles

(b) Divide domain in grid-like pattern

(c) Grid search: calculate minimum distances

(d) Place bubble in optimal position

Figure 3.1: Visualisation of the fallback position process.

Once the bubble has been placed/generated, either by random coordinates generation whilst the maximum number of attempts still has not been surpassed, or by using the fallback

position as a plan B, the last check is made to see through which path the algorithm will continue. In this last check, the algorithm verifies if all bubbles have been assigned a position.

If they have not, the algorithm will go back to the iterative process's first stage and update the iteration number it is on (it will step into the next iteration) to make sure that the bubble it placed instances earlier will not have its coordinates changed, but rather the following bubble will.

On the other hand, if all bubbles have been assigned valid coordinates, i.e the iterative process has gone through all iterations and has been completed, then the algorithm will output the updated and corrected version of the inputted array with all the bubble's coordinates, marking the end of the algorithm.

3.1.1 Results and discussion

Here is where the results related to the formation of bubbles algorithm are presented and discussed.

The first thing to mention is the fact that the generated bubbles' sizes do follow a log-normal distribution as expected. This complies with data obtained from experimental studies on bubble formation on electrodes during water electrolysis.

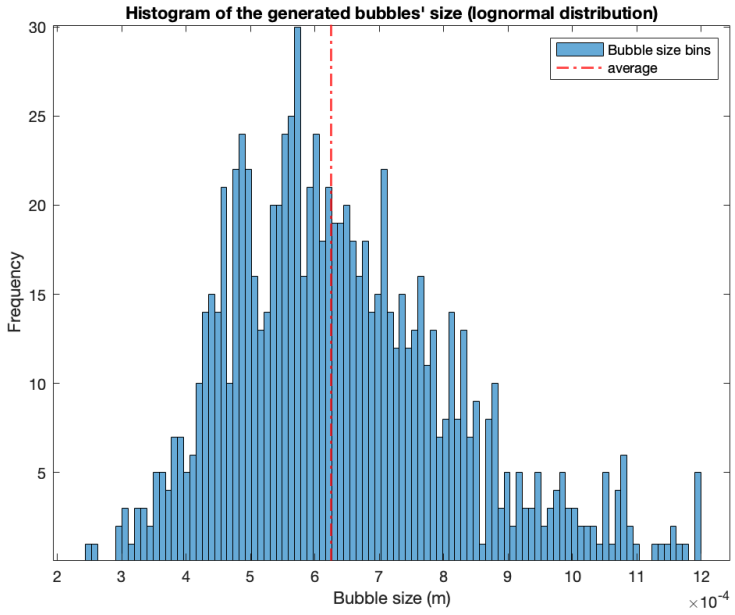

Figure 3.2: Log-normal bubble size distribution of the generated bubbles using the proposed algorithm.

Secondly, the proposed algorithm allows for reproducibility: for the same initial conditions (already mentioned in section 3.1), the results will remain roughly similar. That means that the number of bubbles for given volume fractions, bubble sizes and domain sizes; the

runtime and the shape of the size distribution will remain very similar throughout different simulations. The slight differ in results is because of the small "randomness" inputted into the system (for example, the log-normal distribution of sizes will not always be exactly the same due to its nature and therefore neither will the exact number of bubbles).

One of the observations made during the testing of this algorithm, was that by using a sorting strategy when trying to position the already randomised bubbles instead of placing them in a random order, increased the packing efficiency. Specifically, by sorting bubbles by size in a large-first order, the best packing efficiency is obtained. This means that for the same domain size and same number of bubbles in the same size range, by using this "large-first" sorting strategy, bubbles will be "fit" into the domain in a more efficient way, wasting less space and reducing the number of placement failures, making the algorithm faster. This is because larger bubbles are harder to place as they need more space and have fewer valid positions available. Placing smaller bubbles first reduces the empty space available for the larger bubbles, occupying possible valid positions for the larger bubbles. Also, there is a higher probability of placing correctly a small bubble than a large bubble, as their size allows them to more easily "fill in" gaps. This can be compared to packing luggage when travelling: larger clothes such as hoodies and long trousers should be packed first and smaller pieces such as socks and toiletries last, so that if at some point during the packing the available space does not seem like enough, the socks and toiletries ca be placed in between the larger pieces.

Also, the algorithm can be sped up by "tweaking" a bit the way the random coordinates are assigned. For example, instead of creating all coordinates randomly once per attempt to place the bubble, a multitude of coordinates can be randomly created in a parallel way in each attempt, and then a comparison to find the best position out of those in this attempt can be made. It is as if when trying to find a specific coloured bead in a bag of coloured beads, instead of picking one bead out every time and checking whether the picked bead is the colour you want, you pick out a bunch of beads at the same time, lets say ten beads, and try to find the colour you want out of that small batch. As the picking a bead out of the bag has a fixed cost (in the case of the bubble generation algorithm, each random generation of coordinates has a cost), the probability of finding a bead of the colour you want is the same in both instances, however, finding the coloured bead will be less demanding as you decrease the total cost of picking out beads if you do it by batches.

The function to generate a fallback position is one of the most computationally demanding processes of the algorithm, as it has to compare distances between all bubbles and the distance between the grid test positions and all the bubbles. However, it is a safe way of placing a bubble, which is why it is used as a last resort or safety net in order to place a bubble. Another positive characteristic about this process is that the accuracy of an optimal position determination and the computational cost can be modified or change according to what is wanted or needed: when using a systematic grid search, both the accuracy and cost depend on the amount of grid points. Having more grid points leads to higher accuracy and higher computational cost, whilst less grid points leads to less accuracy and cost. This can be seen in Figure 3.3a, as the higher number of elements in the grid size, the longer the runtime. Therefore, this process is flexible in the sense that it can be modified depending on what is

really needed. Furthermore, this process can be modified further, to provide an optimum for both accuracy and cost, by using an adaptive strategy: start off with a coarse grid search to determine the optimal location based on that, and once the optimal location of the coarse grid is established, then refine the search around it by making the grid finer just around that location. This will ensure higher accuracy than just using a coarse grid search, and a faster run time, i.e less computational demand, than using a fine grid search from the start.

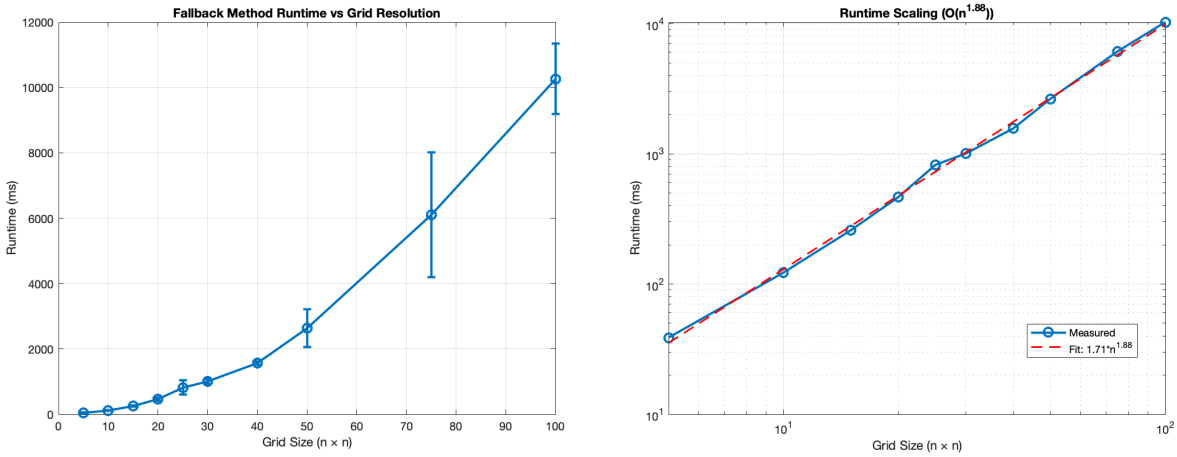

(a) Fallback method runtime as a function of the grid size used.

(b) Fallback method runtime scaling: power law fit.

Figure 3.3: Fallback method performance.

The runtime scaling of the fallback process as a function of the grid size can be approximated by a power law: $t_{run} = C_1 n^{C_2}$, where C_1 and C_2 are constants obtained from fitting an exponential curve to the data points. This fit can be seen in Figure 3.3b with $C_1 = 1.71$ and $C_2 = 1.88$.

Additionally, this algorithm is suitable for multiple different 2D and 3D scenarios, not just for the generation of bubbles on an electrode. By simply changing a bit the algorithm so that instead of having one fixed coordinate, the bubbles have no fixed coordinates and therefore all of the coordinates are randomly generated, distributions of bubbles in space can be generated. For the visualisation of the generated bubbles, this algorithm can be combined or used in different software. Two examples of visualisation are given, one in which ten thousand (10000) bubbles are generated on a vertical planar electrode, and another in which nine hundred (900) bubbles are generated in a three dimensional arrangement around one fixed bubble. The ten thousand bubbles example was created by generating a LAMMPS file with the results of the algorithm and plugging said file into VMD; whilst the nine hundred bubbles example was done using matlab's 3D visualisation tools:

Note: any visual overlaps in either Figure 3.4 or Figure 3.5 are due to either errors in the visualisation software, or due to the camera angle of the image. In reality, there are no

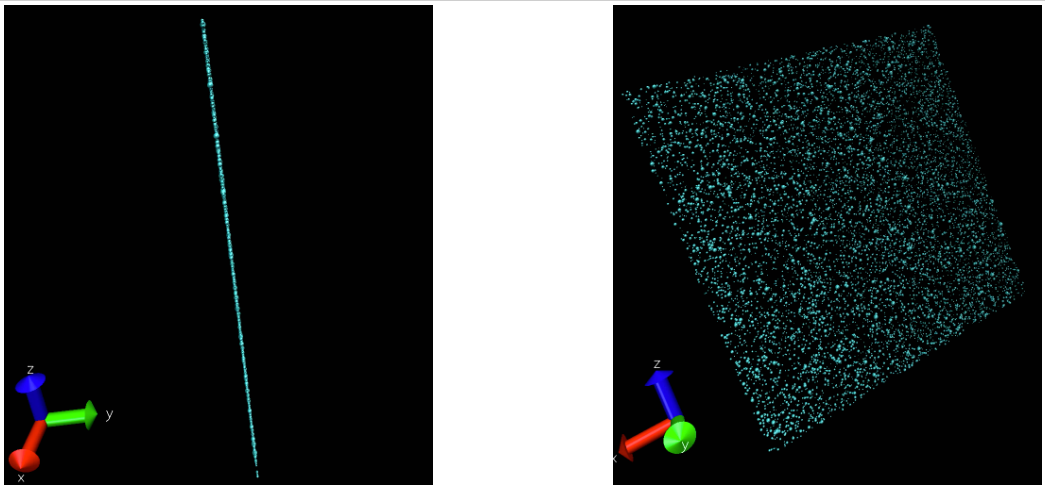

(a) Side view of 10000 bubbles generated. (b) Diagonal view of 10000 bubbles generated.

Figure 3.4: Visualisation of algorithm used to generate 10000 bubbles on a planar vertical electrode using LAMMPS trajectory file in VMD.

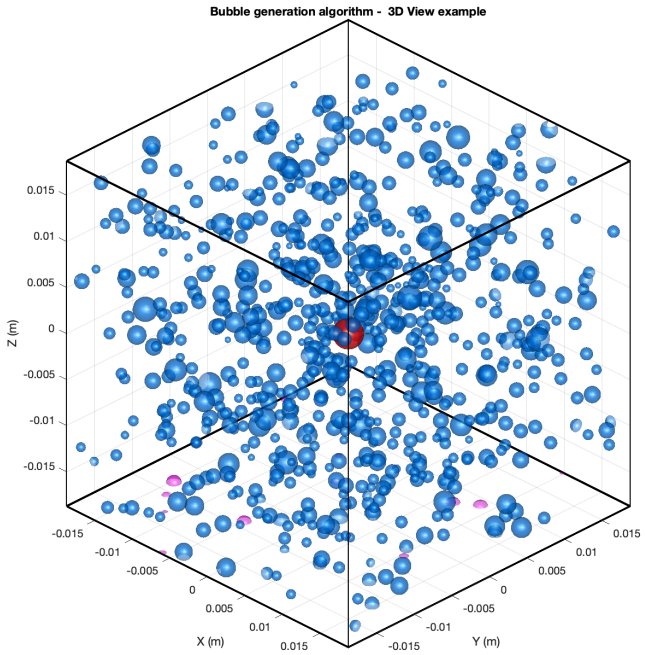

Figure 3.5: 3D visualisation of algorithm for generated bubbles around a fixed bubble.

bubble overlaps in either of the examples.

Finally, this algorithm presents differences in performance between monodisperse and polydisperse distributions of bubbles. Generally, for monodisperse distributions of bubbles,

the algorithm is faster, making it possible to generate a higher number of bubbles in a shorter period of time. Also, for the monodisperse distribution of bubbles, the algorithm is capable of exactly reproducing a space/volume fraction of bubbles when given a desired value of space/volume fraction, as seen in Figure 3.6.

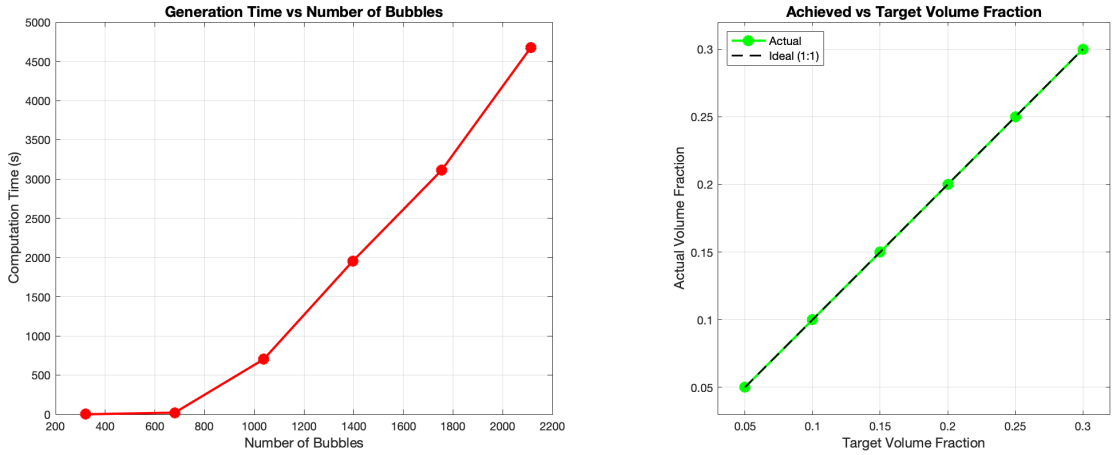

(a) Computation time as a function of the number of bubbles generated.

(b) Achieved vs desired volume fraction.

Figure 3.6: Algorithm performance for monodisperse case.

On the other hand, for polydisperse distributions of bubbles, the algorithm is slightly slower, as it first has to generate the log-normal distribution of bubble sizes and order the bubbles in an descending size order (if a sorting method is included in the algorithm). At the same time, unlike for the monodisperse distribution of bubbles, the algorithm's achieved volume fraction deviates from the desired value of the volume fraction. In most cases, the algorithm overshoots the volume fraction as can be seen in Figure 3.7b.

It is believed that the overshooting of space/volume fraction for the polydisperse distribution of bubbles is due to the fact that, if a desired volume fraction is inputted into the algorithm instead of a specific number of bubbles to generate, the algorithm will calculate the amount of bubbles to generate based on the domain size, and the average bubble size. The way the specific number of bubbles to generate is calculated is as follows: first the average space needed for one bubble is calculated using the average size of a bubble from the inputted range of sizes ($A_{avg,bubble} = [(R_{min} + R_{max})/2]^2 \times \pi$ in the 2D case). Then, the total space needed for all the bubbles, out of the domain space, is calculated by multiplying the desired space/volume fraction times the total domain space: ($A_{bubble,total} = \varphi A_{domain}$ in the 2D case), where φ is the volume fraction. Once both of those values are known, then the number of bubbles to be generated is computed as:

$$n_{bubbles} = \left| \frac{A_{bubble,total}}{A_{avg,bubble}} \right| \tag{3.1}$$

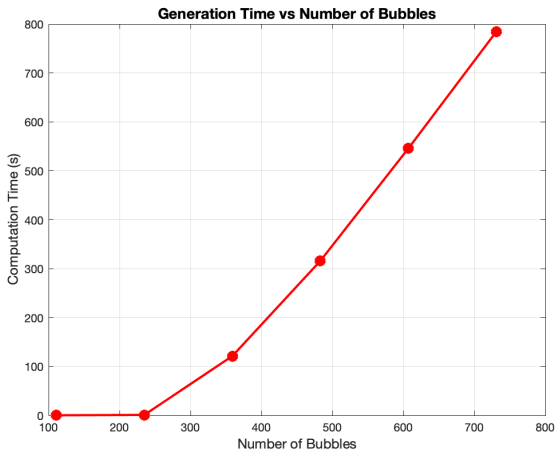

(a) Computation time as a function of the number of bubbles generated.

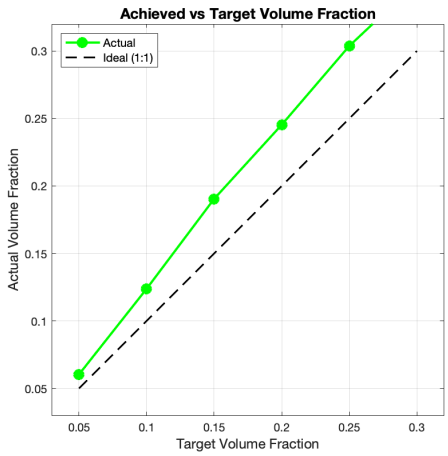

(b) Achieved vs desired volume fraction.

Figure 3.7: Algorithm performance for polydisperse case.

Because in the monodisperse case, the average size of the bubbles is exact (as the bubbles are all of the same size), the amount of domain space reserved for the bubbles is exactly the same as the amount of space needed for one bubble times the number of bubbles to be generated. Thus, once the achieved volume fraction is computed after generating all of the bubbles, this values' difference to the desired volume fraction is negligible: it is a difference of either one bubble more or one bubble less out of thousands generated, due to round-off errors. On the other hand, in the polydispersed case, because the amount of domain space needed for the average sized bubble is not equal to the actual space taken up by all of the generated bubbles (due to the fact that there are bubbles of different sizes that are randomly generated following a log-normal distribution), the achieved space/volume fraction differs from the desired one. Specifically, because the number of bubbles to generate is rounded up, the actual space/volume fraction tends to be higher than the desired one.

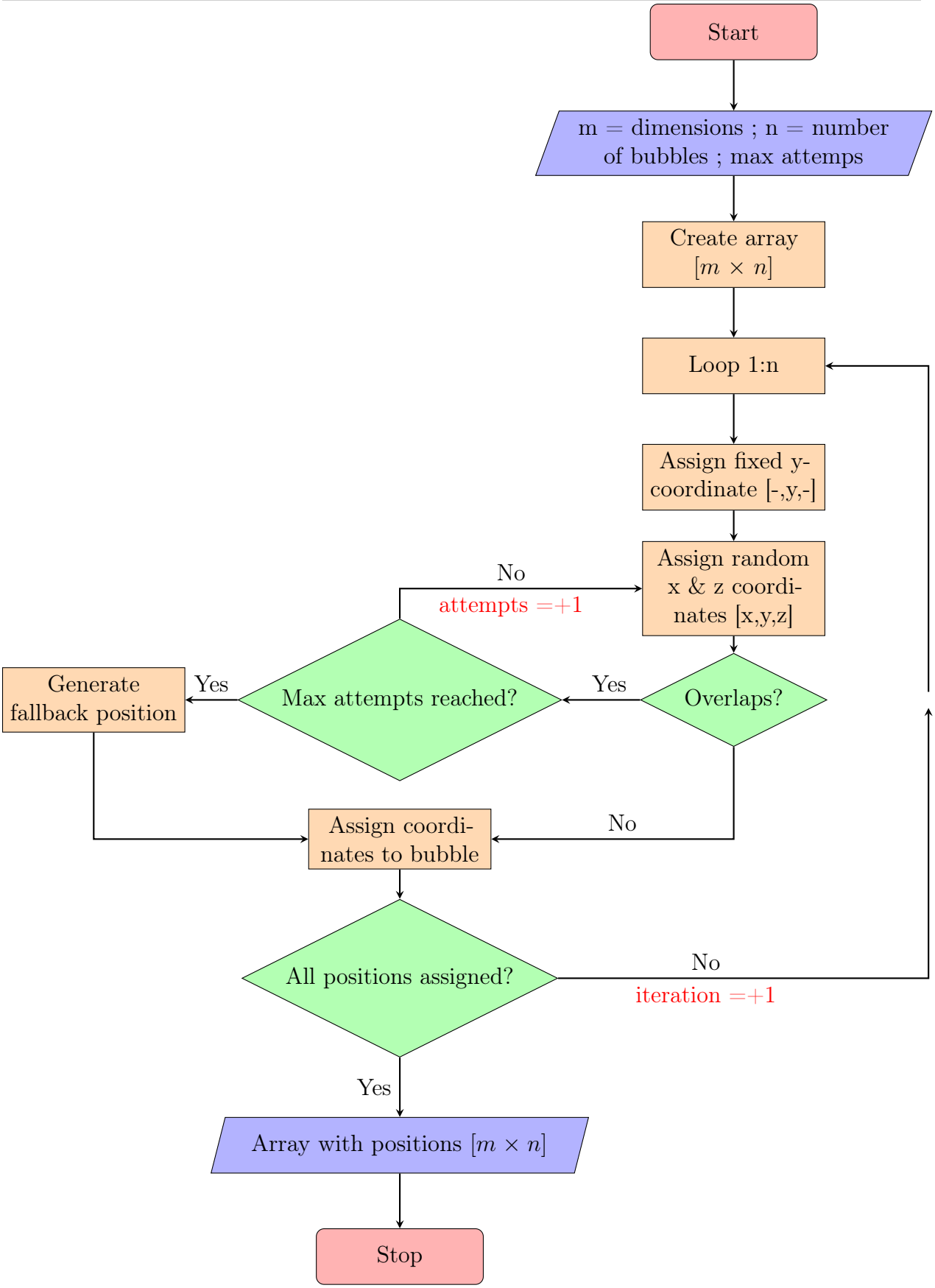

Figure 3.8: Bubble generation algorithm flowchart

3.2 Bubble detachment and advection

To study the bubble detachment and flow inside of the electrolyser channel, two different scenarios were studied: a horizontal planar electrode, and a vertical planar electrode. The main object of this part of the study is to provide a coherent insight into the most important forces that aid in bubble detachment from the electrode, without going into the deep details of this complex phenomena. At the same time, this part of the study helps deliver comprehension as to how the definition of certain forces can change completely the results of the simulation.

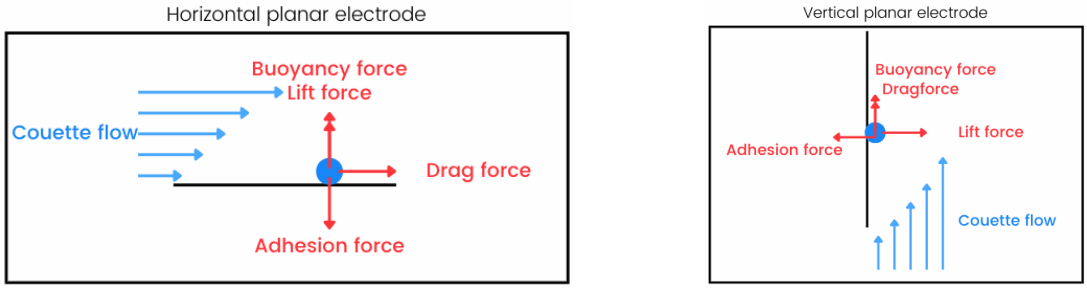

(a) Horizontal planar electrode configuration. (b) Vertical planar electrode configuration.

Figure 3.9: Configurations studied in the bubble detachment and flow section.

In both cases, the assumed flow is a viscous linear flow, either Poiseuille or Couette flow, and the forces studied are the buoyancy force (including the Archimedes force and weight force), the adhesion force, the drag force and the lift force. A few simplifications and definition changes with respect to what was explained in section 2.2 were made in order to reduce the complexity of the problem, whilst still trying to maintain the essence and crucial parts of the problem.

As for the surface tension/ Adhesion force, its definition and the way its calculated was simplified to avoid problems with dynamic contact angles and a moving bubble interface along the electrode. Additionally, it was taken to act in the direction perpendicular to the electrode surface and towards it, hindering the bubble's detachment from the electrode. The force was calculated as:

$$F_{adhesion} = \gamma R_{bubble} \tag{3.2}$$

where γ is the surface tension value of the bubble interface, assumed to be $\gamma = 0.072[N/m]$ (surface tension of water); and R_{bubble} is the instantaneous radius of the bubble attached to the electrode.

The drag force was taken from Oseen's approximations for a sphere in Stokes flow, which was confirmed to be a suitable definition of the drag force by Brenner [47], R.G. Cox [48], W. Chester [49], P.M. Lovalenti and J.F. Brady [50]. It is mentioned in some of these references, that Oseen's expression is not entirely correct for certain cases (such as for bodies not possessing the symmetries described by Oseen), however, it is stated that for perfectly

spherical rigid spheres, Oseen's approximations are accurate enough. Since for this project, the bubbles are assumed to be perfectly spherical and rigid bodies, Oseen's approximation is valid. The direction in which the drag force acts depends on the direction of the velocity vector $\boldsymbol{U}$:

$$F_{drag} = 6\pi\mu L_c \boldsymbol{U}\left(1 + \frac{3}{8}Re_b\right) \tag{3.3}$$

where μ is the fluid's kinematic viscosity, L_c is the characteristic length of the bubbles, i.e the radius of the bubble, $\boldsymbol{U}$ is the relative velocity of the bubble with respect to the fluid flow, and Re_b is the bubble Reynolds number.

As for the buoyancy force, which includes already both the weight of the bubble and the weight of the fluid, it was calculated as the difference in densities between the fluid in which the bubble is immersed in and the gas trapped inside of the bubble, i.e H_2:

$$F_{buo} = \frac{4}{3}\pi R^3 \left(\rho_f - \rho_b\right) g \tag{3.4}$$

where R is the bubble's radius, ρ_f is the density of the surrounding fluid, ρ_b is the density of the gas inside of the bubble, and g is the value of gravity.

Finally, the lift force. This force was specially studied as it is thought to be one of the main contributors to bubble detachment in processes thought to be similar to bubble nucleation and detachment from an electrode, such as boiling.

As mentioned already in section 2.2, the lift force, as defined by Legendre and Magnaudet; is a function of the drag force on the bubble in creeping motion, the magnitude/absolute value of the relative velocity of the bubble, the shear rate and the monotone function $J(\epsilon)$.

$$F_L = \frac{J(\epsilon)}{\pi^2} R\sqrt{\frac{\alpha}{\nu}} F^0 = \frac{4}{\pi}\rho_l \sqrt{\nu} R^2 |U_{rel}| \sqrt{\alpha} J(\epsilon) \tag{3.5}$$

The aforementioned definition of the lift force given my Legendre and Magnaudet presents one problem for the case in which a bubble is rising near a wall: the definition given is for unbounded flow. Due to the fact that the bubble is assumed to be perfectly spherical, using said definition for unbounded flow would result in an only shear-induced lift, caused by the assymetry of the flow surrounding the bubble, know as Saffman lift. Therefore, the resulting lift force would not take into account the presence of the wall near the bubble, which would result in the neglect of asymmetric flow-induced lift and pressure imbalance-induced lift due

to the squeezing of fluid between the bubble and the wall.

Having said this, simulations were carried out using the unbounded flow definition of the lift force, in order to confirm said definition problem.

For the unbounded flow lift, the lift force was taken as stated in Equation 3.5. As for the monotone function $J(\epsilon)$, the definitions given by McLaughlin's "Inertial migration of a small sphere in linear shear flows" [37] were taken. In said study however, the monotone function presents a discontinuity. To deal with the discontinuity of the monotone function $J(\epsilon)$ that is produced when using the asymptotic formulas for the monotone function, a smooth interpolation was performed. The Eq. (3.26) from John B. McLauglin's 1990 "Inertial migration of a small sphere in linear shear flows" is given for epsilon values much larger than unity ($\epsilon >> 1$), while Eq. (3.27) is described as the leading behaviour of the monotone function J for epsilon values much lower than unity ($\epsilon << 1$). Therefore, a discontinuity is produced for values lying around the value 1. In McLaughlin's paper, it is said that in order to obtain values of the monotone function for said range close to unity, it is necessary to evaluate the monotone function by numerical integration.

As $J(\epsilon)$ was already numerically integrated and some results were given in the paper, said numerical integration results were taken to perform the mentioned smoothing interpolation and make the monotone function continuous: Eq (3.26) from McLaughlin's paper was taken for values of epsilon larger than 20 ($\epsilon > 20$) , Eq (3.27) was taken for values smaller than 0.025 ($\epsilon < 0.025$); and as for the range in between, a smoothing spline was introduced using the numerical integration results. The smoothing spline compared to the actual numerical integration values, and the complete monotone continuous function can be seen in Figure 3.10.

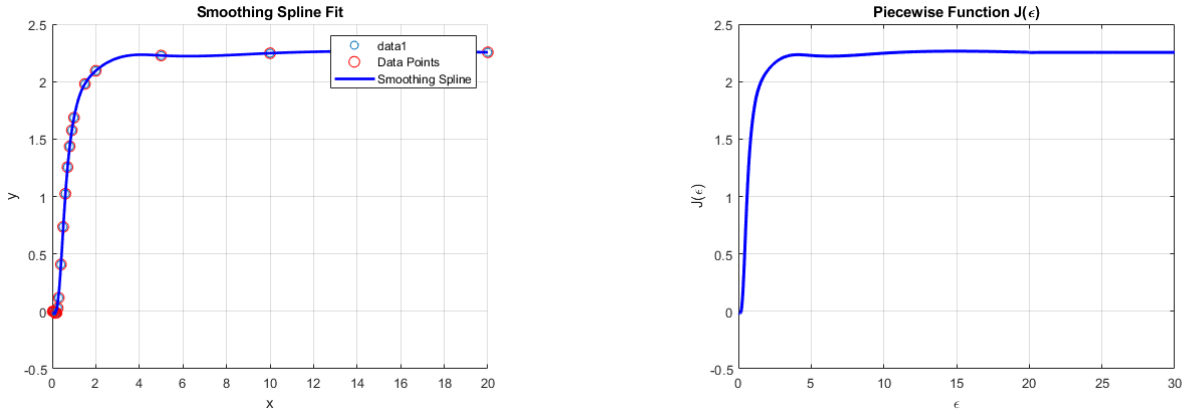

(a) *Smoothing spline* (b) $J(\epsilon)$ *piecewise function*

Figure 3.10: Monotone continuous function J(ϵ)

As a viscous linear shear flow is assumed, specifically Stokes flow, in order to simulate the movement of the bubble, a non-inertial force balance had to be solved. Whilst doing so, the velocity at each time step could be computed as a function of the forces acting upon the

bubble. Different methods could be used in order to solve this iterative process, however, for convenience and simplicity once again, an Euler Forward time discretisation method was used. Of course, when using the Euler Forward discretisation, instabilities may occur that lead to the solution blowing up, however, the parameters for the simulation were chosen so that the simulation would remain stable. The non-inertial dynamics of the bubble present a force balance at each time step, but as the drag and lift forces depend on the relative velocity of the bubble, said iterative process has to be carried out in order to accurately estimate said velocity to be able to compute the forces. Therefore, at the start of each iteration, an initial estimation of the relative velocity of the bubble is done by using the correct value obtained at the previous time step. With said estimate, all forces are computed and the force balance is solved in order to find the value of the relative velocity of the bubble for said force balance. This process, performed at each time step, is repeated until the correct value of the relative velocity of the bubble and forces are calculated.

Additionally, to compare results between unbounded flow lift and the lift force experienced because of the presence of a slip-wall, i.e. the vertical electrode, which will be referred to as "bounded flow lift", simulations were undertaken using an expression for the lift force in bounded flow. The effect of the presence of a wall near the bubble described in Takemura (2010) "On the lateral migration of a slightly deformed bubble rising near a vertical plane wall" [51], results in a migration velocity of a bubble near a wall as seen in Equation 3.7:

$$U_{mig} = \frac{\mu V_{rising}^2}{25\zeta\gamma} \tag{3.6}$$

where V_{rising} denotes the rising velocity of the bubble, μ is the dynamic viscosity of the fluid, γ the surface tension value and ζ is the distance between the bubble interface and the electrode.

Using this, a new expression for the lift force can be defined; as the sum of an unbounded lift (which we take as what we already described in Equation 3.5), and a wall-induced contribution. This of course is assuming superposition/linearity is applicable to the lift force. Therefore, a wall-bounded lift force can be defined as:

$$F_{L,bounded} = FL, unbounded + 6\pi\mu R U_{mig} \tag{3.7}$$

3.2.1 Results and discussion

Firstly, after making the monotone function continuous by using a smoothing interpolation as explained previously, it can be seen that the numerical results given by the definitions used for the lift force and the monotone function $J(\epsilon)$, coincide both numerically and qualitatively with the the dashed and dotted lines in Figure 3.11a, which are the analytical results shown in Legendre and Magnaudet's study [26]. As the Reynolds number Re increases, the lift coefficient C_l decreases. This means that the smoothing interpolation done for the range of ϵ

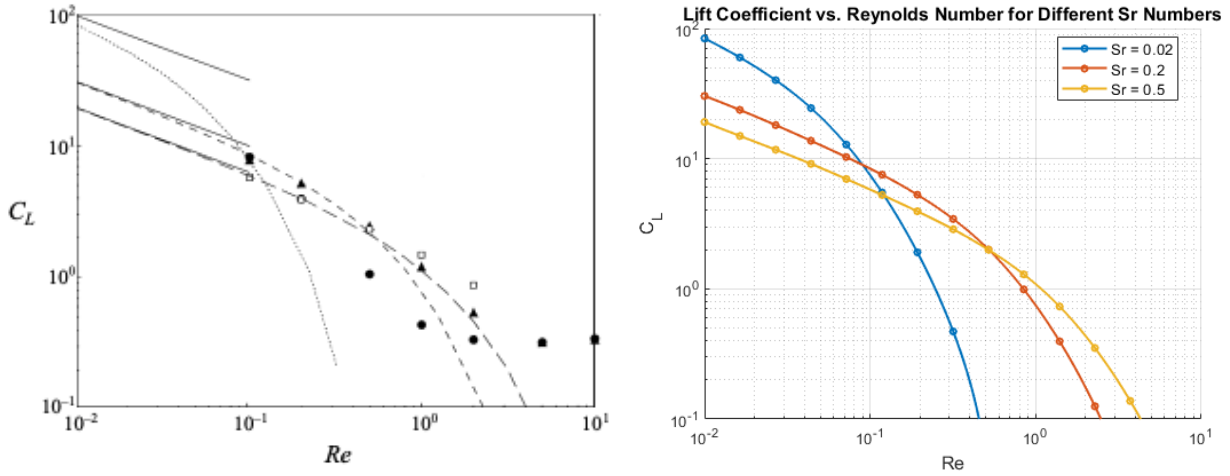

(a) Lift coefficient C_l vs Re, · Sr=0.02; △ Sr=0.2 (Simulation results), ··· Sr=0.02; –Sr=0.2. From Legendre & Magnaudet (1998) [26]

(b) Lift coefficient C_l vs Re from this study.

Figure 3.11: Comparison of lift coefficient for unbounded flows between Legendre and Magnaudet's (1998) work: [26]; and the calculations in this project.

values mentioned previously, does not alter the results.

Secondly, from Figure 3.12, it can be seen that for a range of epsilon values smaller than approximately $\epsilon = 0.0015$ the lift force is negative. Qualitatively, this agrees with D. Legendre and J. Magnaudet's results of the lift coefficient in their work [26], for which at medium to high Reynolds numbers, and for fixed non-dimensional shear rates $Sr = 0.2$ and $Sr = 0.02$, which correspond to small epsilon (ϵ) values, the lift coefficient C_l becomes negative. This is worth mentioning despite said ϵ values representing cases in which the non-dimensional shear rate is very low, or the Reynolds number is very high: unlikely in the case of rising bubbles near a vertical electrode in an electrolyzer, but that could happen. This further suggests that the lift force at some point during the bubble's rise may become negative, making the lift force flip direction and point towards the electrode, inhibiting the separation or lateral movement of the bubble from the electrode. Having said this, this inverted lift force direction case applies to very limited amount of cases for very small ϵ values.

Simulations assuming non-inertial dynamics of the bubble and accounting for the growth of the bubble on the electrode (following the growth laws mentioned, Equation 2.3) and accounting for the detachment of a bubble from the electrode, result in adhesion forces much larger than any other force, suggesting that for said cases of shear stress at the wall (values taken from [24]), a singular bubble does not detach from the wall. However, as this does not match what intuition tells us, another reason as to why this happens can be that the assumptions made to the adhesion force, including its simplification into a definition that only involves surface tension and the radius of a bubble, are incoherent and simplify the physics of adhesion too much, leading to erroneous results. Not accounting for the changing contact area, the changing contact angles and other bubble interface changes, results in an

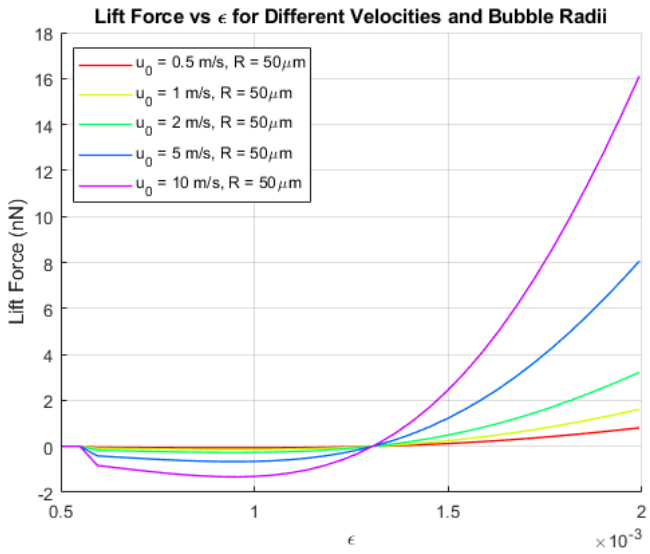

Figure 3.12: Calculated lift force as a function of the non-dimensional number ϵ.

over simplification of the adhesion force.

Because the adhesion force is too large compared to the rest of the forces for the circumstances of the simulation and for the given assumption of the adhesion force, tests without the adhesion force were made to to be able to study the other significant forces, to see the magnitude of the lift force after detachment and to see how much the bubble would move in the direction perpendicular to the electrode.

Worth mentioning is that simulations were also completed assuming inertial dynamics of the bubble, just to see if the results would differ from the non-inertial bubble dynamics simulations. For both inertial and non-inertial cases, the results were the same, so long as there was no numerical instability in the inertial dynamics simulations.

Horizontal electrode simulations

In the simulations made for the horizontal electrode, the evolution of the lift force is not obvious due to it not being the only force that aids in the "pushing" of the bubble away from the electrode. In this case, the buoyancy force also plays a large part in it, although constant once the bubble has detached.

As can be seen in Figure 3.13, the trajectory of the bubble is mostly horizontal, as its movement away from the electrode is smaller than its movement along the flow. Also, from the trajectory it is not possible to see the involvement of the lift force in the bubble's vertical movement; as without it, the trajectory would look similar due to the buoyancy force.

Because of the difficulty in visualizing the involvement and importance of the lift force in the bubble's trajectory for the horizontal electrode case, the vertical electrode cases were studied in more depth.

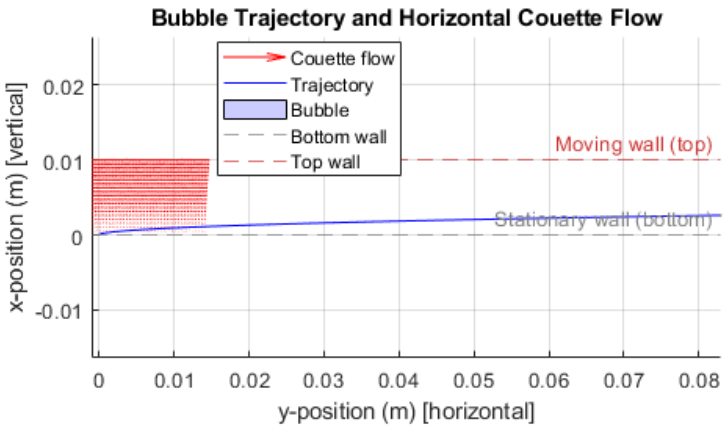

Figure 3.13: Trajectory of a detached bubble from a horizontal electrode using a bounded flow definition of the lift force.

Unbounded flow lift force on a vertical electrode simulations

In said case of non-detachment, the results (Figure 3.14) show that although the wall-induced lift force is not accounted for, as the unbounded flow definition of the lift force was used, the bubble still moves away from the electrode. Furthermore, it can be seen that the velocity on the axis perpendicular to the electrode (x-axis) increases over time. The drag force is the largest force acting upon the bubble and it increases over time, whilst the lift force, although it also increases over time, is smaller than the drag force. The buoyancy force remains constant, as expected, given that the bubble does not grow once it has detached.

Both the drag force and the lift force increase over time, due to the fact that the bubble moves away from the electrode (in the direction perpendicular to it), thus it moves into a region of the flow where the flow velocity is larger. The bubble's change in absolute velocity is not fast enough, and therefore the difference between it's velocity and the flow's velocity increases, making both the drag and lift forces increase. However, the lift force increases at a faster rate than the drag force, making the ratio between drag and lift force decrease, as seen in Figure 3.15.

The displacement of the bubble in the direction perpendicular to the electrode can be seen in Figure 3.16. The graph represents the evolution in time of the ratio between the bubble's x-coordinate (coordinate that indicates how close or far away from the electrode the bubble is) and the bubble's final radius, that is the radius that the bubble has once it has finished growing and has detached. From the plot, it can be seen that said ratio increases, meaning that the bubble moves away from the electrode. For the already mentioned characteristics of the simulation (shear rate, fluid flow, etc), the bubble moves approximately a distance of twenty (20) bubble radius away from the electrode. Meanwhile, in the same amount of time, the bubble rises approximately five hundred (500) radius of distance parallel to the electrode.

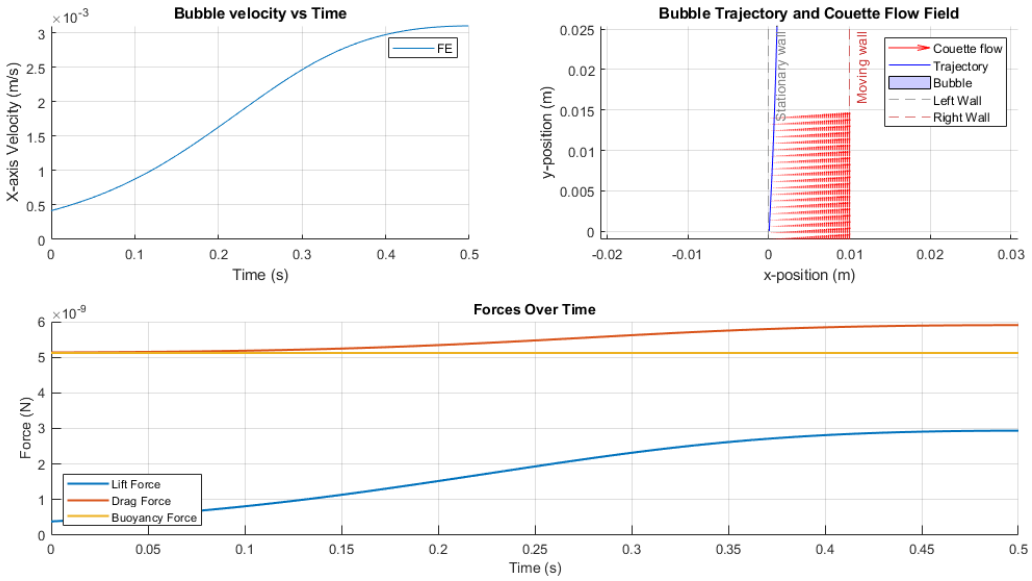

Figure 3.14: Bubble x-velocity, bubble trajectory and bubble forces over time.

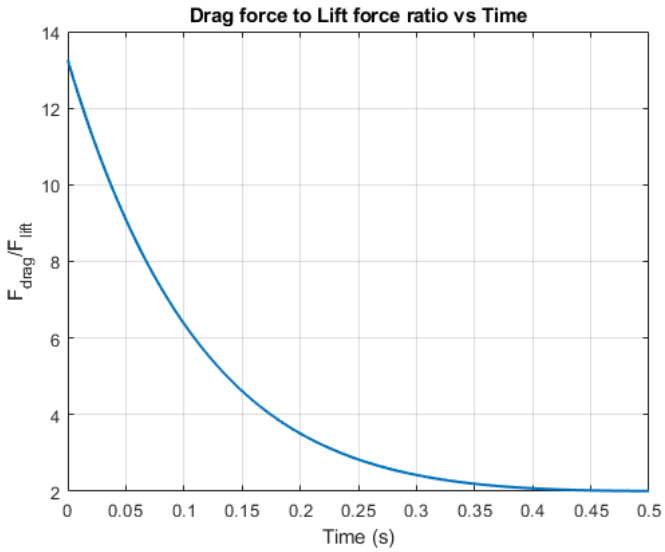

Figure 3.15: Drag to lift force ratio over time for the vertical electrode configuration.

A better comparison between how much the bubble moves parallel to the electrode and perpendicular to it can be seen in Figure 3.17. In mentioned plot, both the ratio between perpendicular and parallel motion relative to the vertical electrode over time, as well as the trajectory of the bubble are seen. The ratio between the bubble's y-coordinate and x-coordinate presents a non-linear shape, meaning that the change in y-coordinate and x-coordinate over time are not the same: for most of the simulation, the bubble moves faster in the y-axis, i.e in the direction parallel to the electrode; than in the x-axis, the direction perpendicular to the electrode. Approximately at $t = 0.125$ there is an inflection

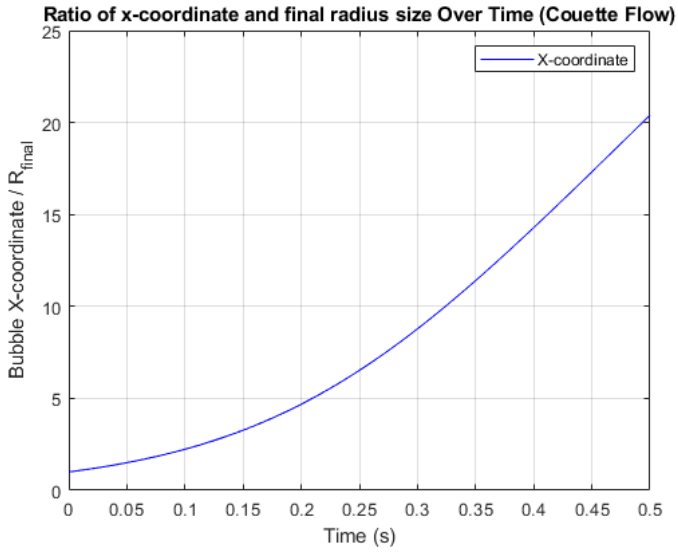

Figure 3.16: Ratio of bubble's x-coordinate to radius over time.

point, suggesting that the motion of the bubble transitions from a buoyancy and drag force dominated motion, to a motion in which shear effects play a bigger role, making the bubble's horizontal motion stronger, as seen in Figure 3.17a. This could be due to the fact that as the unbounded-flow lift force is indirectly a function of the undisturbed fluid's velocity, as the bubble moves away from the electrode, the unbounded-flow lift force increases with increased fluid velocity, making the bubble's horizontal motion greater. Unlike Figure 3.17a, which is a temporal-domain plot, Figure 3.17b shows the trajectory of the bubble, this of course being in the spatial domain. Said graph shows how the bubble translates much further parallel to the electrode than away from the electrode, suggesting that for the bubble to reach the centre of the electrolyser channel, where the majority of the bulk flow is moving, the channel would have to be of great lengths, i.e very tall electrolysers would be needed for said case. Note: the starting point of the bubble's trajectory (green dot in Figure 3.17b), is not at x-coordinate 0. This is because to track the bubble's trajectory, the centre of mass of the bubble is tracked, i.e the centre of the sphere; and the bubble is assumed to have only one singular contact point with the electrode at the moment of detachment.

The fact that the vertical displacement of the bubble is much greater than the horizontal displacement means that unless there are multiple bubble interactions, the space in the electrolyzer channel where bubbles are present, is very close to the electrode. This references the efficiency loss problem in electrolysers: the layer of bubbles close to the wall blocks the active surface of the electrode and decreases the conductivity of the electrode.

As already mentioned, the unbounded-flow lift force increases over time as the bubble moves away from the electrode, whilst at the same time the non-dimensional number ϵ becomes smaller, as seen in Figure 3.18. This is possible due to the fact that, despite the unbounded-flow lift force being directly proportional to the monotone function $J(\epsilon)$, which becomes smaller with decreasing values of ϵ; the unbounded-flow lift force is also a function

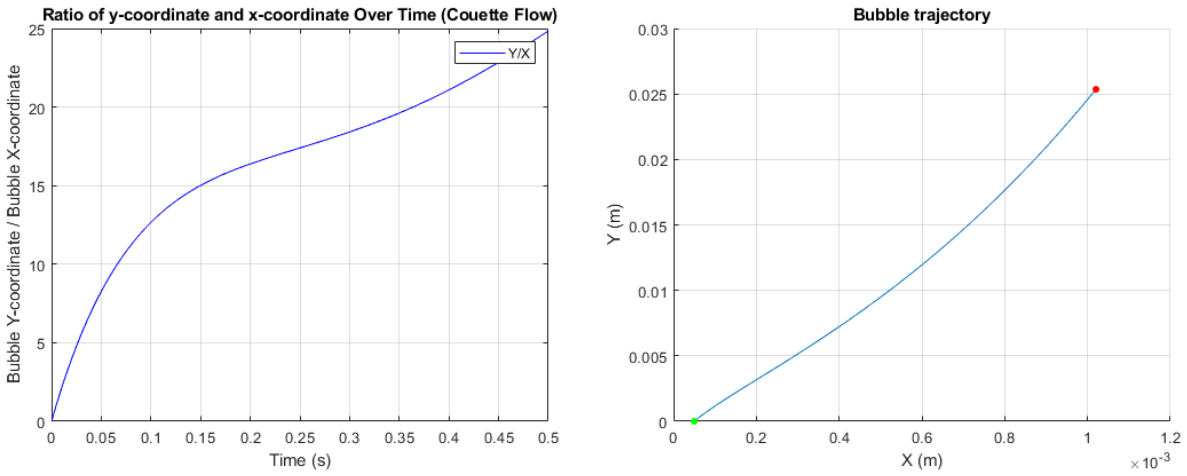

(a) Ratio between bubble y-coordinate and x-coordinate over time.

(b) Bubble trajectory in vertical electrode configuration.

Figure 3.17: Comparison between bubble's parallel and perpendicular motion relative to electrode.

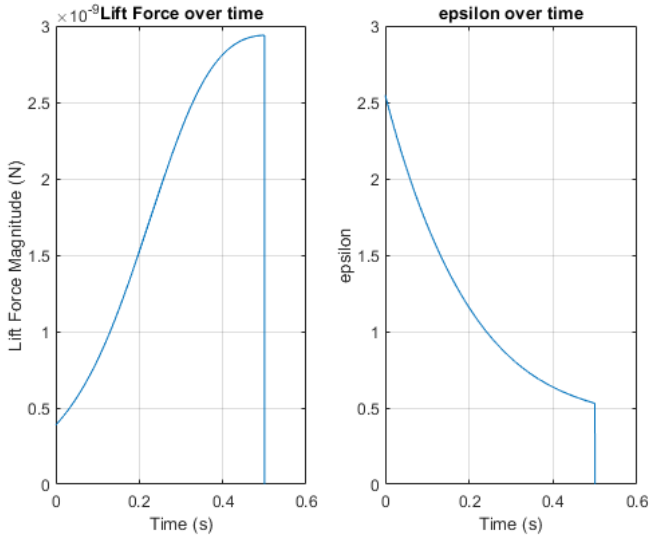

Figure 3.18: Lift force and epsilon values over time.

of the non-disturbed flow velocity. This suggests that the decrease in value of the monotone function $J(\epsilon)$ is slower than the increase in value of the undisturbed flow velocity. Additionally, as already mentioned, for very small values of ϵ it is possible for the lift force's sign to change and become negative. Therefore, it is possible that at a certain point in the bubble's motion, the value of ϵ becomes so small that the lift force changes direction and makes the bubble move once again towards the electrode that it departed from. Note: the simulation ends at $t = 0.5$ (s), thus the drop of lift force and epsilon to 0.

Bounded flow lift force on a vertical electrode simulations

An expression for the combination of the unbounded flow lift force and the lift force resulting from the motion of the bubble near the electrode wall, was used to view the effect of the wall on the bubble's rising motion.

Similar plots to the ones in the subsection of the unbounded flow lift force are shown in this subsection.

From Figure 3.19, it can be seen that when using the expression for the bounded flow lift force, the total lift force over time is larger and grows faster than for the unbounded flow lift force. This results in the bubble moving further away from the electrode than in the case of the unbounded flow lift force. At a certain point, the bubble's lift force surpasses the bubble's buoyancy force which remains constant throughout the simulation. However, this does not result in the bubble moving horizontally more than vertically. This is because the bubble not only rises due to the buoyancy force, but also due to the actual flow of the bulk fluid; whilst the lift force is the only driving force behind the bubble's horizontal movement.

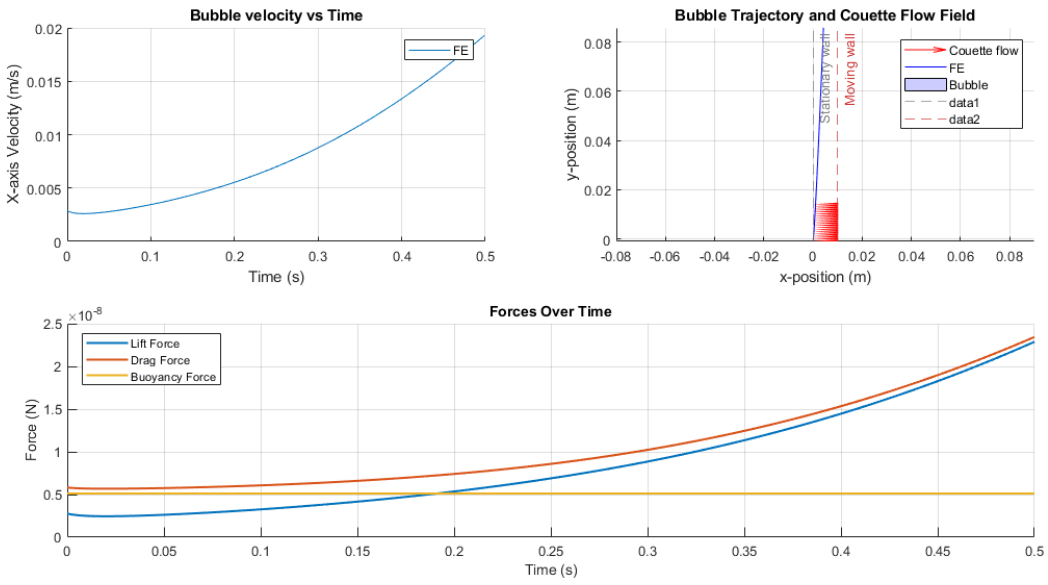

Figure 3.19: Bubble x-velocity, bubble trajectory and bubble forces over time for the bounded flow lift force case.

Both the drag and lift force increase over time, however the lift force grows faster. This is due to the bounded flow lift force being a function of the square of the bubble's velocity, which increases with time, while the drag force presents a linear relation with said velocity. In Figure 3.20, it is visible how the curve increases at the start, when the bounded flow lift force seems like it is not yet accounted for, and then decreases steadily, showing how the lift force's rate of increase is slightly faster than that of the drag force.

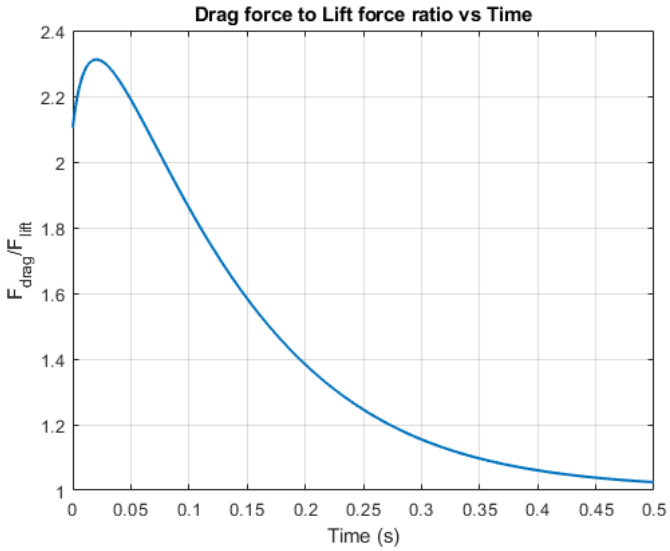

Figure 3.20: Drag to lift force ratio over time for the bounded flow vertical electrode configuration.

The displacement of the bubble in the bounded flow lift force case can be seen in Figure 3.21. When compared to the unbounded case, Figure 3.16, visibly the difference is negligible: the curve presents the same trend, does not present any inflection points and maintains a steady growth. However, quantitively, for the bounded flow case, in the same amount of time, the ratio of the bubble's x-coordinate to final radius grows approximately four times faster than for the case of the unbounded flow. This clearly represents the difference in "strength" between the bounded lift force and the unbounded lift force.

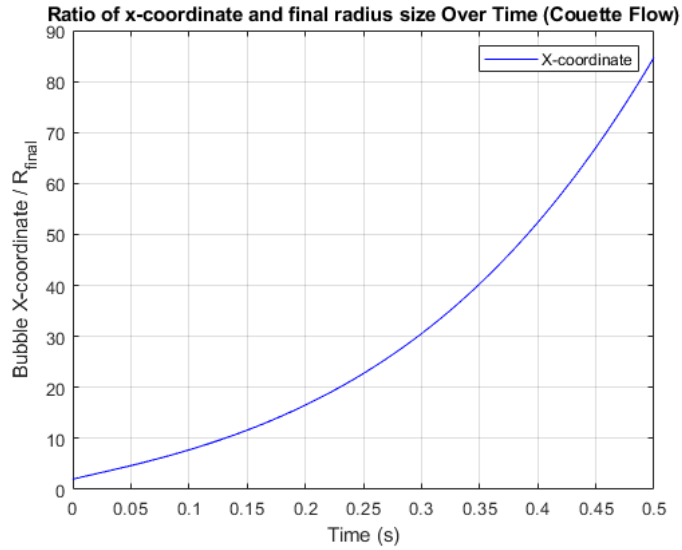

Figure 3.21: Ratio of bubble's x-coordinate to radius over time for the bounded flow case.

As for the ratio of the bubble's y-coordinate to x-coordinate, i.e. the ratio between the bubble's coordinate in the axis parallel to the electrode, and the coordinate perpendicular to the electrode; as well as the bubble trajectory, it can be seen from Figure 3.22, that in the case of the bounded flow, the ratio of y-coordinate to x-coordinate of the bubble does not present an inflection point, as is the case for the unbounded flow. Despite the lift force in the bounded flow case being larger than in the unbounded flow case, the bubble's vertical movement (parallel to the electrode) remains "stronger" than the bubble's horizontal (perpendicular to the electrode) movement, all throughout the simulation. As the bubble moves away from the electrode, it starts to move closer to the bulk flow, where the velocity of the fluid is larger in the vertical direction parallel to the electrode. Thus, the bubble starts to rise faster, as it is pushed by the fluid.

From Figure 3.22b, we can see that the bubble's trajectory remains somewhat similar to the unbounded flow case. However, in the same amount of time, the bubble travels approximately four times the distance of the unbounded flow in the bounded flow case, both in the vertical and horizontal axis. This is due to the bubble's total lift force being higher, making its velocity also faster than for the unbounded flow case.

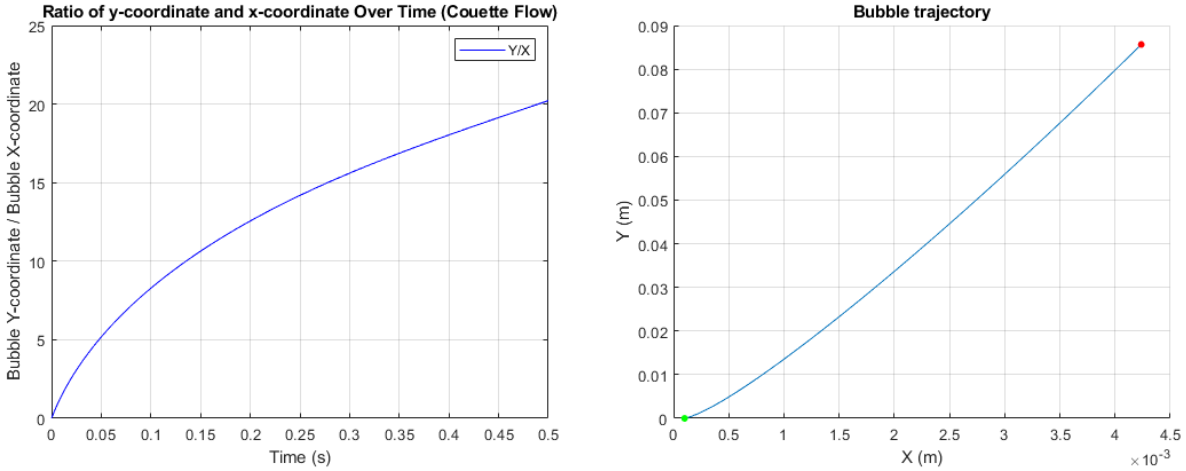

(a) Ratio between bubble y-coordinate and x-coordinate over time for the bounded flow case.

(b) Bubble trajectory in vertical electrode configuration for the bounded flow case.

Figure 3.22: Comparison between bubble's parallel and perpendicular motion relative to electrode for the bounded flow case.

Finally, the lift force over time, as well as the evolution in time of the non-dimensional ratio ϵ, are shown in Figure 3.23. As already mentioned, the lift force increases faster in the bounded flow case than in the unbounded flow case. A slight minimum valley in the lift force is seen at the beginning of the simulation. This is a result of the bubble's starting velocity being zero, as the no-slip condition at the electrode is present. Once the bubble starts moving and its velocity starts increasing, the lift force starts to increase, which is why after the initial minimum valley, the lift force rises steadily. Synonymously, the

value of ϵ initially is large, as the bubble's Reynolds number is small due to its small velocity, but eventually decreases as the bubble picks up speed, making its Reynolds number larger.

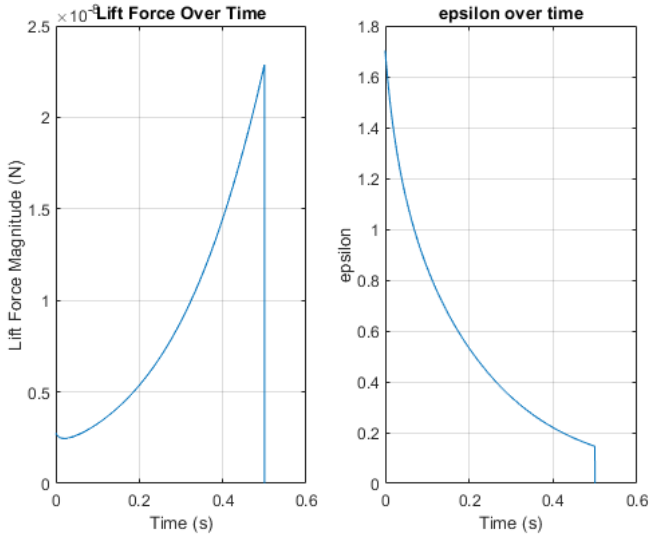

Figure 3.23: Lift force and epsilon values over time for the bounded flow case.

3.3 Modelling of detachment force due to bubble collision

To study and model the detachment of bubbles from the electrode due to the collision between bubbles, simulations were carried out considering the collision physics introduced in section 2.3.

In this project, because the main goal is to study the effect that the bubble layer that is formed near the electrode has on the performance of the electrolyser, and to understand this, it is primordial to know how this bubble layer is formed, a model to study the interaction between bubbles, as well as a model to describe the collision force that a bubble suffers due to the bubbles that collide with it were made.

Due to the complexity of the coalescence phenomena, and further complexity of its modelling, in this project, coalescence of bubbles was neglected and only bubble collisions were studied and modelled.

Additionally, and following the rest of the parts of this project, the bubbles are assumed to be perfectly spherical, and no changes in shape are considered due to the collision of bubbles.

As mentioned in section 2.3, two major forces are involved in the collision of bubbles: the lubrication force due to the "squeezing" of fluid between colliding bubbles, and a short-range electrostatic - nonhydrodynamic repulsive force present in non-pure liquids.

To model the lubrication force, given that the order of magnitude of the "squeeze" lubrication force is much larger than the "shear-flow" lubrication force, only the "squeeze" lubrication force was accounted for out of both of the aforementioned lubrication forces. This squeeze lubrication force acting upon a bubble, was computed as such:

$$\mathbf{F}_{lub} = 6\pi\mu R_{eff}^2 U_{rel} \frac{1}{h}\overline{\mathbf{n}} \tag{3.8}$$

where μ is the viscosity of the fluid, $R_{eff} = R_1 R_2/(R_1 + R_2)$ is the effective radius of the colliding bubble being subjected to the lubrication force being calculated, computed with the radius of both colliding bubbles R_1 and R_2 ; U_{rel} is the relative velocity of the bubble whose lubrication force is being calculated, h is the gap between both bubbles, and $\overline{\mathbf{n}}$ being the vector connecting both centres of the bubbles, which points out of the studied bubble's surface. This definition coincides with the definition given by Equation 2.41, the only differences being that the effective radius of the bubble is used instead of the actual radius, given by the fact that the colliding bubbles may possibly be of different sizes, and that instead of writing κ, its equivalent form in terms of radius and gap ($\kappa = h_0/R$) was written. The sign of the lubrication force is given by the relative velocity: repulsive when bubbles are approaching each other, and attractive when bubbles are moving away from each other after collision.

As for the nonhydrodynamic repulsion force, an electrostatic short range force was chosen for the model, instead of Equation 2.49. This is because said equation is based on the fact that the bubble's shape changes as the gap between bubbles diminishes, making the area of contact between the squeezed fluid and the bubble larger, i.e the inner region of the bubble. However, as for this project perfectly spherical bubbles at all times are assumed, the inner area of the bubble would not change, which would lead to erroneous calculations of the nonhydrodynamic repulsive force, which in turn could possibly lead to overlap between bubbles.

Thus, an electrostatic short range force was chosen instead: said short range electrostatic force, although different in origin and physical meaning, is capable of capturing the exponential divergence of the bubble force inversely proportional to the distance or gap between bubbles, i.e how the repulsive force grows as the gap between bubbles diminishes, which helps avoid overlaps of bubbles when colliding.

The calculation of the electrostatic repulsive force can be seen in the following equation:

$$\mathbf{F}_{rep} = C_1 \frac{1}{h^2}\overline{\mathbf{n}} \tag{3.9}$$

where C_1 is a repulsive coefficient, h is once again the gap between bubbles, and $\overline{\mathbf{n}}$ is again the outward pointing vector that connects both centres of the bubbles.

This electrostatic repulsive force diverges with the square of the gap between bubbles, as electrostatic forces given by Coulomb's Law do.

Said repulsive coefficient C_1 is set up as an arbitrary value, and can be changed according to the desired order of magnitude of the repulsive force. For this study, the value of the repulsive coefficient was chosen by trial and error, in order to make the order of magnitude of both the lubrication force and the repulsive force similar, so that the collision between bubbles can be studied and modelled as a combination of both forces acting on the bubbles at the same time.

Apart from the collision forces, the hydrodynamic forces acting upon a bubble remain the same as previously: buoyancy force and drag force.

In order to be able to study the collision force acting upon a bubble, and obtain an expression for the average collision force on a bubble, a simulation was set up in which a fixed bubble was placed in the centre of a domain, and multiple rising bubbles were generated in that same domain, using the bubble generation algorithm created in this project (explained in section 3.1). Said rising bubbles would then collide with the fixed bubble, exerting a force on it. Different number of bubbles, sizes and distribution types (monodisperse or polydisperse) were simulated in order to gain statistical data of the collision force, and finally obtain an expression for the collision force on a bubble which can then be used in future models in order to save computation time when dealing with collisions. The simulations were run for enough time so that a large number of collisions per simulation was observed between the fixed bubble and rising bubbles, making the statistical data even more coherent.

Worth mentioning is that the way the bubble generation algorithm was employed during the realisation of this part of the project, made it so that the generation/placement of bubbles was not fully random at all times. The bubbles were generated progressively with each iteration in a grid like manner until there was no space to do so any more. Once that was done, then the rest of the bubbles left to be assigned coordinates were generated fully randomly. This was brought about to speed up the process of bubble generation, as during the bubble collision part of the project, the main objective was to study collisions and not the formation of the bubbles.

In order to make the simulation feasible, instead of continuously generating new bubbles throughout the simulation so that many collisions could happen, a set number of bubbles was set during the initialisation part of the code (either the exact number of bubbles or a space/volume fraction was inputted) and was kept throughout the simulation. A simulation domain was set up with periodic boundary conditions at the west and east boundaries, making it so that a bubble that exits the simulation domain at the east boundary, will be re-positioned with the same velocity, size and vertical coordinates at the west boundary; and vice-versa. This not only eliminates the need of generating a new bubble when a moving bubble exits the domain, but also allows to simulate larger systems while only simulating one part of the domain, eliminating any artificial artifacts due to domain size, that could arise in the simulation. As for the north and south boundaries, different conditions were used: a "buffer" region was created under the simulation domain, so that bubbles exiting the

simulation domain through the north boundary would be randomly repositioned in the buffer region. Once the bubbles in the buffer region crossed the north boundary of said buffer region, i.e the south boundary of the simulation domain, they would enter the simulation domain once again. Bubbles in the buffer region follow the same motion and collision physics as the bubbles in the simulation domain, however, their collisions are not accounted for and their presence does not affect the bubbles in the simulation domain. This means that a bubble in the buffer region will not be included for example in the calculation of distances to the fixed bubble.

This "buffer" region was set up to avoid numerical artifacts due to the creation of "channels" or "ways" north of the fixed bubble. When colliding with the fixed bubble, rising bubbles will change their trajectory, and similarly to a flow past a sphere or cylinder, a sort of "wake" is produced. In the case of rising and colliding bubbles, this "wake" is a channel where no bubbles exist. Therefore, using periodic boundary conditions in the north and south boundaries of the simulation domain so that north-boundary exiting bubbles are repositioned in the south boundary; would lead to a channel where no bubbles exist both upstream and downstream of the fixed bubble, meaning the collisions between moving bubbles and the fixed bubble would decrease with time until eventually an equilibrium is reached in which no moving bubbles collide with the fixed bubble.

Thus, to avoid this, the "buffer" region was included south of the simulation domain to eliminate the possibility of having said channel where no bubbles exist. Randomly repositioning rising bubbles exiting the simulation domain through the north boundary in the buffer region, allows for bubbles to re-appear directly south or under the fixed bubble. Thus eliminating the possibility of reaching an equilibrium in which no collisions happen.

A 2D visualisation of the set-up, which represents a front view of a bubble attached to the electrode and detached moving bubbles rising around it, includes the buffer region, as well as a time-evolution of the set-up to represent the random repositioning of the bubbles; is shown in Figure 3.24.

As for the 3D case of this collision study, both a set-up with a fixed bubble in the centre of a simulation domain with no electrode was made in order to study the average collision force acting upon said bubble, and a set-up in which the bubble is attached to the electrode and the bubbles rise parallel to the electrode and collide with the attached bubble. This second set-up was made to study the evolution of the bubble "plume" or "boundary layer" that is produced near the electrode. Both set-ups can be seen in Figure 3.25.

In Figure 3.25a, the buffer region is not directly visible, however bubbles in the buffer region are pink/magenta coloured, whilst bubbles in the simulation domain are blue. The fixed bubble's colour is red. In Figure 3.25b, the electrode is the grey element, the fixed bubble is red, and the moving bubbles are blue. The buffer region is not shown. Note: any visible overlaps in either of the set-ups visualisations are not actual overlaps but just visualisation artifacts/problems made by the software used for the visualisations and animations.

Different models based on different approaches and physical phenomena were come up with and tested in order to model the average collision force on the fixed bubble. The different

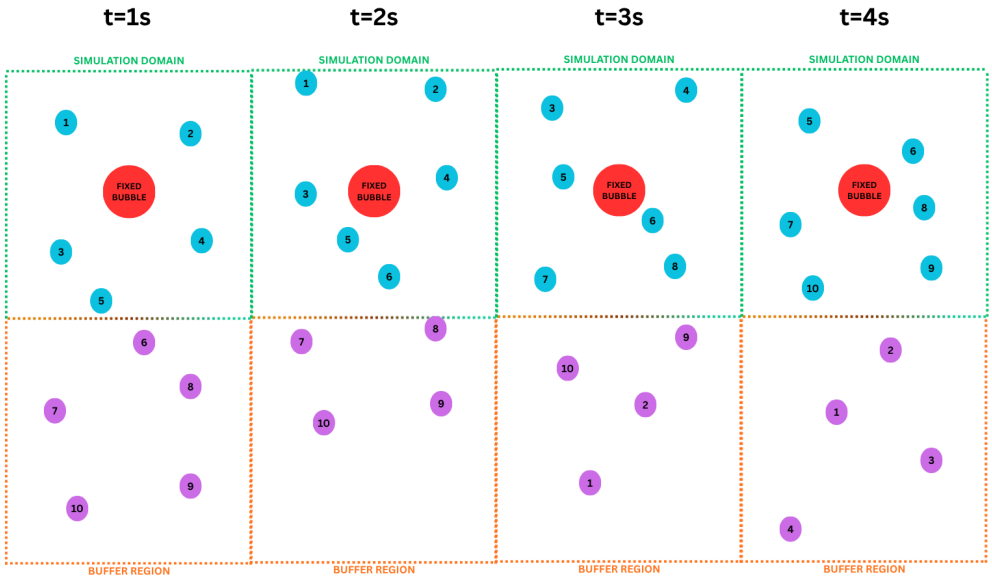

Figure 3.24: 2D visualisation of collisions set-up and random repositioning.

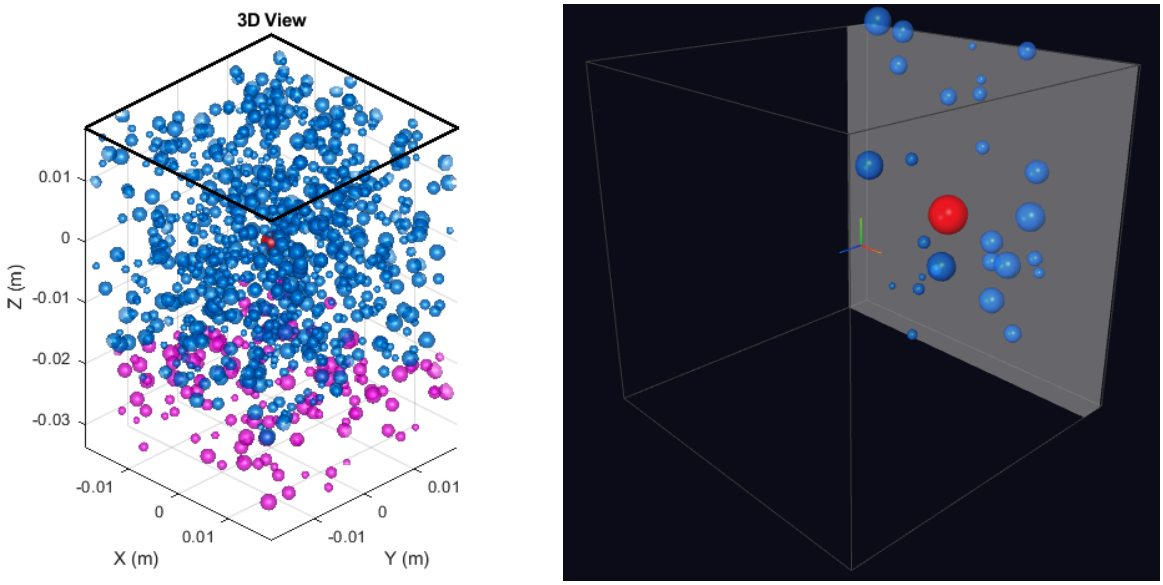

(a) Fixed bubble in the centre of the simulation domain set-up.

(b) Fixed bubble attached to the electrode set-up.

Figure 3.25: Visualisation of the 3D bubble collisions set-ups.

tested models are: "Average buoyancy model", "Momentum Transfer Model", "Kinetic Theory Approach" , "Pressure-based Model" , "Energy dissipation model", and a "Power Law".

The **"Average buoyancy model"** says that the average collision force on a bubble can be approximated by the buoyancy force of the averaged sized bubble in the distribution. The reasoning behind this approximation is that the driving force for the rising motion of the bubbles is their buoyancy force, and when two bubbles collide, the collision force tries to stop the buoyancy-driven motion of the bubbles from making them collide:

$$\overline{F_{coll}} = \frac{4}{3}\Delta\rho\pi g\langle R\rangle^3 \tag{3.10}$$

where $\overline{F_{coll}}$ is the average collision force , $\Delta\rho$ is the difference in densities between the fluid and the bubble and $\langle R\rangle^3$ is the cube of the average radius in the distribution.

The **"momentum transfer model"** arguments that the collision forces arise from a momentum exchange when buoyancy-driven bubbles collide/interact. It states that the average collision force equals the rate of change of momentum of a bubble:

$$\overline{F_{coll}} = \frac{dp}{dt} = \Delta p f_{coll} \tag{3.11}$$

$$\Delta p = m \times v_{coll} = \frac{4}{3}\pi\langle R\rangle^3\rho_b \times \frac{F_{buo}}{6\pi\mu\langle R\rangle} \tag{3.12}$$

$$f_{coll} = n_{dens}\sigma_{coll}v_{coll} \tag{3.13}$$

where p is the momentum of the bubble, m is the bubble's mass, v_{coll} is the velocity at which the collision happens, which can be approximated as the terminal velocity of the bubble, ρ_b is the bubble's density; n_{dens} is the number density of bubbles, which in 3D can be computed as number of bubbles per unit volume; and σ_{coll} is the collision cross section that can be computed as $\sigma_{coll} = \pi(R_{fixed} + \langle R\rangle)^2$. Therefore, the final equation for the average collision force given by the momentum transfer model is:

$$\overline{F_{coll}} = \frac{4}{3\mu}\langle R\rangle^2\rho_b\overline{F_{buo}}f_{coll} \tag{3.14}$$

The **"Kinetic Theory approach"** treats the bubbly system as "molecular gas" where the collisions between bubbles follow kinetic theory principles. It considers the average collision force to be equal to the force per collision, times the number of collisions that happen in the system, which is an idea taken from the impulse-momentum theorem $\sum F \times \Delta t = \Delta p$). The force per collision can be computed as the momentum transfer of each collision over the collision time:

$$\overline{F_{per,coll}} = \frac{\Delta p}{t_{coll}} = \frac{4}{3}\pi\langle R\rangle^3 v_{coll}/\frac{(R_{fixed} + \langle R\rangle)}{v_{coll}} \tag{3.15}$$

where the v_{coll} is the collision velocity, or approach velocity which can be approximated as the terminal velocity of the moving bubble, and the rest of the symbols remain the same.

The collision frequency used in this "Kinetic Theory approach" can be calculated as the gas kinetic theory collision rate, and using the definition of temperature as a function of the kinetic energy of the moving molecules, the following equation can be obtained:

$$f_{coll} = n_{dens}\sigma_{coll}\sqrt{\frac{8K_BT}{\pi m}} = n_{dens}\sigma_{coll}\sqrt{\frac{8K_B\frac{2E_K}{3K_B}}{\pi m}} \approx 0.9n_{dens}\sigma_{coll}v_{coll} \tag{3.16}$$

where all already shown symbols remain the same, T is temperature, K_B is the Boltzmann constant, and E_K is the kinetic energy of the bubble.

Combining the equation of the average force per collision and the collision frequency, the average collision force can be computed as:

$$\overline{F_{coll}} = \overline{F_{per,coll}}f_{coll} \approx 0.9\rho_b\varphi(R_{fixed} + \langle R\rangle)\overline{F_{buo}}^3\frac{1}{6\pi^2\mu^3\langle R\rangle^3} \tag{3.17}$$

where the new symbols φ is the spatial/volume fraction of bubbles in the domain.

The **"Pressure-based model"** models the collision forces as arising from the pressure exerted on the fixed bubble by a "swarm" of bubbles around it. It makes use of the definition of force as pressure times the area the pressure affects and the equipartition theorem (used already in Equation 3.16 to relate the temperature to the kinetic energy). The bubbles are treated once again as molecules, and kinetic theory is assumed:

$$P_{bubble} = n_{dens}K_BT = \frac{1}{3}\varphi\rho_b\left(\frac{\overline{F_{buo}}}{6\pi\mu\langle R\rangle}\right)^2 \tag{3.18}$$

then by using the definition of force:

$$\overline{F_{coll}} = P_{bubble}A_{fixed} = \frac{1}{3}\varphi\rho_b\left(\frac{\overline{F_{buo}}}{6\pi\mu\langle R\rangle}\right)^2 4\pi R_{fixed}^2 \tag{3.19}$$

where A_{fixed} is the area of the fixed bubble (assumed to be a sphere to write Equation 3.19).

The **"Energy Dissipation model"** states that the collision force arises from energy dissipation during inelastic collisions between the bubbles. It makes use of the definition of dissipated power in the system as the product of the average collision force times the average velocity of the bubbles, which is assumed to be the average terminal velocity of the moving bubbles. Combining said definition of dissipated power with the definition of dissipated power as a function of the dissipated energy, the average collision force is calculated.

$$W_{diss} = \overline{F_{coll}} v_{avg} = \overline{F_{coll}} \frac{\overline{F_{buo}}}{6\pi\mu\langle R\rangle} \tag{3.20}$$

$$W_{diss} = E_{diss} f_{coll} = \epsilon E_K f_{coll} \tag{3.21}$$

where W_{diss} is the dissipated power, v_{avg} is the average terminal velocity of moving bubbles, E_{diss} is the dissipated energy per collision, ϵ is an arbitrary value between 0-1 that represents the percentage of kinetic energy dissipated, E_K is the kinetic energy of the moving bubble, and f_{coll} is the collision frequency.

Combining Equation 3.20 and Equation 3.21, an equation for the average collision force can be obtained:

$$\overline{F_{coll}} = \epsilon \frac{4}{6^2} \langle R\rangle^2 \rho_b \overline{F_{buo}} f_{coll} \tag{3.22}$$

Finally, a **"Power Law"** was tested. Two slightly differing power laws were defined using what is thought to be the most important parameters of the bubble simulation: the number of bubbles $n_{bubbles}$, the average buoyancy force $\overline{F_{buo}}$, the volume fraction φ and the collision frequency f_{coll}:

$$\overline{F_{coll}} = C_1 n_{bubbles} \overline{F_{buo}} \varphi^{C_2} \tag{3.23}$$

$$\overline{F_{coll}} = C_1 n_{bubbles} \overline{F_{buo}} \varphi^{C_2} f_{coll}^{C_3} \tag{3.24}$$

where C_1 , C_2 and C_3 are all arbitrary fit constants. The optimal values of said constants were obtained by fitting said power laws to the results obtained in the simulation.

All the models mentioned and tested in this study were come up with using physical intuition and ideas/analogies from what could possibly be similar behaving phenomena like the motion of molecules in a system. None of the models have previously been established as bubble collision models and or validated for said bubble systems. Dimensional analysis was used to obtain the coherent equations used.

The reason why the "**Kinetic Theory approach**" and the "**Pressure-based model**" are different and yield different results despite both being based on using the kinetic energy of the bubbles and both using the equipartition theorem is because they both stem from different physical assumptions. The "**Kinetic Theory approach**" stems from the idea that the bubble collisions are discrete events and in each event momentum is transferred; whilst the "**Pressure-based model**" stems from the idea that the bubble collisions of the moving

bubbles with the fixed bubble are continuous and therefore exert a "pressure" on the fixed bubble.

All models share the fact that they all use the average buoyancy force in their average collision force calculations. Because the buoyancy force is the force that mainly drives the motion of the rising bubbles, it is expected that the buoyancy force of each bubble is a main contributor to the collision force exerted by each moving bubble on to the fixed one. It also makes it easier to calculate the average collision force on a bubble due to the bubbles surrounding it, as it is a parameter that can be calculated by only knowing the density of the fluid and the bubble, and the size of the bubbles; making the model less complex.

3.3.1 Results and discussion

First of all, both 2D and 3D simulations were run using the set-up in which the fixed bubble is placed in the centre of the domain, as shown in Figure 3.26.

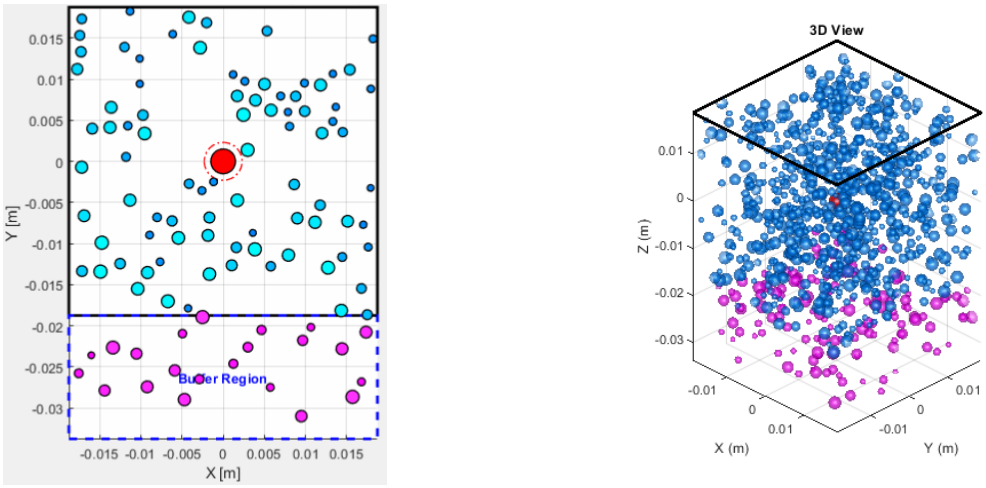

(a) 2D set-up.

(b) 3D set-up.

Figure 3.26: 2D and 3D set-ups for the average collision force analysis in the case of the fixed bubble being in the centre of the simulation domain.

As for the average collision force obtained from the simulations, the results between the 2D and 3D case were very similar. Despite having differences in number of moving bubbles, distribution of sizes of the moving bubbles, total number of collision, etc; as those parameters have a random nature; the average collision force obtained lies in the same order of magnitude: $\overline{F_{coll}} \approx [10^{-4} - 10^{-5}]$ (N).

Moreover, said range of average collision force order of magnitude relates to the order of magnitude of the buoyancy force of the average sized bubble in the distribution; suggesting that the average collision force of the fixed bubble can be computed as the buoyancy force

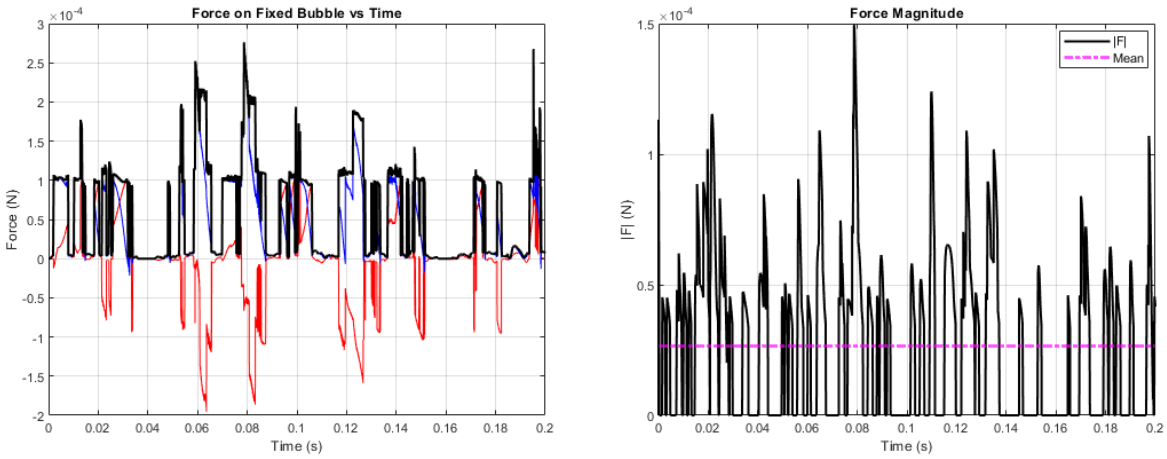

(a) 2D force evolution.

(b) 3D force evolution.

Figure 3.27: Collision force evolution over time for the 2D and 3D fixed-bubble in the centre of the domain simulations.

of the average sized bubble in the distribution. Said results were obtained for both the polydisperse and monodisperse cases.

Furthermore, from the histogram of the 3D case, Figure 3.28, it can be seen that the distribution of collision forces throughout the simulation are arranged in a log-normal distribution that resembles the log-normal distribution of the range of sizes of the moving bubbles.

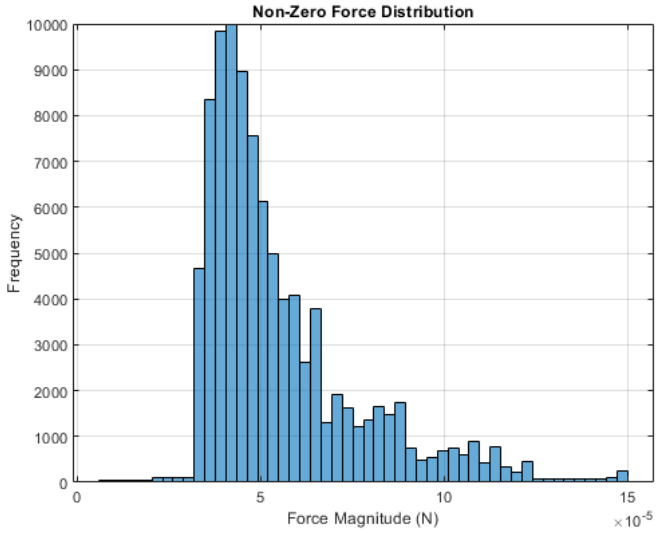

Figure 3.28: Collision force histogram for the 3D fixed-bubble in the centre of the domain simulations

This once again suggests that the collision forces on the fixed bubble have a strong

correlation to the buoyancy force of each bubble, as said buoyancy is the driving force for the motion of the moving bubbles.

Additionally, for both the 2D and 3D cases, the number of bubbles within the repulsive region of the fixed bubble (the region where the fixed bubble starts to actively 'feel" the moving bubbles and thus a force is exerted on it), remains similar throughout the simulations, as seen in Figure 3.29. The number of bubbles in the repulsive region is calculated by setting a distance at which the force exerted on the fixed bubble by a moving bubble is large enough to consider it in the "repulsive region". As seen in the figures, said number is around 3 for both cases, meaning that the maximum number of bubbles directly colliding with the fixed bubble at the same time is 3.

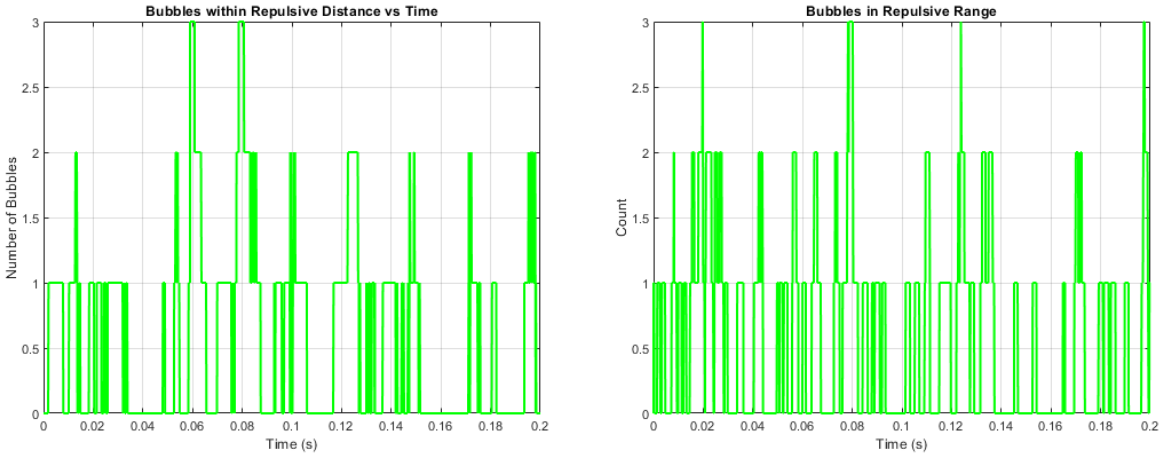

(a) 2D count for bubbles in repulsive region evolution.

(b) 3D count for bubbles in repulsive region evolution.

Figure 3.29: Evolution of the count for the bubbles in the repulsive region over time for the 2D and 3D fixed-bubble in the centre of the domain simulations.

Worth mentioning is that the the curve seen is a step function because only the centre of mass of a bubble crossing the distance threshold is considered when accounting for a bubble in the repulsive region. Therefore, at each iteration a check is made to see whether the bubble is in or out of that repulsive region, and once it is out the count automatically drops.

Similarly, the results for the number of bubbles in the buffer region throughout the simulation is also analogous in the 2D and 3D cases. Of course, quantitatively the results do not necessarily match, as the amount of bubbles in the buffer region depends on the total number of moving bubbles, which can differ from simulation to simulation; as well as the domain size and buffer region size. However, qualitatively, said results are coherent, as can be seen in Figure 3.30.

Although not quite visible in Figure 3.30a, both for the 2D and 3D case, the number of bubbles in the buffer region ends up reaching an equilibrium where said number of bubbles oscillates between certain values. At first, the number of bubbles in the buffer region is 0,

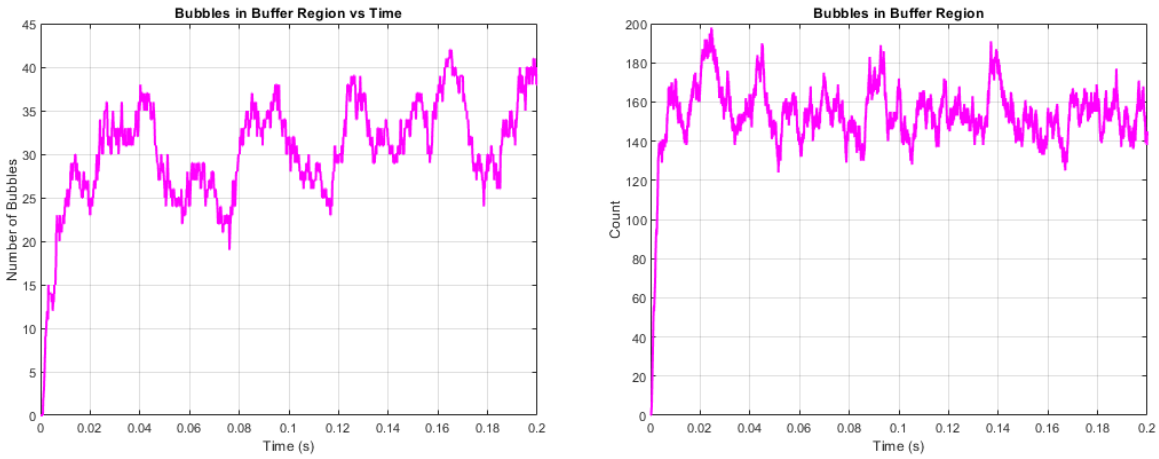

(a) Evolution of number of bubbles in buffer region in 2D case.

(b) Evolution of number of bubbles in buffer region in 3D case.

Figure 3.30: Evolution of the number of bubbles in the buffer region over time for the 2D and 3D fixed-bubble in the centre of the domain simulations.

as all bubbles are initially placed in the simulation domain, however, as bubbles rise and exit the north boundary of the simulation domain, they are re-placed in the buffer region (as previously explained). Once said equilibrium is reached, it can be concluded that the results will not present any errors or miscalculations due to numerical artifacts related to the domain size or periodic boundary conditions.

As for the area of the fixed bubble that suffers collisions, both in the 2D and 3D case, it is visible that the bubble collisions are mostly of course in the bottom part of the fixed bubble, due to the rising motion of bubbles. However, from Figure 3.31, it is observed that bubbles will "roll" around the fixed bubble an amount that is not always the same. This is due to the fact that the collision between fixed bubble and moving bubble is not a 2 body problem, but a multiple body problem: other moving bubbles will collide with the rising bubble that is at collision with the fixed bubble, pushing the rising colliding bubble towards the fixed bubble and not letting it "bounce" away from the fixed bubble. Since for each fixed bubble - rising bubble pair wise collision, the moving bubbles in the surroundings are different at each moment, the amount that the rising bubble "rolls" around the fixed bubble differs: the different bodies of the multiple body problem are different every time.

The evolution of the number of collisions with the fixed bubble can be seen in Figure 3.32. As the plot represents the cumulative total of collisions throughout the simulation, logically the curve is positive (meaning the number of total collisions grows with time). However, the slope of the curve remains somewhat constant along the entirety of the simulation. This suggests that the collisions are independent of time conditions and that once an equilibrium is reached, the collisions are continuous and steady. This statement suggests no numerical artifacts are present in the results of the collision simulations, as they do not influence the collision frequency with the fixed bubble; but instead a constant "stream" of moving bubbles

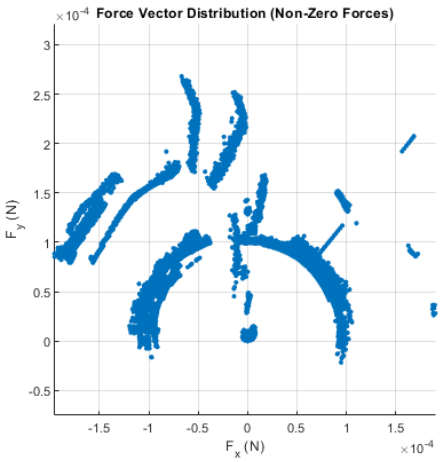

(a) Force vector distribution for the 2D case.

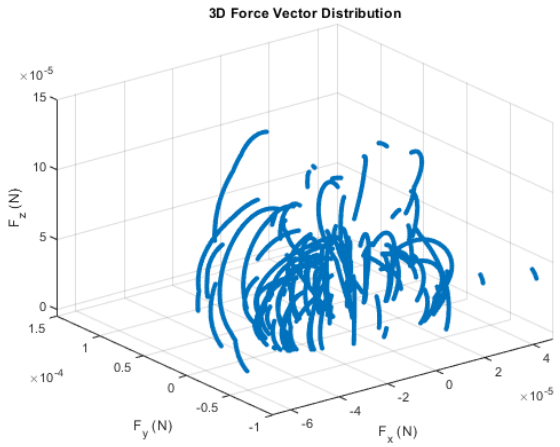

(b) Force vector distribution for the 3D case.

Figure 3.31: Evolution of the number of bubbles in the buffer region over time for the 2D and 3D fixed-bubble in the centre of the domain simulations.

collides with the fixed bubble, as would happen in an electrolyser.

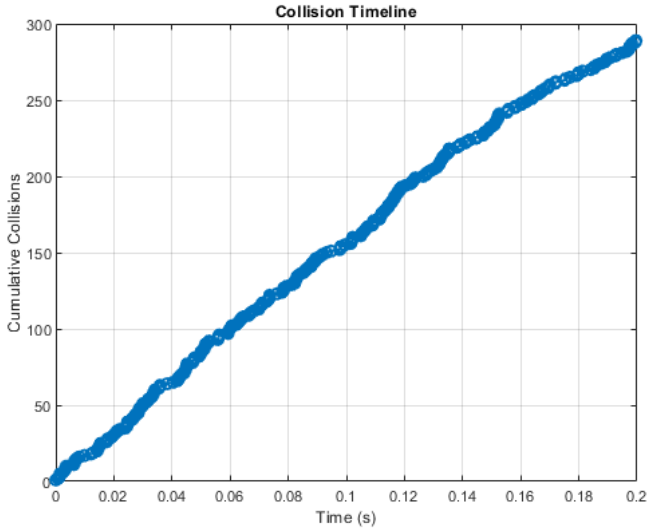

Figure 3.32: Evolution of the total number of collisions with the fixed bubble in time for the 3D fixed-bubble in the centre of the domain simulations.

Note: all the plots shown in subsection 3.3.1, this subsection showing the results of the bubble collisions part of the project, are shown for individual simulations of polydisperse distributions of bubbles. However, the results apply to all cases of 2D and 3D simulations made in which the fixed bubble is in the centre of the simulation domain; for both polydisperse and monodisperse distributions of bubbles.

As for the different models used, the first one tested was the "Average buoyancy model". Said model yields acceptable relative errors when comparing the average collision force calculated using Equation 3.10, and the average collision force obtained from simulations (for all time steps, including the time steps when no bubbles are colliding). The average relative error for this model is approximately 85% , specifically 88% for the polydisperse distribution of bubbles, and 82% for the monodisperse distribution of bubbles, therefore making it slightly better for monodisperse distributions of bubbles, as the average buoyancy force is exactly equal to the buoyancy force of the average sized bubble. For the monodisperse case, against logic, the average buoyancy force model does not yield perfect results when predicting the average collision force on the fixed bubble. This is because, as explained already, when a rising bubble collides with the fixed bubble, its collision is also affected by other moving bubbles near the rising bubble, i.e. it is a multibody problem. This makes the rising bubbles "roll" along the fixed bubble. As the rising bubble rolls, the ratio of collision force to buoyancy force is not exactly one: said ratio is only one when the rising bubble collides with the fixed bubble and both of their centres of mass are in the same vertical axis, aligned with the direction of gravity. Surprisingly, this model works best for simulations in which a low percentage of the total time steps are time steps with collisions. This could be, once again, due to the ratio between collision force and buoyancy force not being equal to one as the moving bubble "rolls" over the fixed bubble: the maximum collision force for a two-bubble collision is the buoyancy force of the moving bubble; therefore assuming the average collision force for all time steps to be the buoyancy force of the average sized bubble neglects the rolling effect during collision.

As for the "Momentum transfer model", "Kinetic theory approach", "Pressure-based model" and "Energy dissipation model", all present non-accurate results, as their relative errors are very high percentages. The "Momentum transfer model" yields an average relative error of 94.5% for the polydisperse cases and 87.55% for the monodisperse cases. The "Kinetic theory approach" presents an average relative error of 99.96% for the polydisperse cases and 99.7% for the monodisperse cases. The "Pressure-based model" shows an average relative error of 99.68% for the polydisperse cases and 99.53% for the monodisperse cases. The "Energy dissipation model" yields an average relative error of 99.99% for both the polydisperse and monodisperse cases.

The high average relative errors of these models are believed to be due to the simplifications and assumptions made when deriving the equations for the average collision force, such as considering the approach velocity of the moving bubble to be the terminal velocity of the bubble at all instances.

Furthermore, the reason as to why for the monodisperse cases said models perform ever so slightly better than for the polydisperse cases, is once again due to the average buoyancy force being exactly equal to the buoyancy force of the average sized bubble for the monodisperse cases. As all models make use of the average buoyancy force, all models share this reason.

Both versions of the "Power Law" model produce the best results out of all suggested models, in terms of average relative error.

In the case of the "Power Law" without including the collision frequency, the smallest average relative error, for the combined case of polydisperse and monodisperse distributions, is of 47.2% for $C_1 = 0.0205$ and $C_2 = 0.1314$. However, treating polydisperse and monodisperse distributions separately, lower relative errors can be obtained: in the polydisperse case, a fit with $C_1 = 0.027$ and $C_2 = 0.1314$, results in an average relative error of 27.56%; whilst for the monodisperse case, for $C_1 = 0.1115$ and $C_2 = 1.1$, an average relative error of 44.18% is obtained.

In the case of the "Power Law" including the collision frequency, the smallest average relative error, for the combined case of polydisperse and monodisperse distributions, is of 49.02% for $C_1 = 19.5$, $C_2 = 0.795$ and $C_3 = -0.9$. Once again, by treating polydisperse and monodisperse distributions separately, lower relative errors can be obtained: in the polydisperse case, a fit with $C_1 = 0.25$, $C_2 = 0.4112$ and $C_3 = -0.2767$, results in an average relative error of 27.58%; whilst for the monodisperse case, for $C_1 = 0.1962$, $C_2 = 1.2258$ and $C_3 = -0.05$, an average relative error of 43.5% is obtained.

Said results of the "Power Law" raise the question whether the collision frequency matters or is relevant for said model.

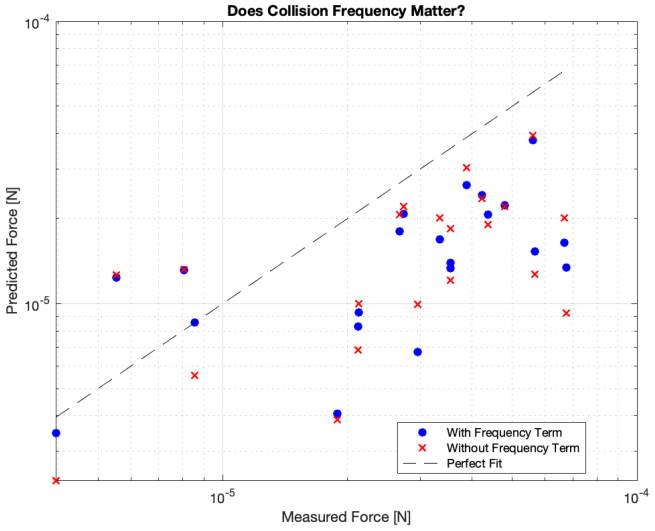

Figure 3.33: Comparison of predicted force vs actual force for both different varioations of the power law (with and without the collision frequency) for both polydisperse and monodisperse cases.

From Figure 3.33, it is visible that the results of the "Power Law" with the collision frequency term and without the collision frequency term are quite similar. Therefore, for the case in which said law is used to describe the average collision force on a large distribution of bubbles, one might be more successful ignoring the collision frequency term, as said term does not add any more accuracy to the model, but adds one more term to an equation that

could ever so slightly increase the computational demand per bubble.

In Figure 3.34 the results for all models considered compared to the correct average collision force are shown. As can be seen in the plot, confirming what has already been stated, the power law models have the highest accuracy of all models, tending to predict the average collision force roughly in the same order of magnitude as the actual average collision force, whilst the other models are not capable of doing so. Having said this, this statement is nuanced, as both versions of the power law were fitted to the data to obtain the optimal values of coefficients and the smallest relative errors, thus of course they are the best performing models. However, the parameters to use in the power law models were chosen out of intuition, i.e what was believed to be most important and coherent to the average collision force. Therefore, if they weren't chosen correctly, the power law models could yield worse results than the other presented models.

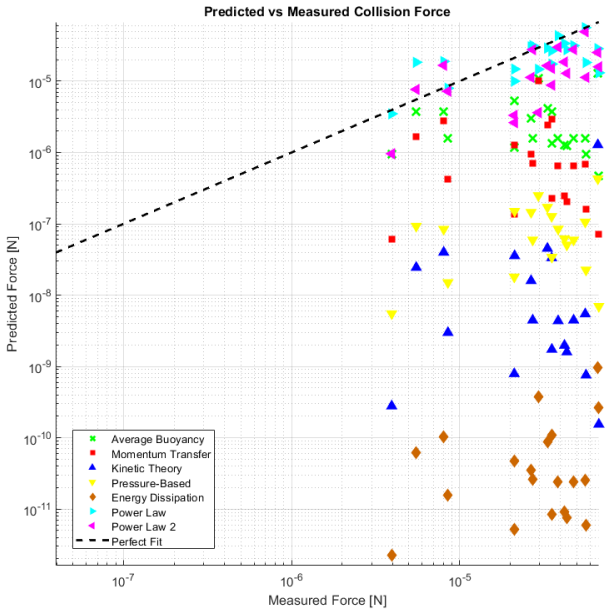

Figure 3.34: Comparison of predicted force vs actual force for all models, for both polydisperse and monodisperse cases.

Using the set-up in which the fixed bubble is attached to the electrode, as seen in Figure 3.25b, a qualitative understanding and result of how the bubble collisions affect the trajectory of the rising bubbles, and how these rising bubbles end up forming a "plume" can be obtained. The evolution of the bubble plume caused by bubble collisions can be seen in Figure 3.35. The snapshots show a side view of the set-up, where the grey area is the flat vertical electrode (given a random width and height), the red bubble is fixed bubble positioned on the electrode to simulate a non-detached bubble still growing with which moving bubbles can collide, and the blue bubbles are the already detached and rising bubbles. It is visible how when bubbles collide, because they can not be pushed towards the

electrode, instead they are pushed away from the electrode. After some time, when more and more bubbles start to collide, a plume is formed due to said "pushing" of bubbles further from the electrode as a result of multiple collisions.

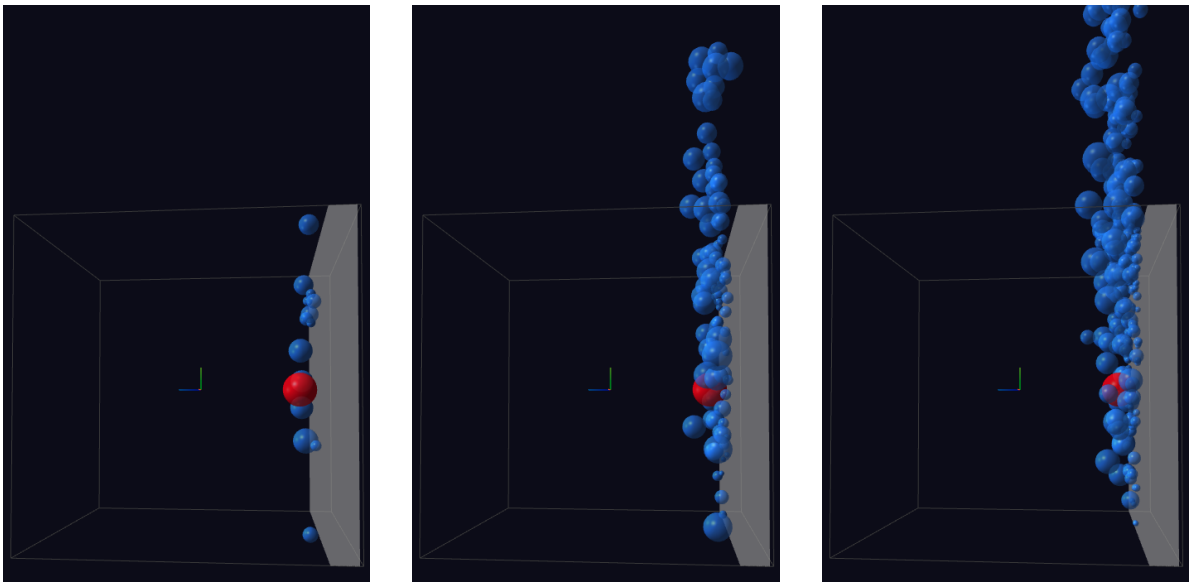

(a) Snapshot 1. (b) Snapshot 2. (c) Snapshot 3.

Figure 3.35: Visualisation of the bubble collisions code and the bubble plume generated.

Chapter 4

Conclusions, research gaps and future lines of study

This thesis studied the formation of bubbles on flat electrodes and their behaviour in an electrolyser, including their detachment, advection and interactions with each other. It is essential to understand how bubbles behave in electrolysers and what causes them to behave in such manner, in order to reduce the efficiency loss of the the electrolysis process at large scales. The objective of this thesis was to develop a point-bubble model capable of working for a large number of bubbles, and to gain insight into the behaviour of bubbles in electrolyser-like flow regimes. This final chapter synthesises the main contributions this research has made into this field of study.

4.1 Conclusions

A comprehensive literature review on the simulation of multiphase bubbly flow for hydrogen production in water electrolysis, as well as the physics and theory behind it has been presented.

4.1.1 An Algorithm for bubble generation

A robust algorithm was created to generate realistic 2D and 3D distributions of bubbles consistent with experimental observations and literature. Its main features and performance include:

The algorithm allows a high volume fraction or high number of bubbles to be generated, staying true to the stochastic nature of bubble nucleation on an electrode and to the distributions of bubble sizes seen in literature.

The possibility of using the algorithm in different simulation methods and set-ups, whilst maintaining a relatively small computational demand, makes it a reliable and powerful tool to pair up with other numerical methods used in the field of bubble simulations. It is a robust and volatile algorithm, capable of creating monodisperse and polydisperse distributions of

bubbles, that counts with a failure of placement safety net, known as the fallback position function, as explained in section 3.1.

The fallback position function's computational demand and runtime scale with the grid size, following a power law given in this thesis. When dealing with volume fractions instead of number of bubbles, as an input to the algorithm, it presents high accuracy when calculating the needed number of bubbles, specially for monodisperse distributions of bubbles.

The flowchart of the logical reasoning and steps the algorithm follows is presented.

4.1.2 Bubble detachment and advection

To study the forces acting on the detachment of a bubble from a flat surface mimicking an electrode, as well as the force acting on the bubble during the bubble's flow after its detachment, different cases were studied.

The major interest of this part of the project was placed on the lift force, as it is believed to be the major contributor to the bubble´s detachment and motion away from the electrode.

The first case was a horizontal electrode set-up for which no conclusions could be drawn about the importance of the lift force to the bubble´s motion away from the electrode. In said horizontal case, the buoyancy force acts as a continuous promoter of the advection of the bubble away from the flat surface.

The other case studied was a flat vertical electrode set-up. For this vertical case, the study of the forces and movement of the bubble after detachment suggest that the lift force plays a major role in pushing the bubble away from the electrode.

The difference between unbounded flow lift force definitions and the inclusion of a bounded flow lift force term in the total lift force suggest mostly quantitative differences: larger displacements, for the same amount of time, are seen in the case of the bounded flow, but similar trajectories are observed.

The lift force is observed to grow at a faster pace than the drag force, whilst the value of the ratio of non-dimensional numbers (ϵ) decreases as the bubble rises and becomes faster.

For both the horizontal and vertical cases, it was concluded that the simple definition of the adhesion force keeping the bubble attached to the electrode, oversimplifies the physics of adhesion, resulting in excessively large adhesion force values that keep the bubble attached to the electrode for many different simulation runs.

4.1.3 Modelling of detachment force due to bubble collision

An attempt to model the force that enhances bubble detachment, that arises due to the collisions between bubbles, was made.

The non-coalescing collision between bubbles was simulated by assuming perfectly spherical, non deformable bubbles, that suffer a lubrication force and electrostatic force when coming close enough to each other.

The bubble generation algorithm presented in this study, was used to create two different set-ups with the intention of studying said collisions.

A first set-up in which a fixed bubble was placed in the centre of the domain, whilst rising bubbles collided with it, was used to gain knowledge of the average collision force exerted on said fixed bubble throughout the simulations. Various different runs were made with different sized bubbles, different domain sizes, and different volume fraction of bubbles in the domain. Parameters such as the collision frequency, force vector distribution and bubbles within collision reach, apart from the main result, the average collision force; were obtained from the simulations.

Once the average collision force was obtained, different models based on slightly different physical phenomena were tested and compared with the simulation results.

Both different variations of the "Power law" model present average relative errors of around 48%. The "Average buoyancy model" yields an average relative error of 85%. The rest of the models presented worse average relative errors, errors up to 99%. Despite the differences in average relative errors, most models suggest that what determines the average collision force is mostly the average buoyancy force of the bubble distribution. As most models make use of said force, they present average collision force predictions either in the same order of magnitude as the actual results, or a few orders of magnitude smaller: they underestimate the average collision force.

The high relative error from such models is believed to be in both cases a result of the "rolling" motion of bubbles when colliding with the fixed one, caused by the collision being a multiple body phenomena. However, no irrefutable evidence is presented that can confirm said statement, but evidence that suggests it is given.

The second set-up in which a fixed bubble was placed on a vertical electrode, was used to visualise the effect of bubble collisions on the evolution of the scale of the "bubble plume" that exists near the vertical electrode and causes the efficiency problems. From the included snapshots in the study, it can be seen that bubble collision promotes the extension of the "bubble plume" into the bulk flow.

4.1.4 Achievements of the thesis

The achievements of this thesis therefore are the following:

- An exhaustive review of existing knowledge on bubble formation, growth and detachment in water electrolysis was carried out.
- A broad analysis of methods used to generate realistic bubble distributions on electrolyser electrodes was completed.
- A study of the most relevant hydrodynamic forces acting on bubbles in water electrolysis was performed.
- A code capable of generating bubbles on the electrode, that complies with the knowledge obtained from the study of methods already used to create realistic distributions, was created.
- A code capable of replicating the motion of a bubble in both horizontal and vertical shear flow was generated.
- A code capable of representing bubble-bubble collision as well as multiple-bubble collision was produced.
- Numerical models describing the collision force experienced by a bubble attached to the electrode were come up with and tested.
- Insights into why bubble "plumes" are formed in electrolysers, and how said plumes happen, were obtained.

Furthermore, this literature review has touched upon the challenges associated with modelling bubble behaviour during water electrolysis such as modelling the moment bubbles begin to nucleate, or modelling bubble's changing contact angle with the electrode.

4.2 Research gaps and limitations

4.2.1 Research gaps and limitations general to bubbly flows in water electrolysis

Despite all of the knowledge gained during the literature review, and the progress made in understanding and simulating bubbly flows during water electrolysis, further investigation is needed to cover the existing general research gaps in this field of study:

- A large portion of the research done on this field of bubbly flow simulation for water electrolysis focuses on singular bubbles. However, and as mentioned already, in reality many bubbles are generated at a time in the electrode, and their interactions play a role in the electrolyser's performance: bubbles may coalesce to form bigger bubbles

or push each other due to collisions, up to a point where a "wall" or "plume" of bubbles is formed on the electrode, decreasing the electrode's available reaction area significantly. Therefore, numerical models capable of simulating large number of bubbles and capturing the interactions between them at a reasonable computational cost, are needed. Existing numerical methods like the Point-Particle method developed in this study, although efficient for large number of bubbles, require more accurate closure laws for hydrodynamic interactions between particles, to achieve higher accuracy and fidelity.

- More accurate constituent equations, i.e definitions of the forces, are needed. Despite the existence of said definitions, that capture the essence of the main hydrodynamic forces acting upon the bubbles, such as the buoyancy force, calculating the less studied and more subtle forces that are not so straightforward to compute, because they depend on gradients of variables for example, is still challenging. For that reason, there are less refined consituent equations that calculate said subtle forces, which may still be of great importance to the hydrodynamics of bubbles. Additionally, simpler but accurate definitions are needed, to reduce the computational demand of simulating bubbles, whilst reasonably maintaining the essential physics. The absence of simpler models and the excess of complex definitions and models of forces lead to erroneous oversimplifications like the adhesion force simplification made in this study.

- A closer interplay of the fluid dynamics of bubbles, and the electrochemical reactions happening in water electrolysis, is needed. Most studies treat both phenomena somewhat separately. The integration of both phenomena in one, would result in a more realistic representation of what is really happening in water electrolysis, specially for simulations of large number of bubbles.

- There is a need for more detailed experimental data on bubble formation, growth, detachment and flow evolution to validate the numerical models and simulations of this phenomena. Specially for conditions relevant to the scale-up of said process, i.e. for conditions seen in the large scale water electrolysis industry. Data such as the collision frequency of bubbles in water electrolysis for given volume fractions, the average moving velocity of bubbles during water electrolysis, the percentage of total time in which a bubble suffers a collision, etc. are suggested to be imperative for the study. Without this data, conclusions as to if the models are coherent with what happens in reality can not be drawn, and therefore they could be deemed useless. Said data can also help improve model's predictive capabilities. The results obtained in this study, although promising, are not useful unless they are validated experimentally.

- The uniqueness of possible scenarios in this field of study, leads to incoherent data and results. Much research has been done into the formation, detachment, transport and interaction of bubbles in water electrolysis, however most available literature presents unique scenarios. Having such variance of set-ups, conditions and parameter values makes it hard to determine whether results are valid and represent the underlying physics correctly, or if the results are tailored to the specific conditions of the simulations.

4.2.2 Research gaps and limitations specific to this study

As for the major limitations or constraints specific to this study, most of them derive from assumptions and simplifications made to the intricate underlying physics in this phenomena.

First of all, throughout the simulation, the bubble shape is considered to be perfectly spherical and non-deformable. Of course, this is a significant simplification of the true behaviour of bubbles, as in reality many bubbles will change shape depending on the forces acting on them and their interactions with other bubbles.

Secondly, the developed algorithm for bubble generation focuses on heterogeneous nucleation, i.e. the formation of bubbles on the electrode. This results in the neglect of homogeneous formation if bubbles in the electrolyser.

Third, due to the complexity of modelling an adhesion force with a changing contact angle with the electrode, a fully dynamic and complex detachment force is not addressed or used in this study. Therefore, the conclusions related to the detachment of the bubble are limited.

Finally, the study presents a limited electrode configuration. The developed code, and therefore the results obtained from the study, are only available for planar electrodes. This restricts the application of this study to cases in which the electrode geometry is not planar.

4.3 Future lines of study

Having mentioned research gaps relevant to this thesis' theme, several future lines of study both for the general case of the existence of bubbles in electrolysers, as well as specific to this study, can be proposed:

- Developing hybrid models that resolve different scales could help reduce the computational cost of simulations with high number of bubbles. By combining high resolution methods such as Interface-Resolved simulations for the bubble dynamics near the electrode, with less computationally demanding methods such as the Point-Particle method, with improved closure-laws, for tracking bubbles further away from the electrode (in the bulk flow) or for generating said bubbles in the domain, could be a way to simulate larger systems, with more accuracy, whilst keeping the computational strain low.

- Improving the research on the less known hydrodynamic forces and their impact on the bubble's dynamics is needed. Once that is done, incorporating that knowledge into existing numerical models would improve simulation accuracy.

- Improving the knowledge on bubble-bubble interactions and coalescence using high resolution methods such as Direct Numerical Simulation (DNS). By doing so for small, simpler domains and small number of bubbles; valuable insights can be obtained which can then later be applied to larger systems. Once found reliable, said mentioned

high-fidelity simulations can also serve as benchmark for newly developed and less computationally demanding models such as the one presented in this study.

- Attempting to make the bubble generation algorithm faster and less computationally demanding. Other ideas that came up during the realisation of this project were not tested due to the computational and time constraints, as well as the programming knowledge cap. Different methods to generate bubbles that were not tried are for example, making the generation of coordinates parallel and sequential at the same time: have an iterative loop without limit to randomly generate the bubble coordinates. For every iteration, all coordinates of all bubbles are randomly generated. The coordinates that are valid and therefore create bubbles that do not overlap are left untouched going into the following iteration. In the following iteration, only the coordinates that were not deemed as valid are re-randomised in the current iteration. The process is repeated until all coordinates are valid. This process, as mentioned, has not been tested or tried, but may lead to faster run times and lower computational demand, as the process is parallelized and each parallelization can be handled by different cores.

- Improving adhesion force modelling to further understand the implications of said force on the detachment of the bubble, and how it compares or competes with the forces aiding in the detachment of the bubble.

- Investigating the "rolling" motion of colliding bubbles during multi-body collisions, and how it affects the average collision force. Then more accurate collision force models will be able to be created, that implement said knowledge on the rolling effect.

- Conducting a sensitivity analysis on the key operational parameters (bubble radius, electrolyte flow, wall shear stress, etc) and electrode characteristics (electrode size, electrode geometry, etc), can lead to more accurate simulations and models, resulting in knowledge on how to obtain a more optimized electrolyzer performance.

- Developing open-source simulation tools can help boost the research in this field, as communal sharing of knowledge by the experts in the field can lead to a wider range of ideas employed.

In conclusion, while significant progress has been made in the field of water electrolysis and multiphase flow simulations, continued research is needed to fully understand and solve this complex phenomena. Only then will improvements in the efficiency and scalability of green hydrogen production via water electrolysis, and therefore a step closer to a sustainable energy future, be possible.

References

[1] K. T. Møller, T. R. Jensen, E. Akiba, and H.-w. Li. "Hydrogen - A sustainable energy carrier". In: *Progress in Natural Science: Materials International* 27.1 (2017), pp. 34–40. ISSN: 1002-0071. DOI: https://doi.org/10.1016/j.pnsc.2016.12.014. URL: https://www.sciencedirect.com/science/article/pii/S1002007116303240.

[2] IEA. *Distribution of hydrogen production worldwide in 2022, by technology [Graph]*. url. Graph. Sept. 2023. URL: https://www.statista.com/statistics/1464120/hydrogen-production-share-by-technology/.

[3] F. Khalighi, N. G. Deen, Y. Tang, and A. W. Vreman. "Hydrogen bubble growth in alkaline water electrolysis: An immersed boundary simulation study". In: *Chemical Engineering Science* 267 (2023), p. 118280. ISSN: 0009-2509. DOI: https://doi.org/10.1016/j.ces.2022.118280. URL: https://www.sciencedirect.com/science/article/pii/S000925092200865X.

[4] W. Wang, B. Han, B. Cao, and J. Mo. "Three-dimensional numerical simulation of bubble dynamics and design optimization of microchannel in proton exchange membrane water electrolyzers". In: *International Journal of hydrogen energy* 48 (June 2023), pp. 36240–36253.

[5] F. Sepahi, R. Verzicco, D. Lohse, and D. Krug. "Mass transport at gas-evolving electrodes". In: *Journal of Fluid Mechanics* 983 (2024), A19. DOI: 10.1017/jfm.2024.51.

[6] H. Vogt. "Superposition of microconvective and macroconvective mass transfer at gas-evolving electrodes—a theoretical attempt". In: *Electrochimica Acta* 32.4 (1987), pp. 633–636. ISSN: 0013-4686. DOI: https://doi.org/10.1016/0013-4686(87)87054-8. URL: https://www.sciencedirect.com/science/article/pii/0013468687870548.

[7] X. Lu, D. Yadav, B. Ma, L. Ma, and D. Jing. "Rapid detachment of hydrogen bubbles for electrolytic water splitting driven by combined effects of Marangoni force and the electrostatic repulsion". In: *Journal of Power Sources* 599 (2024), p. 234217. ISSN: 0378-7753. DOI: https://doi.org/10.1016/j.jpowsour.2024.234217. URL: https://www.sciencedirect.com/science/article/pii/S037877532400168X.

[8] S. S. Kumar and H. Lim. "An overview of water electrolysis technologies for green hydrogen production". In: *Energy Reports* 8 (2022), pp. 13793–13813. ISSN: 2352-4847. DOI: https://doi.org/10.1016/j.egyr.2022.10.127. URL: https://www.sciencedirect.com/science/article/pii/S2352484722020625.

[9] Y. Liu, S. Li, H. Wu, and Y. Shi. "Experimental investigation and analysis for the bubble size distribution during alkaline water electrolysis by using a wire electrode". In: *DeCarbon* 5 (2024), p. 100052. ISSN: 2949-8813. DOI: https://doi.org/10.1016/j.decarb.2024.100052. URL: https://www.sciencedirect.com/science/article/pii/S2949881324000180.

[10] F. Khalighi. "Bubble dynamics in electrolysis: an immersed boundary simulation study". PhD thesis. Mechanical Engineering, Dec. 2024.

[11] S. S. Kumar and V. Himabindu. "Hydrogen production by PEM water electrolysis – A review". In: *Materials Science for Energy Technologies* 2.3 (2019), pp. 442–454. ISSN: 2589-2991. DOI: https://doi.org/10.1016/j.mset.2019.03.002. URL: https://www.sciencedirect.com/science/article/pii/S2589299119300035.

[12] P. van der Linde. "On electrolytic bubbles". PhD thesis. Netherlands: University of Twente, Apr. 2019. DOI: 10.3990/1.9789036547413.

[13] L. L. Qianjin Chen and H. S. White. "Electrochemical Generation of a Hydrogen Bubble at a Recessed Platinum Nanopore Electrode". In: *Langmuir* 31.15 (2015), pp. 4573–4581. DOI: https://doi.org/10.1021/acs.langmuir.5b00234.

[14] L. Zhengmao, L. Zhang, R. Iwata, E. N. Wang, and J. C. Grossman. "Transport-Based Modeling of Bubble Nucleation on Gas Evolving Electrodes." In: *Langmuir 36* 49 (2020), pp. 15112–15118. DOI: 10.1021/acs.langmuir.0c02690.

[15] S. G. Panpan Zhao Chaoyang Zhang. "Size Ranges of Effective Nucleation Cavities on Gas-Evolving Surfaces". In: *Langmuir* 39.45 (2023), pp. 16101–16110. DOI: https://doi.org/10.1021/acs.langmuir.3c02235.

[16] L. Deng, L. Jin, L. Yang, C. Feng, A. Tao, X. Jia, Z. Geng, C. Zhang, X. Cui, and J. Shi. "Bubble evolution dynamics in alkaline water electrolysis". In: *eScience* (2024), p. 100353. ISSN: 2667-1417. DOI: https://doi.org/10.1016/j.esci.2024.100353. URL: https://www.sciencedirect.com/science/article/pii/S2667141724001526.

[17] O. Kessels. "Simulation of Hydrogen Bubbles during Electrolysis". Student thesis: Bachelor. Eindhoven University of Technology, 2024.

[18] P. Chandran, S. Bakshi, and D. Chatterjee. "Study on the characteristics of hydrogen bubble formation and its transport during electrolysis of water". In: *Chemical Engineering Science* 138 (2015), pp. 99–109. ISSN: 0009-2509. DOI: https://doi.org/10.1016/j.ces.2015.07.041. URL: https://www.sciencedirect.com/science/article/pii/S0009250915005278.

[19] M. Gallo, F. Magaletti, and C. M. Casciola. "Heterogeneous bubble nucleation dynamics". In: *Journal of Fluid Mechanics* 906 (2021), A20. DOI: 10.1017/jfm.2020.761.

[20] S. Peng, V. Spandan, R. Verzicco, D. Lohse, and X. Zhang. "Growth dynamics of microbubbles on microcavity arrays by solvent exchange: Experiments and numerical simulations". In: *Journal of Colloid and Interface Science* 532 (2018), pp. 103–111. ISSN: 0021-9797. DOI: https://doi.org/10.1016/j.jcis.2018.07.111. URL: https://www.sciencedirect.com/science/article/pii/S0021979718308750.

[21] X. Deng et al. "Direct measuring of single–heterogeneous bubble nucleation mediated by surface topology". In: *Proceedings of the National Academy of Sciences* 119.29 (2022). _eprint: https://www.pnas.org/doi/pdf/10.1073/pnas.2205827119, e2205827119. DOI: 10.1073/pnas.2205827119. URL: https://www.pnas.org/doi/abs/10.1073/pnas.2205827119.

[22] T. van der Linden. "DNS investigation on the lift force of single bubbles". Student Thesis: Master. Eindhoven: Eindhoven University of Technology.

[23] A. Bashkatov, X. Yang, G. Mutschke, B. Fritzsche, S. S. Hossain, and K. Eckert. "Dynamics of single hydrogen bubbles at Pt microelectrodes in microgravity". In: *Phys. Chem. Chem. Phys.* 23.20 (2021). Number: 20, pp. 11818–11830. DOI: 10.1039/D1CP00978H. URL: http://dx.doi.org/10.1039/D1CP00978H.

[24] N. Valle and J. W. Haverkort. "Self-similar solution for laminar bubbly flow evolving from a vertical plate". In: *Journal of Fluid Mechanics* 996 (2024), A38. DOI: 10.1017/jfm.2024.793.

[25] J. Magnaudet. "THE FORCES ACTING ON BUBBLES AND RIGID PARTICLES". In: June 1997.

[26] D. Legendre and J. Magnaudet. "The Lift Force on a Spherical Bubble in a Viscous Linear Shear Flow". In: *Journal of Fluid Mechanics* 368 (Aug. 1998), pp. 81–126. DOI: 10.1017/S0022112098001621.

[27] G. G. Stokes. "On the Effect of the Internal Friction of Fluids on the Motion of Pendulums". In: *Transactions of the Cambridge Philosophical Society* 9 (Jan. 1851), p. 8.

[28] C. Oseen. *Über die Stoke'sche Formel und über eine verwandte Aufgabe in der Hydrodynamik: Mitteilung 2*. Arkiv för matematik, astronomi och fysik v. 1. Almqvist & Wiksell, 1911. URL: https://books.google.nl/books?id=SB64nQEACAAJ.

[29] C. Oseen. *Neuere Methoden und Ergebnisse in der Hydrodynamik*. Mathematik und ihre Anwendungen in Monographien und Lehrbüchern. Akademische Verlagsgesellschaft, 1927. URL: https://books.google.nl/books?id=2lWHugEACAAJ.

[30] T. D. Taylor and A. Acrivos. "On the deformation and drag of a falling viscous drop at low Reynolds number". In: *Journal of Fluid Mechanics* 18.3 (1964), pp. 466–476. DOI: 10.1017/S0022112064000349.

[31] A. TOMIYAMA, I. KATAOKA, I. ZUN, and T. SAKAGUCHI. "Drag Coefficients of Single Bubbles under Normal and Micro Gravity Conditions". In: *JSME International Journal Series B* 41.2 (1998), pp. 472–479. DOI: 10.1299/jsmeb.41.472.

[32] J. P. McHale and S. V. Garimella. "Bubble nucleation characteristics in pool boiling of a wetting liquid on smooth and rough surfaces". In: *International Journal of Multiphase Flow* 36.4 (2010), pp. 249–260. ISSN: 0301-9322. DOI: https://doi.org/10.1016/j.ijmultiphaseflow.2009.12.004. URL: https://www.sciencedirect.com/science/article/pii/S0301932209001967.

[33] V. Levich. "The motion of bubbles at high Reynolds numbers". In: *Zh. Eksp. Teor. Fiz* 19.18 (1949), 436ff.

[34] D. W. Moore. "The boundary layer on a spherical gas bubble". In: *Journal of Fluid Mechanics* 16.2 (1963), pp. 161–176. DOI: 10.1017/S0022112063000665.

[35] S. v. d. Heuvel. "Hydrodynamic Forces Acting on Vertically Rising Bubbles". PhD thesis. Sept. 2023. URL: http://essay.utwente.nl/97212/.

[36] F. TAKEMURA, S. TAKAGI, J. MAGNAUDET, and Y. MATSUMOTO. "Drag and lift forces on a bubble rising near a vertical wall in a viscous liquid". In: *Journal of Fluid Mechanics* 461 (2002), pp. 277–300. DOI: 10.1017/S0022112002008388.

[37] J. B. McLaughlin. "Inertial migration of a small sphere in linear shear flows". In: *Journal of Fluid Mechanics* 224 (1991), pp. 261–274. DOI: 10.1017/S0022112091001751.

[38] T. Auton, U. of Cambridge, U. of Cambridge. Department of Applied Mathematics, and T. Physics. *The Dynamics of Bubbles, Drops and Particles in Motion in Liquids*. The Author, 1983. URL: https://books.google.nl/books?id=T07kGwAACAAJ.

[39] J. Klausner, R. Mei, D. Bernhard, and L. Zeng. "Vapor bubble departure in forced convection boiling". In: *International Journal of Heat and Mass Transfer* 36.3 (1993), pp. 651–662. ISSN: 0017-9310. DOI: https://doi.org/10.1016/0017-9310(93)80041-R. URL: https://www.sciencedirect.com/science/article/pii/001793109380041R.

[40] X. WANG, X. PENG, Y. DUAN, and B. WANG. "Dynamics of Spreading of Liquid on Solid Surface* *Supported by the National Natural Science Foundation of China (Nos.50636020, 50406001)." In: *Chinese Journal of Chemical Engineering* 15.5 (2007), pp. 730–737. ISSN: 1004-9541. DOI: https://doi.org/10.1016/S1004-9541(07)60154-2. URL: https://www.sciencedirect.com/science/article/pii/S1004954107601542.

[41] S. Orvalho, P. Stanovsky, and M. C. Ruzicka. "Bubble Coalescence in Electrolytes: Effect of Bubble Approach Velocity". In: *Chemical Engineering Journal* 406 (2021), p. 125926. DOI: 10.1016/j.cej.2020.125926. URL: https://doi.org/10.1016/j.cej.2020.125926..

[42] A. Chesters and G. Hofman. "Bubble coalescence in pure liquids". In: *Applied Scientific Research* 38.1 (1982), pp. 353–361.

[43] É. Guazzelli, J. Morris, and S. Pic. *A Physical Introduction to Suspension Dynamics*. Cambridge Texts in Applied Mathematics. Cambridge University Press, 2011. ISBN: 9781139503938. URL: https://books.google.nl/books?id=TFICnEwZS7YC.

[44] T. Heng-Kwong and D. L. Koch. "Collisions of Slightly Deformable, High Reynolds Number Bubbles with Short-range Repulsive Forces". In: *Physics of Fluids 6* 6.8 (1994), pp. 2591–2605. DOI: 10.1063/1.868149.. URL: https://doi.org/10.1063/1.868149..

[45] J. Dukovic and C. W. Tobias. "The influence of attached bubbles on potential drop and current distribution at gas-evolving electrodes". In: *Journal of the Electrochemical Society* 134.2 (1987), p. 331.

[46] C. Gu and L. Botto. "FIPI: A fast numerical method for the simulation of particle-laden fluid interfaces". In: *Computer Physics Communications* 256 (2020), p. 107447. ISSN: 0010-4655. DOI: https://doi.org/10.1016/j.cpc.2020.107447. URL: https://www.sciencedirect.com/science/article/pii/S0010465520302095.

[47] H. Brenner. "The Oseen Resistance of a Particle of Arbitrary Shape". In: *Journal of Fluid Mechanics* 11.4 (1961), pp. 604–610. DOI: 10.1017/S0022112061000755. URL: https://doi.org/10.1017/S0022112061000755..

[48] B. H and C. RG. "The resistance to a particle of arbitrary shape in translational motion at small Reynolds numbers." In: *Journal of Fluid Mechanics* 17.4 (1963), pp. 561–595. DOI: 10.1017/S002211206300152X.

[49] W. Chester. "On Oseen's approximation." In: *Journal of Fluid Mechanics* 13.4 (1962), pp. 557–569. DOI: 10.1017/S0022112062000932.

[50] P. M. Lovalenti and J. F. Brady. "The Hydrodynamic Force on a Rigid Particle Undergoing Arbitrary Time-Dependent Motion at Small Reynolds Number." In: *Journal of Fluid Mechanics* 256 (1993), pp. 561–605. DOI: 10.1017/S0022112093002885.

[51] F. Takemura and K. Sugiyama. "On the lateral migration of a slightly deformed bubble rising near a vertical plane wall." In: *Journal of Fluid Mechanics* 662 (2010), pp. 209–231. DOI: 10.1017/S0022112010003149.

[52] S. Das, L. D. Weerasiri, and W. Yang. "Influence of surface tension on bubble nucleation, formation and onset of sliding". In: *Colloids and Surfaces A: Physicochemical and Engineering Aspects* 516 (2017), pp. 23–31. ISSN: 0927-7757. DOI: https://doi.org/10.1016/j.colsurfa.2016.12.010. URL: https://www.sciencedirect.com/science/article/pii/S0927775716310445.

[53] H. Jo, M. Kaviany, S. H. Kim, and M. H. Kim. "Heterogeneous bubble nucleation on ideally-smooth horizontal heated surface". In: *International Journal of Heat and Mass Transfer* 71 (2014), pp. 149–157. ISSN: 0017-9310. DOI: https://doi.org/10.1016/j.ijheatmasstransfer.2013.12.040. URL: https://www.sciencedirect.com/science/article/pii/S0017931013010843.

[54] B. D. Johnson, R. M. Gershey, R. C. Cooke, and W. H. S. J. and. "A Theoretical Model for Bubble Formation at a Frit Surface in a Shear Field". In: *Separation Science and Technology* 17.8 (1982). Publisher: Taylor & Francis _eprint: https://doi.org/10.1080/01496398208060267, pp. 1027–1039. DOI: 10.1080/01496398208060267. URL: https://doi.org/10.1080/01496398208060267.

[55] Q. Cao, Z. Li, and Z. Cui. "Nanoscale Investigation of Bubble Nucleation and Boiling on Random Rough Surfaces". In: *Langmuir* 39.36 (Sept. 12, 2023). Publisher: American Chemical Society, pp. 12754–12761. ISSN: 0743-7463. DOI: 10.1021/acs.langmuir.3c01483. URL: https://doi.org/10.1021/acs.langmuir.3c01483.

[56] E. Lozano, D. Roehl, W. Celes, and M. Gattass. "An efficient algorithm to generate random sphere packs in arbitrary domains". In: *Computers & Mathematics with Applications* 71.8 (2016). Number: 8, pp. 1586–1601. ISSN: 0898-1221. DOI: https://doi.org/10.1016/j.camwa.2016.02.032. URL: https://www.sciencedirect.com/science/article/pii/S0898122116300864.

[57] S. M. Mehdi and S. Kim. "Theoretical study of motion of small spherical air bubbles in a uniform shear flow of water". In: *Nuclear Engineering and Technology* 47.1 (2015). Number: 1, pp. 126–134. ISSN: 1738-5733. DOI: https://doi.org/10.1016/j.net.2014.11.001. URL: https://www.sciencedirect.com/science/article/pii/S1738573314000059.

[58] N. Hidman, H. Ström, S. Sasic, and G. Sardina. "The lift force on deformable and freely moving bubbles in linear shear flows". In: *Journal of Fluid Mechanics* 952 (2022), A34. DOI: 10.1017/jfm.2022.917.

[59] R. Manica, E. Klaseboer, and D. Y. C. Chan. "The hydrodynamics of bubble rise and impact with solid surfaces". In: *Advances in Colloid and Interface Science* 235 (2016), pp. 214–232. ISSN: 0001-8686. DOI: https://doi.org/10.1016/j.cis.2016.06.010. URL: https://www.sciencedirect.com/science/article/pii/S0001868616300537.

[60] J. Magnaudet and D. Legendre. "Some Aspects of the Lift Force on a Spherical Bubble". In: *Applied Scientific Research* 58.1 (Mar. 1997). Number: 1, pp. 441–461. ISSN: 1573-1987. DOI: 10.1023/A:1000844026662. URL: https://doi.org/10.1023/A:1000844026662.

[61] R. ZENIT, Y. H. TSANG, D. L. KOCH, and A. S. SANGANI. "Shear flow of a suspension of bubbles rising in an inclined channel". In: *Journal of Fluid Mechanics* 515 (2004), pp. 261–292. DOI: 10.1017/S0022112004000461.

[62] R. ADOUA, D. LEGENDRE, and J. MAGNAUDET. "Reversal of the lift force on an oblate bubble in a weakly viscous linear shear flow". In: *Journal of Fluid Mechanics* 628 (2009), pp. 23–41. DOI: 10.1017/S0022112009006090.

[63] D. Kitajima, R. Misumi, Y. Kuroda, and S. Mitsushima. "Relationship between bubble generation behavior and hydrogen evolution reaction performance at high current densities during alkaline water electrolysis". In: *Electrochimica Acta* 502 (2024), p. 144772. ISSN: 0013-4686. DOI: https://doi.org/10.1016/j.electacta.2024.144772. URL: https://www.sciencedirect.com/science/article/pii/S0013468624010120.

[64] P. S. Epstein and M. S. Plesset. "On the Stability of Gas Bubbles in Liquid-Gas Solutions". In: *The Journal of Chemical Physics* 18.11 (Nov. 1950). Number: 11, pp. 1505–1509. ISSN: 0021-9606. DOI: 10.1063/1.1747520. URL: https://doi.org/10.1063/1.1747520.

[65] H. Kusuno, H. Yamamoto, and T. Sanada. "Lift force acting on a pair of clean bubbles rising in-line". In: *Physics of Fluids* 31.7 (July 2019). Number: 7, p. 072105. ISSN: 1070-6631. DOI: 10.1063/1.5100183. URL: https://doi.org/10.1063/1.5100183 (visited on 03/18/2025).

[66] L. Bureau, G. Coupier, and T. Salez. "Lift at low Reynolds number". In: *The European Physical Journal E* 46.11 (Nov. 2023). Number: 11, p. 111. ISSN: 1292-895X. DOI: 10.1140/epje/s10189-023-00369-5. URL: https://doi.org/10.1140/epje/s10189-023-00369-5.

[67] P. Oresta, R. Verzicco, D. Lohse, and A. Prosperetti. "Heat transfer mechanisms in bubbly Rayleigh-Bénard convection". In: *Phys. Rev. E* 80.2 (Aug. 2009). Number: 2, p. 026304. DOI: 10.1103/PhysRevE.80.026304. URL: https://link.aps.org/doi/10.1103/PhysRevE.80.026304.

[68] P. Snabre and F. Magnifotcham. "I. Formation and rise of a bubble stream in a viscous liquid". In: *Eur. Phys. J. B* 4 (Jan. 1998), pp. 369–377. DOI: 10.1007/s100510050392.

[69] W.-t. Xu, S.-s. Li, L.-m. Pan, and Z.-c. Li. "Experimental investigation about the lift force of a single bubble in the water at a linear shear flow". In: *International Journal of Multiphase Flow* 145 (2021), p. 103819. ISSN: 0301-9322. DOI: https://doi.org/10.1016/j.ijmultiphaseflow.2021.103819. URL: https://www.sciencedirect.com/science/article/pii/S0301932221002494.

[70] Y. Murai, T. Shiratori, I. Kumagai, P. A. Rühs, and P. Fischer. "Effective viscosity measurement of interfacial bubble and particle layers at high volume fraction". In: *Flow Measurement and Instrumentation* 41 (2015), pp. 121–128. ISSN: 0955-5986. DOI: https://doi.org/10.1016/j.flowmeasinst.2014.10.006. URL: https://www.sciencedirect.com/science/article/pii/S0955598614001253.

[71] R. Mundhra, R. Lakkaraju, P. K. Das, M. A. Pakhomov, and P. D. Lobanov. "Effect of Wall Proximity and Surface Tension on a Single Bubble Rising near a Vertical Wall". In: *Water* 15.8 (2023). Number: 8. ISSN: 2073-4441. DOI: 10.3390/w15081567. URL: https://www.mdpi.com/2073-4441/15/8/1567.

[72] N. G. Deen, S. H. L. Kriebitzsch, M. A. v. d. Hoef, and J. A. M. Kuipers. "Direct numerical simulation of flow and heat transfer in dense fluid–particle systems". In: *Chemical Engineering Science* 81 (2012), pp. 329–344. ISSN: 0009-2509. DOI: https://doi.org/10.1016/j.ces.2012.06.055. URL: https://www.sciencedirect.com/science/article/pii/S0009250912004204.

[73] R. I. Eddington, D. B. R. Kenning, and A. I. Korneichev. "Comparison of gas and vapour bubble nucleation on a brass surface in water". In: *International Journal of Heat and Mass Transfer* 21.7 (1978), pp. 855–862. ISSN: 0017-9310. DOI: https://doi.org/10.1016/0017-9310(78)90177-1. URL: https://www.sciencedirect.com/science/article/pii/0017931078901771.

[74] S. S. Hossain, A. Bashkatov, X. Yang, G. Mutschke, and K. Eckert. "Force balance of hydrogen bubbles growing and oscillating on a microelectrode". In: *Phys. Rev. E* 106 (3 Sept. 2022), p. 035105. DOI: 10.1103/PhysRevE.106.035105. URL: https://link.aps.org/doi/10.1103/PhysRevE.106.035105.